Naval Research Laboratory
Stennis Space Center, MS 39529-5004

NRL/MR/7332--93-7068

Estimating the Oceanic Sound Speed Environment for Long-Range Acoustic Propagation

JANICE D. BOYD

Ocean Science Branch
Oceanography Division

August 1993

DISCLAIMER NOTICE

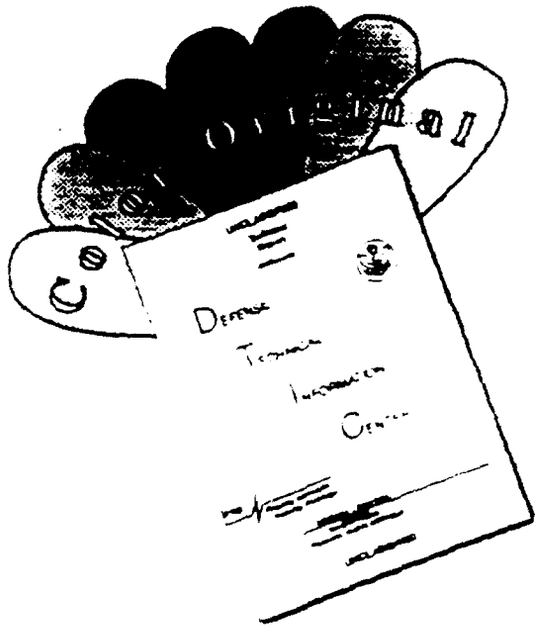

THIS DOCUMENT IS BEST QUALITY AVAILABLE. THE COPY FURNISHED TO DTIC CONTAINED A SIGNIFICANT NUMBER OF COLOR PAGES WHICH DO NOT REPRODUCE LEGIBLY ON BLACK AND WHITE MICROFICHE.

REPORT DOCUMENTATION PAGE

Form Approved
OBM No. 0704-0188

1. Agency Use Only *(Leave blank).*	2. Report Date.	3. Report Type and Dates Covered.
	August 1993	Final

4. Title and Subtitle.

Estimating the Oceanic Sound Speed Environment for Long-Range Acoustic Propagation

5. Funding Numbers.

Program Element No.	0602435N/ 0602314N
Project No.	
Task No	RJ35D04/ RJ14D04
Accession No.	DN258033/ EX155-034
Work Unit No.	73-2308-A3

6. Author(s).

Janice D. Boyd

7. Performing Organization Name(s) and Address(es).

Naval Research Laboratory
Oceanography Division
Stennis Space Center, MS 39529-5004

8. Performing Organization Report Number.

NRL/MR/7332--93-7068

9. Sponsoring/Monitoring Agency Name(s) and Address(es).

Office of Naval Research
800 N. Quincy Street
Arlington, VA 22217-5000

10. Sponsoring/Monitoring Agency Report Number.

NRL/MR/7332--93-7068

11. Supplementary Notes.

12a. Distribution/Availability Statement.

Approved for public release; distribution is unlimited.

12b. Distribution Code.

13. Abstract *(Maximum 200 words).*

The High Gain Initiative (HGI) Program was established in 1987 as a focused Block Program of the Office of Naval Technology (now part of the Office of Naval Research). One of its objectives was to investigate the oceanic environment and its effects on long-range sound transmission. One potential important factor was identified as imprecise knowledge of the oceanic sound speed field. Substantial Program resources were therefore invested in devising and executing sound speed measurement programs for two major field experiments, VAST (Various Acoustic Systems Tests) and MDA (Multi-Dimensional Array), which took place in 1989 in the Northeast Pacific and in 1991 in the western Subtropical Atlantic, respectively. This document reviews available oceanic sound speed measurement techniques, describes the combinations of techniques and strategies that made up each experiment's measurement plan, summarizes the results and the sound speed environment during each experiment, and evaluates what the work has revealed to date about sound speed uncertainties and long-range sound transmission.

14. Subject Terms.

HGI, VAST, MDA, Long-Range Acoustic Propagation, Sound Speed, Physical Oceanography, North Pacific Subarctic Front, North Atlantic Subtropical Front

15. Number of Pages.

91

16. Price Code.

17. Security Classification	18. Security Classification of Report.	19. Security Classification of This Page.	20. Limitation of Abstract. of Abstract.
Unclassified	Unclassified	Unclassified	SAR

TABLE OF CONTENTS

LIST OF TABLES

LIST OF FIGURES

Estimating the Oceanic Sound Speed Environment for Long-Range Acoustic Propagation

1.0 INTRODUCTION

The High Gain Inititative (HGI) Program was established in 1987, managed by the Office of Naval Technology (ONT), now part of the Office of Naval Research (ONR). One of its requirements was to provide information on the oceanic environment and its effects on sound transmission in the ocean. A preliminary experiment, SVLA (Single Vertical Line Array experiment) was conducted in 1987, and then two more large-scale experiments, VAST (Various Acoustic Systems Test) and MDA (Multi-dimensional Array), took place in 1989 and 1991, respectively. For reasons detailed below, a major aspect of the Program involved determining the sound speed field in the experimental areas as accurately as possible with available technology. This document summarizes the present-day technology for estimating the oceanic sound speed field, describes the experimental procedures employed to determine the sound speed fields during the VAST and MDA experiments, and gives an overview of the results and the sound speed environments encountered during the experiments. More details are available from the publications listed in Section 7.0, Resulting Publications.

Sound propagation through the ocean is a function of a variety of parameters, but the single most important variable is the sound speed. The sound speed distribution vertically and horizontally influences all acoustical phenomena. In an ocean environment where sound speed varies only with depth (the range independent case), the sound speed profile, or variation of sound speed with depth, is the dominant factor in the distribution of energy among the various acoustic ray paths. Even the amount of energy directed from the water into interaction with the seafloor is determined by the profile of sound speed in the water column. In cases where the sound speed also varies with horizontal distance (the range dependent case), acoustic energy is further redistributed as it propagates in the horizontal. Thus, in cases where long propagation ranges are considered and where the ocean temperature and salinity structure varies significantly with range, for certain purposes a very good estimate of the sound speed structure is required in order to optimize and/or predict system performance.

One advanced processing technique that has received quite a bit of interest is matched field processing (MFP) (see, for example, Bucker 1976). If the sound speed field is completely known, then through modeling the propagation paths, a comparison can be made between the actual acoustic pressure field as measured by each receiver in a hydrophone array and the calculated acoustic field modeled at the array by assuming a particular source position. A high level of correlation between the two fields indicates a high probability that a source is at the assumed depth-range-azimuth position. This technique is a potentially powerful tool, but theoretical studies have suggested it is highly sensitive to the accurate specification of the sound speed field (Porter et al. 1987). One of the Program objectives was to examine this sensitivity from an experimental viewpoint.

The sound speed structure scales of interest for acoustic propagation depend upon the wavelength of the acoustic energy. If the wavelength of sound is large compared with scales of variation in the sound speed field, the acoustic waves do not "see" the sound speed field. If the acoustic wavelengths are small compared to the sound speed structure scales, then the energy is refracted by the sound speed field. For low frequency acoustic energy (say 75 to 200 Hz), the acoustic wavelengths of interest are about 20 m down to 7.5 m. In the vertical, the sound speed structure has considerable variability on these scales and thus the sound speed field must be vertically sampled on comparable scales (say 1 to 10 m, depending upon location in the water column -- in the more variable upper layers more dense sampling is required). In the horizontal, the sound speed structure varies more gradually so that the scales of interest are determined by the variation in the sound speed field and not the acoustic wavelength. Typical horizontal variations in the sound speed structure depend very strongly upon the type of oceanic feature, as illustrated in Table 1-1. Thus, horizontal sampling scales must depend upon the location of interest and its relation to the location of fronts, eddies, and other high gradient features. Typically the horizontal sampling should be at least half the distance of the dominant scale of variability.

Preliminary work has indicated that the usefulness of advanced techniques involving long-range acoustic propagation could be limited by the imprecise knowledge of the the sound speed field. In particular, the sound speed fluctuations resulting from mesoscale and larger/longer oceanic processes could be limiting if th energy (variance) in the mesoscale range could not be measured with sufficient accuracy -- estimated to be 95 - 99%.

On the other hand, it has been argued that the sound speed fluctuations due to submesoscale and fine scale processes (largely internal wave induced; see Table 1-1) could also be limiting over long distances. A nominal frequency-range bound of 20,000 wavelengths was established using techniques described in Flatte (1979). That is, at frequency-range combinations yielding propagation distances beyond 20,000 wavelengths, unknown submesoscale sound speed fluctuations along the propagation path would severely limit the ability to do useful analyses. Conversely, if the propagation distance in wavelengths was less than about 20,000 wavelengths, the submesoscale uncertainties should not significantly limit the propagation.

These limitations led to the definition of several major issues involving the sound speed field and long-range propagation. They included: first, how should sound speed fluctuations resulting from mesoscale and larger oceanic processes be measured and what accuracy is required? Second, what are the limits imposed by the submesoscale and smaller/faster sound speed variations?

To achieve the sound speed structure resolution required for investigating these questions, a variety of techniques had to be considered. At one extreme (a very stable water mass over short propagation ranges) a single profile of sound speed might adequately describe the sound speed field. At the other extreme (in a front or at a location of strong temporal variation) a virtually continuous monitoring of sound speed in time and space might be required to perform matched field processing on acoustic arrivals; this would necessitate

Table 1-1. Types and scales of oceanic variability.

Feature	Examples	Horizontal Scales
Basin-scale ocean circulation systems	Climatological ocean pilot charts (e.g., Fig. 3-6)	10,000 - 5,000 km
Major boundary currents	Gulf Stream, Kuroshio, California Current	5,000 - 1,000 km
Mesoscale features	Gulf Stream rings, other warm and cold eddies, some frontal zones, Levitus climatology	1,000 - 100 km
Sub-mesoscale features	Some frontal zones, inertial oscillations, paired vortex eddies, Gulf Stream shingles, GDEM climatology	100 - 1 km
Fine-scale or sub-mesoscale features	Internal waves, tides, surface mixed layers	1 km - 1 m
Microscale features	Turbulence, double diffusion	1 m - 1 mm

frequent shipboard (for depth coverage) and airborne (for temporal and spatial coverage) measurement of the region of interest. In practice, a combination of techniques must be used depending upon the availability of resources and the variability of the ocean. A combination of synoptic measurements from ships, satellite, and aircraft combined with historical databases or climatologies is the most readily available method of estimating the sound speed field. More recently, acoustic tomography has been attempted as a method of describing and tracking the temporal evolution of the sound speed field. All methods have drawbacks, and in practice, a careful matching of resources with locations and other requirements is required.

Thus, there is no one readily available and low cost measurement method for the sound speed field. A number of techniques must be employed, all with their particular advantages and disadvantages. This reality was factored into the design of the VAST and MDA environmental sampling plans, as it must be considered for any application involving long-range propagation. Sound speed estimates need to be derived from in-situ and remote

measurements (perhaps including acoustic tomography), climatologies and databases, and ocean numerical models. Inputs from satellite, ship, and aircraft combined with modern modeling techniques show some promise of providing sound speed fields of sufficient accuracy. At present, the available nowcast/forecast capabilities are of coarse resolution and limited accuracy. They may be adequate in low variability environments, but they are not suitable for range varying environments. On the other hand, they are a "first cut" and are often better than pure climatology or sound speed derived from archived databases.

2.0 SOUND SPEED FIELD DETERMINATION

The general problem of determining sound speed in the ocean is many-fold. First, instruments that directly measure sound speed ("sound velocimeters") are costly and more difficult to calibrate and use than instruments that measure parameters which directly influence sound speed in the ocean: temperature, salinity (or conductivity), and pressure (or depth). A number of equations have been derived to calculate sound speed from these three parameters. Three have been most widely used. The first widely accepted equation was Wilson's equation (Wilson 1960). His equation was derived from laboratory investigations using pure water, and later investigations (including Frye and Pugh 1971) revealed inconsistencies in his data. A second equation by Chen and Millero (Chen and Millero 1977) was accepted as the UNESCO (United Nations Educational, Scientific, and Cultural Organization) standard (Fofonoff and Millard 1983). However, recent experiments with acoustic tomography (Dushaw et al. 1993) have indicated that a third equation, that of Del Grosso (1974) probably more accurately represents the speed of sound in sea water, especially at depth. All sound speed calculations in this document have been made using Del Grosso's equation.

A second problem in determining the oceanic sound speed field is simply the magnitude of the undertaking in making simultaneous measurements of the field over large four-dimensional (latitude/longitude/depth/time) ocean areas. Compromises must be made to obtain an "adequate" estimate of the sound speed field using a judicious combination of direct measurements, climatologies and archived databases, inferences from satellite data, acoustic tomography, and numerical ocean models. These will be discussed individually in the following sections.

2.1 DIRECT MEASUREMENTS OF SOUND SPEED

Traditionally, sound speed in an ocean area has been determined by the measurement of temperature, depth or pressure (one may be calculated from the other), and either the direct measurement of conductivity (or salinity) or an assumed salinity value. Temperature and depth measurements are obtained most commonly through the use of expendable bathythermographs (XBTs), air dropped XBTs (AXBTs), or conductivity-temperature-depth sensors (CTD or XCTD, for the expendable version). Less commonly used sensors are sound velocimeters (expendable -- XSVs and AXSVs -- or nonexpendable) and salinity-temperature-depth (STD) sensors. A summary of most of the commonly used instrumentation for measuring the environmental parameters that effect sound speed is given in Table 2-1.

From temperature, salinity, and pressure or depth, sound speed is calculated using one of the equations mentioned above. The effect of temperature is nearly four times more important than salinity in typical ocean conditions and the variation with pressure is primarily hydrostatic, so that for many upper ocean conditions (assuming salinity doesn't

Table 2-1. An outline of selected types of instrumentation commonly used to make physical oceanographic measurements and which can be used to obtain sound speed and other parameters of interest for long-range propagation. Accuracies given are estimates of optimistic achievable accuracies under field conditions; static test accuracies or manufacturer's quoted accuracies may be greater.

DIRECT MEASUREMENT INSTRUMENTATION FOR PHYSICAL OCEANOGRAPHIC DATA

Abbreviations:

- T: Water temperature
- C: Water conductivity
- S: Salinity
- z: Depth
- SS: Sound speed
- SST: Sea surface temperature

Instrument	What it Measures	Properties	Considerations
Shipboard:			
XBT	T vs z	Expendable, deployed under way; relatively simple acquisition system; costs ~$100, depending upon model (different models for different maximum depths)	Depth extent ~460 up to ~1830 m (depends on model); accuracy ~0.2° C; depth accuracy ~5%, can be improved with calibration
XSV	SS vs z	Expendable, deployed underway; relatively simple acquisition system; costs ~$350. Two depth models.	Depth extent ~850 and ~2000 m. Manufact. claimed accuracy of 0.25 m s^{-1} probably not at-sea accuracy; depth accuracy probably comparable to XBT (~5%). Little or no comparisons made in field with other sound speed instrumentation
XCTD (still experimental as of FY93)	T and C vs z; hence T and S vs z, yielding SS vs z	Expendable, deployed under way; relatively simple acquisition system; costs ~$300	Depth extent ~1000 m; not as accurate as CTD; manufacturer's claimed accuracies 0.03°C (T) and 0.03 mS/cm (C): achievable accuracies not yet known

XCP	Baroclinic currents vs z	Expendable, deployed under way; requires special acquisition and processing unit; rel. expensive (~$900);	Max. depth 1500 m; gives instantaneous current snapshot incorporating all sorts of processes and may not be representative of longer term conditions; current accuracy probably several cm s^{-1}, depth accuracy probably comparable to XBT (5%); <90% reliability
CTD	T and C vs z; hence T and S vs z, yielding SS vs z	Ship must be stationary; deep cast takes several hours; requires specialized equipment, personnel, calibration; most models expensive to purchase	If treated properly, highly accurate and can go from surface to bottom. T accuracy ~0.005°C, S ~0.01 psu, z ~1 m
STD	T and S vs z, yielding SS vs z	Same limitations as CTD	No longer made: was essentially a CTD that computed S internally from C and T. Computers now do that calculation external to the unit itself.
Sound velocimeter	SS vs z	Deployed from stationary ship in same fashion as CTD; cost comparable to low-end CTD ($7500-$4000)	If calibrated properly, highly accurate and can go from surface to bottom. Manufacturer's claimed SS accuracy 0.15 m s^{-1}, z accuracy 0.01%.
Acoustic Doppler Current Profiler (ADCP)	Horizontal currents vs z (real time continuous display)	Must be mounted on ship in well; takes trained personnel; expensive (~$50-100k) Mooring deployed and bottom mounted units also available	Max depth ~300 m (deeper are under design); gives currents in depth bins; accuracy 1 cm s^{-1} or better
Current Meter	Horizontal currents at fixed z (many units have T and C sensors as well)	Deployed at discrete depths on a mooring; require specialized handling; expensive to purchase	Give highly accurate time series; usually data available after mooring recovery although telemetry, etc, can be done

XMOOR (under development)	Expendable oceanographic mooring: sensors depend upon configuration but examples are SST, air temperature, baro pressure, T and C vs z at discrete depths, horizontal currents at fixed z, ambient noise	Cost effective enough to be considered expendable	Parameter accuracies will be at least as good as with expendable instruments and probably better. First tests planned for FY93.
Aircraft:			
AXBT	T vs z	Expendable, deployed from specialized ACFT with specialized equipment; cost $175-250	Accuracies comparable to XBT (Navy standard 0.56°C in T, 5% in z: can be improved with calibration to ~0.2°C in T, 2% in z); can provide near synoptic coverage of large areas; depth ~800 m but deeper depth being developed; closer spacing than ~10 nmi requires clever flight planning
AXSV	SS vs z	Expendable, deployed from specialized ACFT with specialized equipment; cost ~$600	Maximum depth 850 m; accuracies probably comparable to XSV (manufacturer claims 0.25 m s^{-1} in SS and 5% in z) but very little if any work done on field comparison with other sound speed instrumentation; because of ACFT speed, sampling closer than ~10 nmi requires spedial effort
AXCP	Baroclinic currents vs z	Air-launched version of ship-deployed XCP	Same as XCP; same problems with close sampling as with AXBT or AXSV
AXCTD (not available as of 1993 but will be at some point)	T and C vs z, giving T and S vs z from which SS vs z may be computed	Planned to be same probe as shipboard, just ACFT deployed. Will require specialized acquisition instrumentation	

Drifting buoys (sonobuoy sized, also called A-sized)	Various model configurations, but can obtain SST, air temperature, baro pressure, T vs z at discrete depths, ambient noise	Deployed from ACFT (incl. operational P-3) or ship. Data transmitted via satellite every hour or so, and thus in almost real time. Buoy lifetimes > 1 mo; costs ~$2-5K each, depending upon model. Various models have various sensor suites.	Meteorological units and units with 300 m and 600 m thermistor tails and ambient noise hydrophones in existence, other sensors being considered
XMOOR (under development)	Same as ship deployed version	Air-deployed version. All but very simple instrumentation suites are deployed from bomb bay or external pod	First tests of air deployed version planned for FY94

vary too much with location), a set of temperature versus depth measurements yields an estimate of the sound speed profile good enough for many purposes. An estimated salinity value is obtained using a mean value characteristic of the region or from the T-S (temperature-salinity) correlation curves which are quite stable, particularly at depth, in many parts of the world ocean. Below about 1000 to 1500 m (the exact depth depends upon geographical region), the vertical temperature and salinity gradients become very small and pressure becomes a dominant effect on the sound speed, although deep ocean sound speed variability of up to 0.5 m s^{-1} can exist.

The classical method of making high accuracy shipboard observations of sound speed is to take CTD or STD measurements and calculate sound speed. Such measurements have the advantage of being highly accurate and covering the full range of ocean depths. Their major disadvantage, however, is that they are time consuming (at a typical lowering rate of 1 m per second, a 5000 m cast takes nearly 3 hr) and non-synoptic (long time between horizontal samples, since oceanographic vessels rarely travel at much more than 10 kt). To overcome this problem, techniques were developed to rapidly sample temperature versus depth using free falling sensors (expendable bathythermographs, or XBTs). These shipboard techniques traded off accuracy and depth of observation for improvements in synopticity (measurements could be taken while underway) and cost. Expendable techniques gradually evolved to include measurements other than temperature (conductivity, direct sound speed, etc.) and eventually became deployable from aircraft, vastly improving the aerial coverage and synopticity.

2.2 CLIMATOLOGIES AND DATABASES

Climatologies are atlases of oceanic parameters (for example, temperature and salinity) derived from archived databases whose data have in some fashion been processed or averaged to yield values at various standard depths and on a uniform grid in latitude and longitude. The two most commonly used climatologies for the determination of sound speed both spatially and temporally are the Levitus Climatology (Levitus 1982) and the Generalized Digital Environmental Model (GDEM) (Davis et al. 1986 and Teague et al. 1990).

Levitus (1982) published the first world-wide climatology, the Climatological Atlas of the World Ocean. This "Levitus climatology" contains temperature, salinity, and dissolved oxygen data analyzed at up to 33 standard depth levels on a one-degree latitude/longitude grid between the surface and ocean bottom (maximum depth of 5500 m). Depth spacing is closer together in the upper regions of the water column. Both annual and seasonal analyses were produced. The data used in the analysis were from the National Oceanographic Data Center (NODC) and included all XBT and Mechanical BT data available as of the first quarter of 1977 and all ocean station data as of the first quarter of 1978. A Successive Correction Method (SCM) objective analysis technique was used to calculate the gridded values. The Levitus climatology is the most widely available and the most frequently used database of its kind, especially by academic and non-US Navy

researchers.

In his 1982 report on the climatology, Levitus discussed several caveats to consider in using the database which are relevant for all climatologies. Because many regions contain little data, all data that is available must be used in the analysis. As a consequence, data in a particular one-degree square may not be well distributed in time, and the analyzed value may not be particularly representative of the true long term climatological value. Adjacent boxes may contain data from very different sets of years, and the analyzed values may be quite different from each other even if the true climatological means are similar. Second, a climatology can only describe large-scale, quasi-permanent ocean features; it cannot describe mesoscale and smaller features with any reliability because of their temporal and spatial variability. Events such as the variability of the position of the Kuroshio Current or the El Nino phenomenon cannot be well-depicted, nor can eddies and frontal meanders. The impact of internal waves can not be included. And finally, biases may be exist because certain anomalous areas (such as warm and cold eddies) may be overly represented in the archives.

A second commonly used climatology, especially by US Navy researchers and contractors is GDEM: the Generalized Digital Environmental Model. GDEM was developed at the US Naval Oceanographic Office (NAVOCEANO) using the 1986 version of the Master Oceanographic Observations Set (MOODS) and other data available at NAVOCEANO to generate on a one-half degree latitude-longitude grid and at standard depth levels a set of analyzed temperature and salinity values on seasonal and annual time scales. Coefficients describing sea surface temperature are available on a monthly time scale to allow modification of the near-surface values of the climatology to more accurately represent monthly variations. The depth grid has up to 36 standard depths, with closest spacing near the surface and progressively wider spacing at greater depths.

As obtained from NAVOCEANO, GDEM consists of sets of stored coefficients that are used in expanding functional forms over several depth regimes. The squared amplitude response of a Butterworth filter with an exponential tail is used to fit temperature in the upper 400 m. An orthogonal Gram polynomial is used to model temperature and salinity between 200 to 2450 m and salinity between 0 to 400 m. From 2000 m to the bottom a quadratic is used for both temperature and salinity. RMS errors in the depth ranges are given in Table 2-2 (from Davis et al. 1986).

Table 2-2. Approximate GDEM RMS errors

Depth Range	Parameter
0 - 400 m	Temperature: 0.5°C Salinity: 0.1 ppt (Effective sound speed error ~2.5 m s^{-1})

400 - 2450 m	Temperature: 0.25°C Salinity: 0.05 ppt (Effective sound speed error ~1.3 m s^{-1})
2000 m - bottom	Temperature: 0.25°C Salinity: 0.05 ppt (Effective sound speed error ~1.3 m s^{-1}

More information on GDEM and the merging of values in the overlapping depth ranges is given in Davis et al. (1986) and Teague et al. (1990).

Higher resolution versions of GDEM have been constructed for selected areas of high Navy interest and are on 10-minute by 10-minute grids or finer. Another approach used in regions where multiple water masses abut one another has been to develop GDEMs for the particular water masses in the area and to have a rule whereby the user may determine which GDEM to use at a particular point (for example, from satellite data). More information is available in Teague et al. (1990). GDEM is not widely available to the general public and is generally restricted to use within the US Navy. It is, however, used in many numerical models being developed with US Navy support to determine the temperature, salinity, and sound speed character of an ocean area.

Teague et al. (1990) compared dynamic height fields computed from both climatologies. Results were mixed. Like Levitus, GDEM appeared to give a good representation of larger-scale ocean features. They preferred GDEM over Levitus when investigating seasonal variability and in frontal areas because of its one-half rather than one-degree grid spacing. They pointed out, however, that other sorts of comparisons are needed before more definitive conclusions may be drawn. Our experience with GDEM versus Levitus has tended to favor Levitus for the estimation of regional sound speed profiles, as is discussed later in the section on HGI Measurement Programs.

A third widely-used physical oceanographic database is the National Oceanographic Data Center (NODC) master data files. These archives include data collected by federal, state, and local government agencies; universities and research institutions; private industry; and data of foreign origin acquired through bilateral exchange with other countries. Data are stored in two formats, one by NODC cruise number, the other by geographic location (referred to as the "geofile"). The geofile contains data sorted by a geographic gridded numbering system, each consisting of a 10 degree square area. All data are subject to a variety of NODC quality control procedures that include subjective review of the data set, running the data through a suite of error-checking programs, and comparisons with environmental model results to determine whether the data fall within an acceptable climatic range.

The types of measured temperature and salinity data available from the NODC master files include: low depth resolution Oceanographic Station (OS) data, high resolution conductivity-temperature-depth/salinity-temperature-depth (CTD/STD) data, and low resolution CTD/STD data. (For a description of the contents of these files, refer to the NODC Users

Guide, U.S. Department of Commerce 1992.) The OS data consist of data from mostly Nansen casts and other water samples, with some more recent CTD/STD data included. The high resolution CTD/STD data files are archived as provided by the originator, and may have been subject to averaging, filtering or interpolation. Low resolution CTD/STD data files were derived from the high-resolution CTD/STD files by picking off data values at up to 106 user-specified depths. The temperature/salinity data files represent data collected at specific locations, with no attempt to interpolate spatially or temporally (with the exception that a data request can be made to obtain data at NODC standard depths, obtained using a three-point Lagrangian interpolation). The amount of data contained in any specified geofile is variable and can produce spatial and temporal biases. Data can be obtained for any 10-degree latitude/longitude square or combination of squares by contacting the User Services Branch of NODC's Information Services Division in Washington, DC. A data request can also include calculated values of sound speed (using Wilson's equation), density, and dynamic height anomaly, if specified at the time of request. Output can consist of data listings, CD-ROM (for some areas) or other products, but are more commonly available on magnetic tape and floppy disk (for smaller requests).

A fourth archived database used primarily by the US Navy is the updated version of the MOODS database itself (Jugan and Beresford 1991), containing both unclassified and classified data. The database contains random data points which can be extracted from within a four corner latitude/longitude box. Data included in MOODS are obtained through NODC, academic institutions, NAVOCEANO survey data, and other sources that can be verified. The data are edited for a variety of errors and are checked against the Levitus climatology (a four standard deviation envelope is allowed). However, the data extracted from any one particular latitude-longitude box varies in quantity and quality depending upon how frequently and with what techniques the region of interest has been sampled. Such an archive allows the examination of individual profiles and hence can give an estimate of the variability to be expected in local sound speed profiles.

2.3 MEASUREMENT ERRORS

Any set of hydrographic observations will have a certain variability associated with it, a set of statistics. At a minimum these statistics are the mean and the variance. The variance has two components: signal variance and noise variance. The signal variance is associated with variability occurring on scales resolved by the spatial and temporal sampling scheme. The noise variance is often termed "measurement errors." Daley (1991) classifies these measurement errors into two types:

Natural error:	instrument error
	error of representativeness
Gross error:	improperly calibrated instruments
	incorrect reading of observations
	incorrect coding of observations
	telecommunication errors

These errors may be either uncorrelated or spatially or temporally correlated with each other.

Careful quality control will often eliminate gross errors, but not in every case. For example, the calibration of satellite-based instruments can often drift. Boyd (1987) and Boyd and Linzell (1993a and b) and others have shown the presence of systematic errors in the fall rate equations of expendable probes such as the XBT and AXBT. A CTD system on board a ship for a number of months or subjected to some shock such as hitting bottom or hitting the side of the ship upon deployment or recovery may have its calibration drift.

Gross errors are distinguished from instrumental errors in that, in principal, gross errors may be eliminated by proper calibration. Instrumental errors are errors inherent in the accuracy and resolution of the instrument itself. In practice, however, the distinction between the two becomes somewhat blurred. Boyd and Linzell (1993a) have shown, for example, that the effective accuracy of population calibrated T-5 XBTs is about 0.15°C. Taken as a population, XBTs, then, have an instrumental error of 0.15°C, but viewed as individual instruments which could be individually calibrated, this value is a gross error which might be reduced by as much as an order of magnitude by individual instrument calibration, leaving a much smaller residual instrument error.

White and Bernstein (1979) were among the first to point out that, if obvious gross errors are eliminated, both types of instrumental error can be shown to be negligible compared to the second type of "natural error," the error of representativeness or, as it is often called, the geophysical error. Geophysical error is the unresolved variability originating in time and space scales smaller than those resolved by the sampling. Geophysical spectra are typically "red," that is, they fall off rapidly with frequency or wave number. Fig. 2-1 (from Daley 1991) illustrates this for the atmosphere, but much the same holds true for the ocean, although observational difficulties have meant that the spectral structure is less well understood than in the atmosphere. Panel 1 shows the wavenumber (spatial) spectrum and panel 2 a frequency (temporal) spectrum. By far more energy exists at longer space and time scales, but energy does exist at all scales. Panel 3, a two dimensional space-time spectrum, indicates that longer space scales are associated with longer time scales, and conversely.

Phenomena with scales less than about twice the sampling frequency (the "Nyquist criterion") will be poorly represented by the sampling and variance at these smaller scales will show up as variance at longer scales (aliasing). The error of representativeness or the geophysical error is that error introduced by the misrepresentation of all scales smaller than that resolved by the sampling. Since internal waves dominate the ocean variability spectrum from a few cycles per hour (the Brunt Vaisala or buoyancy frequency) to approximately a cycle per day (the inertial frequency), for scales smaller than those resolved by the sampling grid used in the High Gain experiments (25 km to 150 km and several hours to several days), common wisdom attributes perhaps half of the cause of this geophysical error to the effects of internal waves. Fortunately, because geophysical spectra are red, the aliasing error usually only reduces the accuracy of measurements and does not obscure the phenomena being investigated.

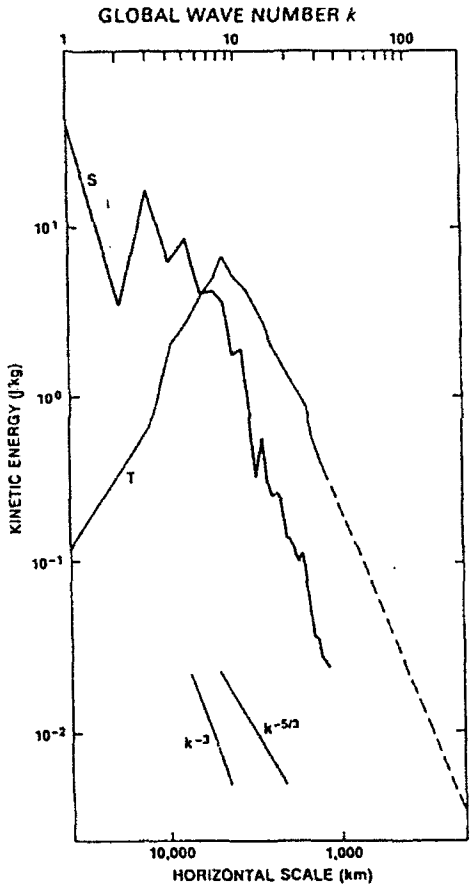

Spatial spectrum of atmospheric kinetic energy. (Curves S and T are from Boer and Shepherd, *J. Atmos. Sci.* 40: 164, 1983. The American Meteorological Society, with dashed portion of T curve inferred from Brown and Robinson, *J. Atmos. Sci.* 36: 270, 1979. The American Meteorological Society.)

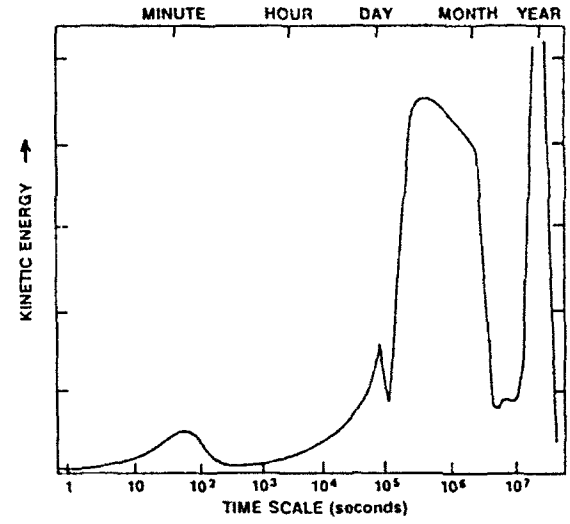

Temporal spectrum of atmospheric kinetic energy. (After Vinnichenko 1970)

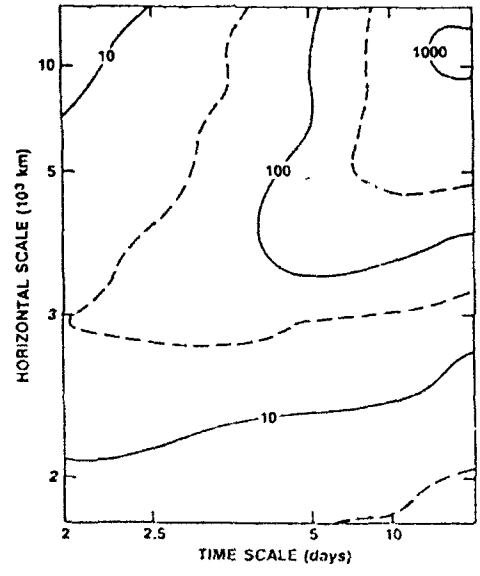

Space/time spectrum of atmospheric variance. (From Pratt, *J. Atmos. Sci.* 36: 1681, 1979. The American Meteorological Society.)

Figure 2-1. Atmospheric space, time, and combined space-time spectra. More energy is at the longer space and time scales, although energy exists at all scales. Longer space scales are associated with longer time scales, and conversely. Oceanic spectra are qualitatively similar. (From Daley, 1991.)

2.4 SATELLITE REMOTE SENSING

A surveillance system based on High Gain technology depends upon accurate knowledge of the sound speed field in the search volume. However, direct measurement of the sound speed field is impractical on a continuous basis. New developments in satellite remote sensing, while not able at the present time to provide highly accurate volumetric sound speed fields, may be the basis for practical large area continuous monitoring of the sound speed field. Remote sensing data will undoubtedly provide major data input to future operational oceanographic analysis and prediction systems described in section 2.6.

Satellite remote sensors currently available to the US Navy community measure only the surface features of the ocean. Infrared (IR) imagery detects the thermal signal of the upper few millimeters of the ocean surface, while the microwave altimeter senses the distance between the satellite and the ocean surface to give the sea surface topography. Methods have been developed to extend that information with depth to provide the subsurface thermal field. Sound speed fields can then be derived from the temperature, salinity, and depth field generated from the surface data. Future research will undoubtedly develop techniques which are significant improvements over what is currently possible.

Three primary methods of inferring the subsurface structure of the ocean are currently being used. The first is to directly infer the thermal structure of the water column through the creation of "synthetic bathythermographs" or "synthetic BTs" or "synthetic STDs." Khedouri et al. (1983) and Kao (1987) demonstrated that the subsurface temperature and density structure in the Gulf Stream region could be derived from sea surface heights calculated from satellite altimeter measurements. Carnes et al. (1990) used the relationship between the sea surface height (actually the dynamic height[1] at the surface relative to the 1000 dbar level) and subsurface temperature provided by regressing the dynamic height and the amplitudes of EOFs of the vertical temperature structure derived by deWitt (1987) for the Gulf Stream and Kuroshio regions. Monthly EOFs of vertical temperature structure were computed using a third order polynomial. The EOFs extended only to 1000 meters because of the lack of information below that depth. The rms differences between observed and estimated temperature profiles were from 0.6° to about 1.8°C, yielding an rms sound speed error of around 3 - 9 m s^{-1}. In highly dynamic areas such as the Gulf Stream, this is often an improvement over what a climatology could give.

The second method for determining the subsurface structure of the ocean is through the use of front and eddy maps of the surface features of the ocean, constructed from infrared imagery, altimetry, and in situ data. From this map the principal water masses in the area are identified at each location of interest and some algorithm is used to assign a canonical profile to that location. One approach is to assign a certain climatological profile to each point based upon the water mass analysis. In a more complex approach, Bennett et al.

---

[1]dynamic height is a measure of the height of the water column above a reference level due to the differential density distribution in the ocean, which, in turn, is intimately related to a major component of the oceanic circulation, the geostrophic flow.

(1989) in the Gulf Stream region assumed a certain thermal structure for the center of the Gulf Stream. Planes orthogonal to the Stream were constructed and temperatures were assigned to points away from the Stream based on depth and distance from the midpoint. A linear gradient was assumed across the width of the core of the stream. Water mass EOFs have also been used to generate profiles at desired locations, with the front and eddy map determination of water mass specifying which set of EOFs to use (Cummings and Ignazewski 1991). Amplitudes of the expansion coefficients of the vertical EOFs were computed using multiple regression equations involving sea surface temperature, location, and time.

Another approach for inferring subsurface structure is through the use of feature models. A feature model is a diagnostic model of an ocean feature that describes its typical three-dimensional structure. Given the surface manifestation -- from a front and eddy map, for example -- the feature model provides a way of projecting the structure below the surface. As an example, a frontal feature model might describe the typical width, slope with depth, and temperature gradient across the front. This technique is used in the Optimal Thermal Interpolation System (OTIS 3.0), discussed further in the section on Numerical Modeling and Operational Products. Bennett et al. (1992) discuss a feature model of the Iceland Faeroe Front in which up to three segments are used to describe the subsurface shape of the front from where it intersects the bottom to its surface manifestation. How many segments are used and what their vertical slopes are depend upon the water depth and the position of the surface point relative to the bottom path. A profile at a desired analysis point is constructed by blending the two relevant water mass climatologies according to weights which depend on the lateral and vertical distance of the analysis point to the front.

2.5 ACOUSTIC TOMOGRAPHY

Satellite information can provide good two-dimensional resolution of ocean surface features, but the extrapolation of this information to depth is not trivial. One technique which has shown promise for the determination of the full three-dimensional (four, if time is considered) oceanic sound speed field on scales from about 100 km to 1,000 km (the mesoscale) is acoustic tomography, first proposed by Munk and Wunsch (1979). Basically, the travel times of sound waves along many different paths within the volume are measured periodically and the best estimate of the sound speed and current field that could cause such travel times is computed. A tomographic array consists of a number of acoustic sources and receivers which span an ocean volume of interest which is typically from 300 - 1000 km across (Fig. 2-2a). Acoustic pulses are emitted every few minutes at a frequency of about 250 Hz and the sound travel times (about 11 minutes for 1000 km) are measured between each transmitter/receiver pair (Fig. 2-2b). The travel times are affected not only by the properties of the water through which the sound travels, but also by the currents within the volume. Currents travelling with the sound will reduce travel times, and those travelling against it will increase travel times.

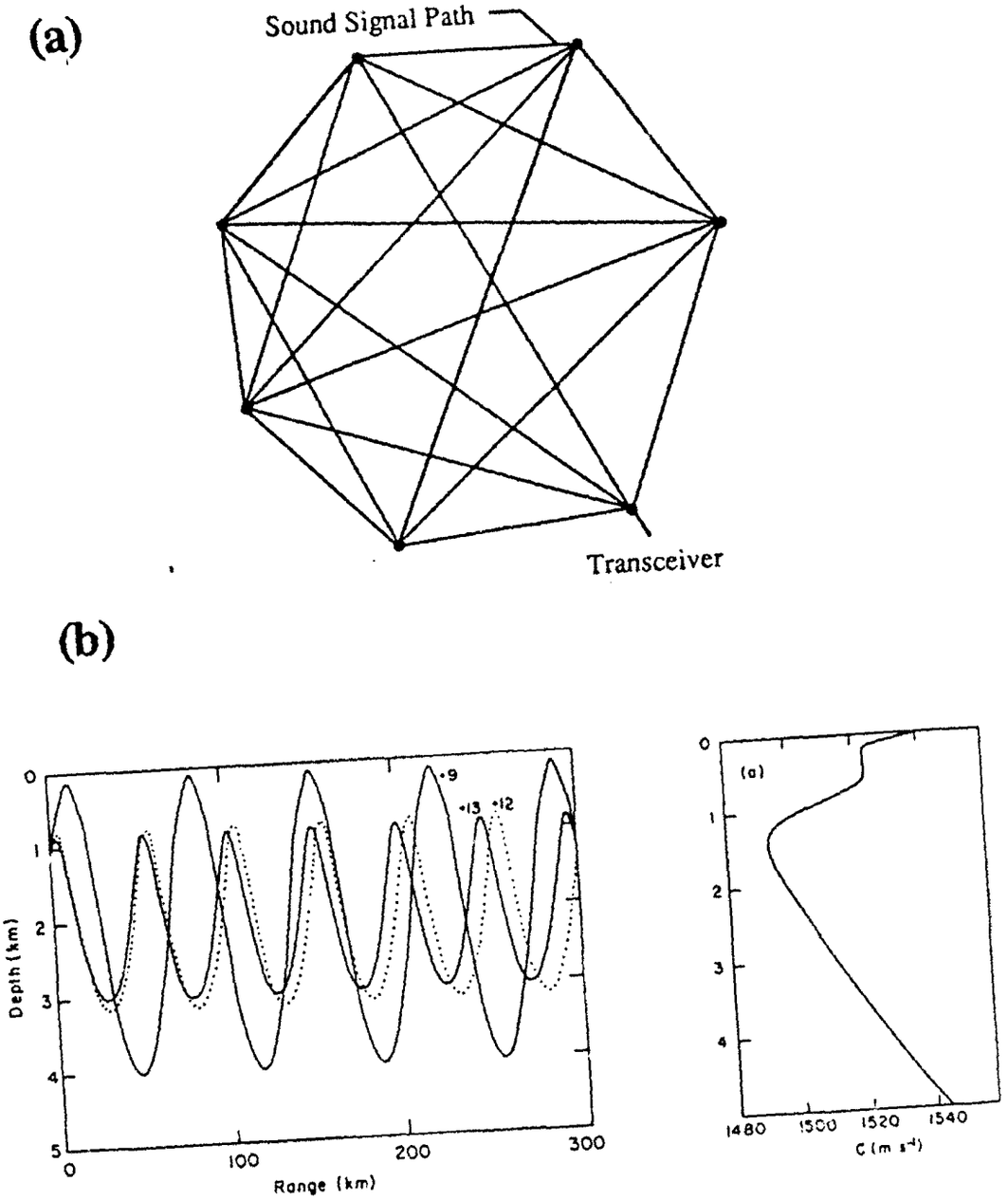

Figure 2-2. (a) Horizontal view of a possible tomographic array, showing the multiple transmission paths. (Redrawn from Spindel and Worcester 1990) (b) Example of the paths taken by three rays which were identified during a 1983 tomography experiment. Each ray leaves the source at the same time, but because of the different path each ray takes, they arrive at the receiver at different times. The mean sound speed profile is shown to the right of the ray paths. (From Stoughton et al. 1986)

Operation of a tomographic system begins with the initialization of the array. A reasonable approximation of the sound speed field and the current velocity field is required at the initial moment of operation to identify the acoustic paths that connect the sources and receivers. Thereafter, as these paths change with time, they can be traced by the system. A climatology such as Levitus is often used for the initialization. Frequently the current field is neglected, since typical oceanic currents have speeds 10^{-3} that of the sound speed in water.

The mathematical problem of determining the sound speed and current fields, given their effect on travel times, is made tractable by the process of assuming an initialization field and subsequent tracking of anomalies. The ocean variables to be estimated (e.g., sound speed and currents) are unknown functions of position. The travel time data can be expressed as summations of the effects of the variables over the various paths that cross the volume; that is, they are expressed as path integrals of the unknown functions of position. Thus, the travel time data contain information concerning the unknown functions, but this information is not directly related to the values of those functions at any particular point. This information is incomplete, however, because the acoustic paths do not sample all points within the volume. The mathematical problem is, therefore, one of forming the best possible estimate of the unknown functions from incomplete and indirect information concerning them. The solutions are found by applying perturbative inverse techniques to the travel time anomalies and to the travel time differences between reciprocal transmission paths to optimally reconstruct the four-dimensional sound speed and flow fields, respectively.

Because of the potential utility of using acoustic tomography to determine the volumetric sound speed field for a High Gain-type system, tomographic experiments were conducted during the three major High Gain field efforts in 1987, 1989, and 1991. Brief comparisons of the tomographic and directly measured sound speed fields are given later in this document.

2.6 NUMERICAL OCEAN MODELING AND OPERATIONAL PRODUCTS

Any future operational High Gain-type system would undoubtedly have to rely largely upon operational products for the sound speed field in its search region rather than upon dedicated measurements, although the field might perhaps be enhanced with additional measurements made in specific critical regions. Both the Naval Oceanographic Office (NAVOCEANO) at the Stennis Space Center in Mississippi and the Fleet Numerical Oceanography Center (FLENUMOCEANCEN, also referred to as FNOC) in Monterey, California, are tasked to provide "global and regional meteorological and oceanographic analyses and forecasts" in support of U.S. Naval and other Department of Defense operations, as well as for authorized civilian users of the products. Using conventional and satellite-derived data gathered world-wide, the centers sort, edit, and analyze the present atmospheric and oceanic conditions. FNOC, for example, currently ingests and processes in near real time ~237,000 world-wide observations each day (Fig. 2-3). An overview of

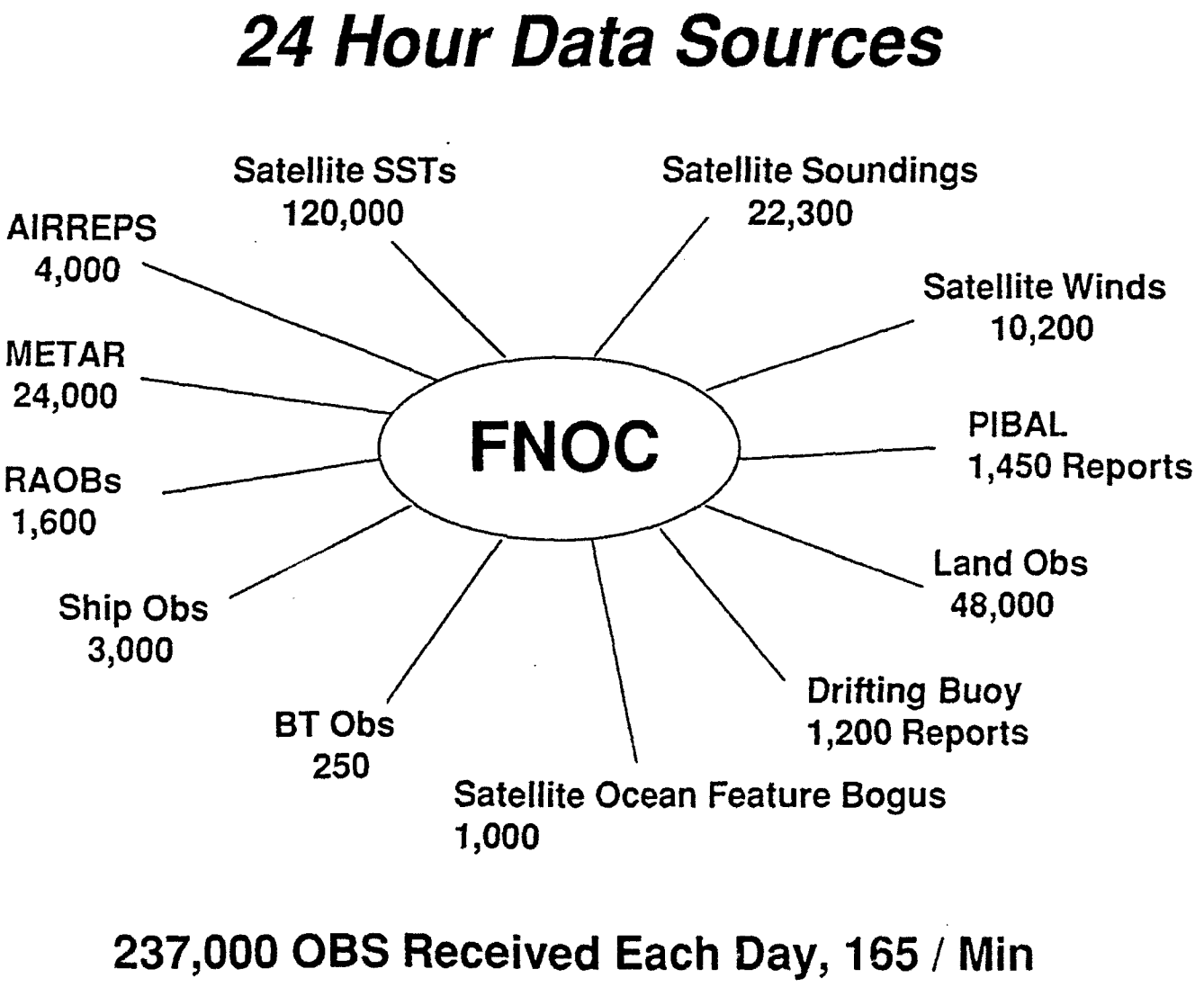

Figure 2-3. Example of the data received daily at the Fleet Numerical Oceanography Center.

the analysis and prediction systems at FNOC is found in Nelson and Aldinger (1992), Clancy and Sadler (1992) and other articles in that issue. From the analyses, numerical models are used to predict the future state of the atmosphere and of the ocean. Other models use these analyses and predictions to generate atmospheric, oceanographic, and acoustic products tailored to the specific needs of naval weapon and sensor systems and platforms. In addition, the environmental analyses and forecasts are transmitted to other naval activities world-wide for use as guidance when responding to direct fleet operational requirements. The ability of these centers to nowcast and predict sound speed over the full water column and on a global basis will be improved in the future as a result of products under development by the Navy Ocean Modeling and Prediction (NOMP) program of the Office of Naval Research.

The Fleet Numerical Oceanography Center is responsible for global scale and open-ocean regional scale oceanographic products. The global ocean thermal structure in near-real-time is generated by the OTIS/TOPS system at FNOC. The most sophisticated version (3.0) is currently only used on a regional basis. OTIS 3.0 functions in a analysis-prediction-analysis cycle, with TOPS providing the prediction, via an optimum interpolation (OI) technique. In contrast to earlier versions, it uses OI decorrelation scales keyed to individual water masses, and relies heavily on water-mass climatologies, synthetic salinity-temperature-depth (STD) algorithms and ocean feature models to map the three-dimensional temperature and salinity (and hence sound speed) of fronts and eddies. Fronts and eddies are initially identified primarily by a subjective analysis of satellite IR imagery to produce an "ocean bogus" that is input to OTIS.

TOPS is a synoptic mixed-layer model consisting of conservation equations for temperature, salinity, and momentum covering the top 400 meters of the ocean. OTIS provides the initial conditions and the geostrophic component of currents to TOPS, which provides a prediction for the upper ocean based on surface forcing from the Navy's atmospheric prediction models. This prediction is then in turn used in the next day's OTIS analysis and tends to control the vertical temperature profile shape immediately below the sea surface.

At present TOPS uses geostrophic currents from OTIS, and fronts and eddies are identified subjectively and over a limited set of regions. There are plans for a global "fronts and eddies" nowcast and prediction system, termed OCEANS, to be implemented in phases over the next three to four years. This will be based on ocean circulation models with six "Lagrangian" layers in the vertical and with 1/8th degree horizontal resolution, sufficient for eddies larger than about 100 km across in mid-latitudes. Lagrangian layers in the vertical are a very efficient way to represent the ocean, since the layers can be associated with water masses and thus often will be natural inflection points for the sound speed structure. The resulting sound speed profiles will be more accurate estimates than would result from interpolation between six fixed depth points. OCEANS will be coupled to OTIS, or a replacement analysis scheme, which will extract full temperature and salinity profiles from OCEANS and any other available data sources. The initial system is scheduled to be delivered to FLENUMOCEANCEN by the Naval Research Laboratory at the end of FY93 and will include 1/8th degree models of the North Pacific and North Atlantic (north of 20°

S) and a 1/4 degree reduced gravity global model (Hurlburt et al. 1992; Thompson et al. 1992). Initially, observational data coming into FLENUMOCEANCEN will only be automatically assimilated into the system in western boundary current regions (in particular, the Gulf Stream and Kuroshio Extension), and subjective front and eddy maps based on IR satellite images will still be required. In these western boundary current regions OCEANS will generate nowcasts and predictions of fronts and eddies. Elsewhere the initial version of the system will only account for oceanic phenomena characterized by slow (weeks to months), direct, and integrated response to atmospheric forcing. This includes the El Nino phenomenon and much of the tropical ocean circulation and also the large scale interannual variations in mid-latitude gyres.

The full OCEANS system is due on line by the end of FY95. It will provide global coverage (72° S to 72° N) at 1/8th degree resolution and will assimilate data globally, and eventually may be able to replace the subjective fronts and eddies maps. The primary sources of data will be satellites, particularly satellite altimetry, but other sources of real time and near-real time data, including acoustic travel times from tomographic arrays, will also be assimilated. As a nowcasting system, the primary advantage of OTIS/TOPS/OCEANS is that OCEANS will fill in the spatial and temporal gaps in the primary data sources (a satellite altimeter, for example, takes 10 to 35 days to give full global coverage), and can provide a better picture of subsurface structure than OTIS's synthetic STDs can do alone. In addition, predictions from OCEANS may show skill (significant predictive capability) for a month or more. This skill will be translatable to improved sound speed fields, providing detailed knowledge of the very upper ocean, where the mixed-layer dominates, is not required. The mixed layer is directly driven by atmospheric forcing, and shares the two to five day time scale of atmospheric prediction.

Significant Navy predictive capability in coastal regions and semi-enclosed seas is only now beginning to be developed. The Naval Oceanographic Office (NAVOCEANO) has the responsibility for developing real-time operational analyses and forecasts in nearshore regions and semi-enclosed seas. NAVOCEANO presently has operational numerical models for the Persian Gulf and the Red Sea (Horton et al. 1992). These have about 7 km and 14 km horizontal resolution, respectively, with 15 to 20 levels in the vertical, using sigma-coordinates (terrain following vertical levels). The application of the same ocean model to other shallow semi-enclosed seas of high Navy interest should be relatively straight forward. The need for updating with observational data is assumed to be less in these cases, since shallow seas are dominated by atmospheric forcing.

The OCEANS system at FNOC will include the majority of deep marginal seas; e.g., the Sea of Japan, South China Sea, and the Mediterranean. However, a limitation of OCEANS is that it only includes areas deeper than 200 m, effectively eliminating many shallow marginal seas such as the Yellow Sea. In addition, ice cover can be a factor in shallow seas at high latitudes, and the effect of ice is not included in OCEANS. Several research and development projects are underway with the goal of providing greater capability than OCEANS for selected marginal seas. These will be targeted at regions of high Navy interest, for example, the Yellow Sea, the Okhotsk Sea, and the Mediterranean Sea, and,

when operational, will be run at the Naval Oceanographic Office. Several modeling approaches are being tried: 1/16th degree layered models, sigma-coordinate models, and others. The proper approach or approaches have not yet emerged, but the goal is to have a capability in the mid to late 90's that augments OCEANS for selected marginal seas.

At present, the adequacy of current numerical models or of operational products to supply sound speed fields for matched field processing has not been formally or quantitatively evaluated. If an accuracy requirement of 1 or 2 m s^{-1} is required, it is unlikely that present models or products would be able to adequately describe conditions in the upper several hundred meters of the ocean or where strong features such as fronts or eddies exist. In a simple minded test, this could be investigated by comparing a modeled sound speed field with a measured field (say by subtracting the two) and evaluating how closely the modeled field matches the measured field. A test involving more effort and requiring the availability of suitable acoustic data would be to make a suite of matched field processing runs on both a modeled field and a measured field and compare the signal gain degradation. A series of such tests in selected areas would constitute a first step at determining the adequacy of numerical models and operational products for matched field processing purposes, and would build an experience base for directing model and product upgrades.

A more appropriate' evaluation of the required accuracy of sound speed fields requires feedback from matched field processing on the HGI tests (SVLA, VAST, and MDA) that have already taken place. Little more can be said about the adequacy of various types of sound speed fields for matched field processing until its success on the already measured sound speed fields is evaluated. Since MDA (and to a lesser extent VAST) sound speed field determinations represent a state-of-the-art measurement achievement, it would not be prudent to improve on this achievement until matched field processing requirements are more carefully quantified.

2.7 COMBINATIONS OF MEASUREMENTS

In practice, combinations of techniques are required to provide adequate estimates of the sound speed field. When wide-area or rapid horizontal coverage is required, emphasis is on airborne measurements. When smaller area coverage or high precision data is required, shipboard instrumentation is typically used. Expendable instrumentation allows more rapid sampling but sacrifices accuracy and depth extent. There is no one best suite of instrumentation, and combining measurements to give suitable sound speed fields of the highest possible accuracy is as much an art as a science.

One issue that usually arises when measurements of the sound speed field are made is that full surface to bottom sound speed fields are needed but the measurements are not to the bottom. This is often the case when expendable probes (e.g., XBTs, AXBTs) are used, but can also be the case with instruments which have full depth capability but for which insufficient time is available for such deep measurements. The usual solution is to append in some smooth fashion to the shallow profile another suitable profile. This suitable profile

might be a climatological profile from GDEM or Levitus, it might be the closest deep CTD cast made during the experiment, it might be the average of some archived data, or it might be a synthetic profile constructed using EOFs. Almost as many approaches exist as there are researchers, but appending a climatology is a common solution. One approach used by Boyd et al. (1992a) was to use a least squares approach to estimate the EOF expansion coefficients from a shallow profile, then reconstruct the full depth profile and append the reconstructed profile onto the bottom of the shallow profile. Where a stable set of EOFs exist, this can be a very good solution.

A common technique for appending is to compute the difference between the profile to be appended and the deepest measured value and to decay this difference exponentially over some depth scale which is typically a few hundred meters. The profile below the maximum measurement depth then becomes the appending profile minus the decayed difference. Much below the scale depth the result approaches the appending profile.

Once a set of profiles to a suitable depth exist, the question arises how to combine them into suitable two dimensional cross sections or three dimensional fields. This is an area of active research and there is no one best answer. A sample of often used techniques is discussed in the following paragraphs.

To create interpolated two dimensional fields, one can simply fit some sort of curve at each desired depth to the sound speed field and interpolate to the desired linear grid. The interpolation could be over the whole range or piecewise over several nearby measurements. The approach, however, does not always preserve features such as the mixed layer of sound channels. To avoid this problem, another approach is to describe each profile as a piecewise linear function of depth, with each vertex corresponding to some important defining point on the curve that can be identified on each profile. The depths at which these vertices are located is then interpolated (usually linearly) in range, allowing a new piecewise linear profile to be constructed at any point. This technique has the problem of being hard to automate in most cases.

Various two-dimensional function fitting approaches can also be used. This technique assumes that the field can be expanded in terms of a set of basis functions and their coefficients, and the interpolation becomes the problem of calculating the unknown expansion coefficients and evaluating them at the desired range and depth points. Daley (1991) discusses some of the caveats in this approach, although from a horizontal surface fitting rather than a vertical surface fitting perspective. Many suitable computer programs exist for this type of surface fitting.

A widely used technique for two dimensional surface fitting is known as statistical interpolation. Statistical interpolation assumes knowledge of a background field, which is often climatology or numerical model output, and the calculations are performed upon observed anomalies, which are the differences between the observations and the background field. The interpolated value at any desired point is computed as the background field plus the weighted sum of all the observed anomalies. The statistical interpolation technique

allows calculation of the optimum weights such that the resulting analysis error is minimized in a least squares sense. The basic problem with the technique is that it requires knowledge of statistical parameters which often is very hard to come by. Required are the statistics describing the resolvable and unresolvable variability and the instrument error characteristics, plus the space-time autocorrelation function. In addition, statistical homogeneity is assumed. However, variants of statistical interpolation are widely used in meteorology and oceanography, and the results are fairly robust to variations in the statistical parameters. Daley (1991) discusses the procedures at length.

Estimation of three dimensional volumetric sound speed fields is more difficult than estimation of two dimensional transects. One approach is to perform multiple transect calculations to build up a set of two dimensional fields. A similar approach is to calculate multiple horizontal fields at a variety of depths. Such techniques can have the shortcoming that information from the third dimension is not included in the calculations, but in principal this objection could be eliminated with a statistical interpolation scheme. However, while the adequacy of two dimensional fields computed using different techniques is only faintly understood, meaningful comparisons of three dimensional fields are even rarer.

In the future, data assimilation techniques such as are being developed at NAVOCEANO and FNOC will be useful in combining observations, climatologies, and numerical model output to generate volumetric sound speed fields that might be required by a High-Gain type system. In addition, advances in inverse methods that combine ocean observations with ocean models will undoubtedly be incorporated into operational products once the techniques progress into the applied arena.

3.0 ESTIMATING THE SOUND SPEED ENVIRONMENT DURING THE HGI EXPERIMENTS

3.1 REQUIREMENTS FOR SOUND SPEED DATA

Experience has shown that comparing a given measured sound speed profile with one extracted from standard sound speed databases such as the GDEM or Levitus climatologies yields discrepancies as large as 5 - 10 m s^{-1} in the upper several hundred meters down to differences on the order of 1 m s^{-1} in the deeper parts of the ocean. Thus, for much of the oceanic world of interest, reliance on databases is only a partial solution -- higher accuracies, especially in the upper regions, require some input from measured data.

As stated earlier, one of the goals of the HGI program was to examine experimentally the sensitivity of matched field processing to sound speed errors. One of the goals of the measurement program, then, was to achieve sound speed accuracies on the order of 1 - 2 m s^{-1} rms throughout the water column. Since the primary determinant of sound speed in the open ocean is temperature, this is equivalent to a temperature error of about 0.2°C.

Total instrument temperature error at a given depth is due to two factors: thermistor/thermometer error and depth error. The anticipated error in CTD profiles falls within the bounds of 1 - 2 m s^{-1}: temperature error is less than 0.01°C or about 0.05 m s^{-1} and depth error is about 5 m, which in a high vertical gradient of 0.1 m s^{-1} per m gives a sound speed error of about 0.5 m s^{-1}. The total error due to thermistor/thermometer error and depth error is then less than 0.6 m s^{-1} for the CTDs.

To maximize the accuracy of the expendable probes, calibration experiments were run on both XBTs and AXBTs to correct both temperatures and fall rates from the values given by the manufacturers. The calibration experiments run on AXBTs and T-5 XBTs during MDA are described in Boyd and Linzell (1993a and b). In summary, the results were that uncalibrated probes gave combined thermistor-depth rms temperature errors on the order of 0.25°C (about 1.25 m s^{-1}), while calibrated probes had errors of about 0.15° C (0.75 m s^{-1}). With the VAST data an attempt to calibrate the XBTs and AXBTs by comparing profiles with CTDs fairly close in time and space was attempted, described in Boyd (1990a). This approach was not as accurate as the true calibration studies, but probably improved the accuracy to an estimated 1 m s^{-1}. Estimated salinity values were also needed for sound speed computations. The estimated maximum salinity error was on the order of 0.1 psu, contributing up to 0.1 m s^{-1} to the total sound speed instrument error. Hence we estimate the total instrument error from the expendable probes during VAST to be about 1.1 m s^{-1} and during MDA about 0.85 m s^{-1}.

Another source of sound speed error can be undersampling, either in the vertical or the horizontal. Based upon vertical sound speed gradients, a criterion of 1 - 2 m s^{-1} translates roughly to needed vertical resolutions of a few meters to 10 meters in the upper few hundreds of meters of the ocean and tens to a hundred meters in deeper regions. Using

the acoustic criterion that at least several depth points per vertical wavelength are needed in regions of significant variability yields a sampling interval of roughly 10 m. The data were retained at every 2 m, which should mean that vertical undersampling contributed only a small amount to the total sound speed error budget over most of the water column.

What sampling schemes to use horizontally and temporally were much more problematic than the vertical sampling scheme and had to be based more upon resources available (time, money, platform capacity) rather than upon statistical calculations.

Based upon resources available, CTD sampling along the VAST and MDA ship tracks was set at 100 km, while XBT and XSV sampling along the tracks during VAST was 10 - 30 km and during MDA every 2 hr and 4 hr, which, when the ships were underway, meant every 20 to 40 km. AXBT spacings along the tracks were 25 km (low horizontal gradient) and 12.5 km (high gradient) during VAST and 46 km (low gradient) and 25 km (high gradient) during MDA. AXBTs were also deployed in a grid over both the VAST and MDA regions. Grid spacing during VAST was 37 - 56 km and during MDA, 25 - 46 km. Time scales in the surface mixed layer are on the order of minutes to hours, but below this highly dynamic region, near-surface decorrelation time scales are often taken as five days to a week, and all grids during VAST and MDA were completed within this time scale. The three VAST grids were completed over 4, 2 and 3 days, respectively, and both MDA grids over 4 days.

3.2 MEASUREMENT PROGRAMS FOR THE HGI EXPERIMENTS

3.2.1 SVLA

The HGI sea tests started in 1987 with SVLA (Single Vertical Line Array), a simple exploratory experiment to test some of the concepts of the Program. SVLA was conducted in a relatively benign environment in the northeast Pacific (not far from the 1989 VAST experiment discussed below), with acoustic instrumentation suspended from FLIP located near 35°N, 126°W. Environmental measurements consisted of about two dozen CTD casts along a radial, and results were sufficiently promising that a second experiment, VAST, was planned.

3.2.2 VAST

VAST (Various Acoustic Systems Test), the second of the High Gain Initiative experiments, took place in July 1989 in the Northeast Pacific 2000 km west of California (Fig. 3-1). The experiment was a complex multi-instrument suite, multi-platform undertaking with the goal of utilizing several acoustic systems to test the feasibility of matched field processing under a variety of environmental conditions. Measurement tracks were laid down across a frontal region expected to be environmentally complex (Track F) and across a non-frontal region expected to be environmentally benign (Track W). One set of environmental measurements was also made along a track (Track B) between Tracks F and W. VAST was closely

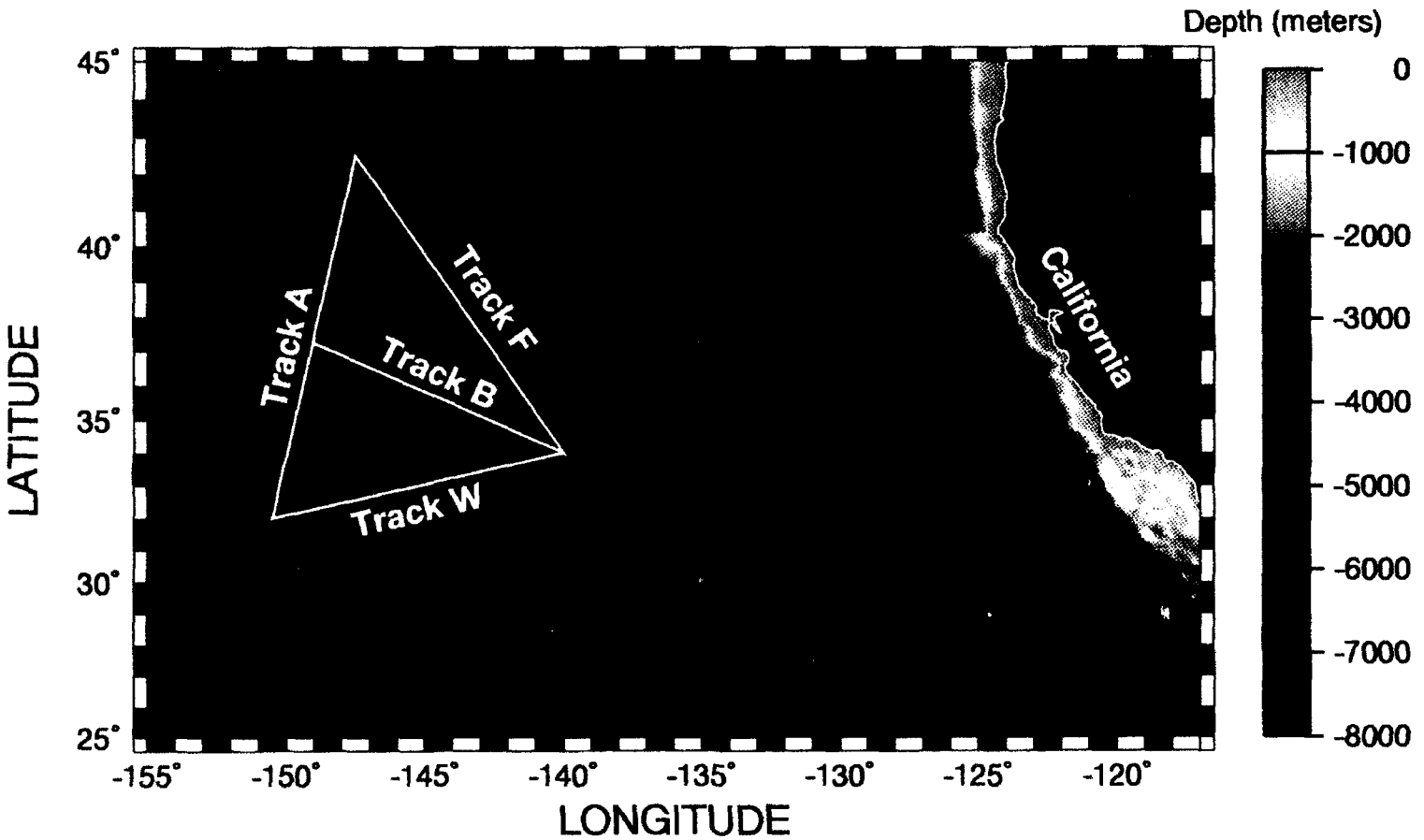

Figure 3-1. Location, bathymetry, and exercise geometry for VAST experiment, summer 1989.

coordinated with the field efforts of several other projects, including:

(1) Northeast Pacific Modeling Project (NEPAC) of the Naval Ocean Research and Development Activity (NORDA -- now part of the Naval Research Laboratory), sponsored by the Office of Naval Technology;

(2) Single Slice Tomography Experiment (SLICE89) of The University of Washington Applied Physics Laboratory (UW/APL) and Scripps Institution of Oceanography, sponsored by the Office of Naval Research and Office of Naval Technology;

(3) Downslope Conversion Experiment of the Scripps Institution of Oceanography Marine Physical Laboratory (Scripps MPL), sponsored by the Office of Naval Research;

(4) Horizontal Random Array (HRA) Experiment of the Naval Ocean Systems Center sponsored by the Naval Air Systems Command and the Office of Naval Technology;

(5) Transient Source Extraction and Classification Test (TRANSECT) of the Scripps Institution of Oceanography Marine Physical Laboratory, sponsored by the Office of Naval Research.

The objective of the environmental measurement program was to measure and otherwise derive the sound speed field with sufficient accuracy and temporal and spatial resolution to meet the "requirements of matched field processing." Since the "requirements of matched field processing" were also being defined during the VAST experiment, the accuracy and time and space sampling of the environmental measurements was a compromise between the best estimate of required accuracy (felt to be on the order of 1 to 2 m s^{-1}), the greatest accuracy of available measurement systems and the optimization of resources (dollars and time) available.

Because of the close coordination between the VAST and NEPAC experimental programs, an enormous quantity and variety of environmental data was obtained (Fig. 3-2, 3-3, and 3-4) which allowed an excellent characterization of the environment above 1000 m. An overview of the environmental measurements made by these two programs is given in Table 3-1. More information is available in Boyd (1989, 1990a and 1990b).

The VAST acoustic instrumentation was located at the intersection of tracks W and F. Two acoustic source towing ships traversed tracks W, A, and F, and environmental measurements were made along the tracks and within the triangular volume determined by the tracks in order to determine the sound speed field. The source ships dropped temperature and sound speed expendable probes along the W and F tracks, nominally every 30 km in regions with small horizontal gradients and every 10 km in higher gradient regions (as established by aircraft flights). To establish T-S relationships along the tracks, a third ship conducted

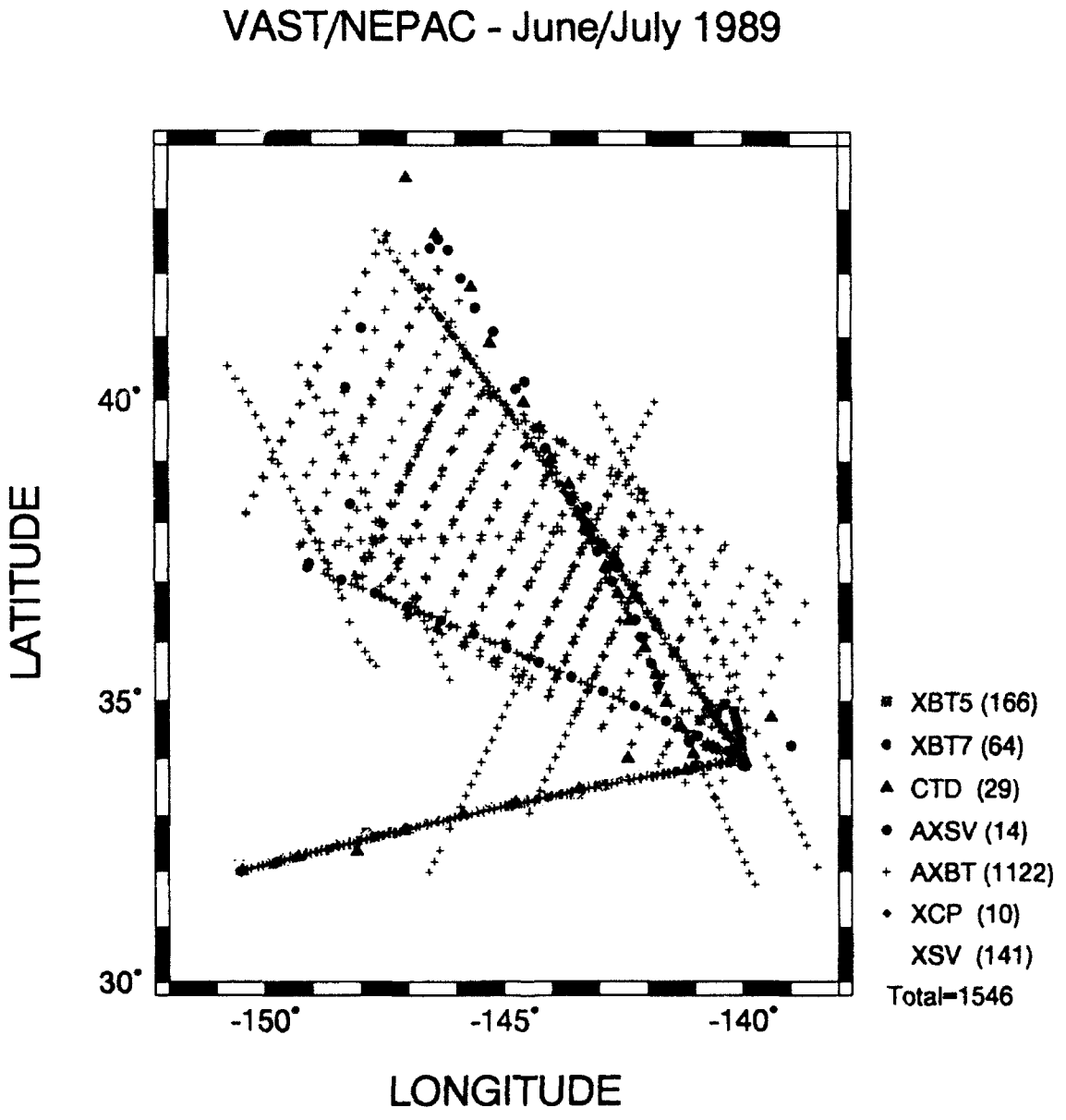

Figure 3-2. Summary of all environmental data taken by the VAST and NEPAC experiments, summer 1989. Different symbols indicate the different measurement types. The number of each measurement type is indicated by the symbols ar : numbers to the right of the plot.

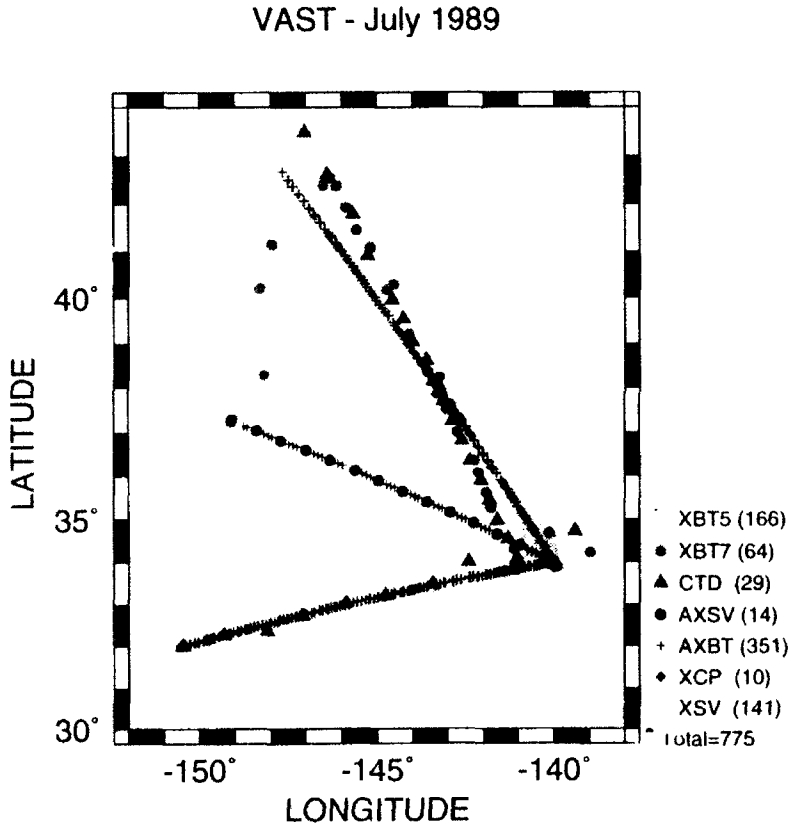

Figure 3-3. Same as in Fig. 3-2, except only VAST data is shown.

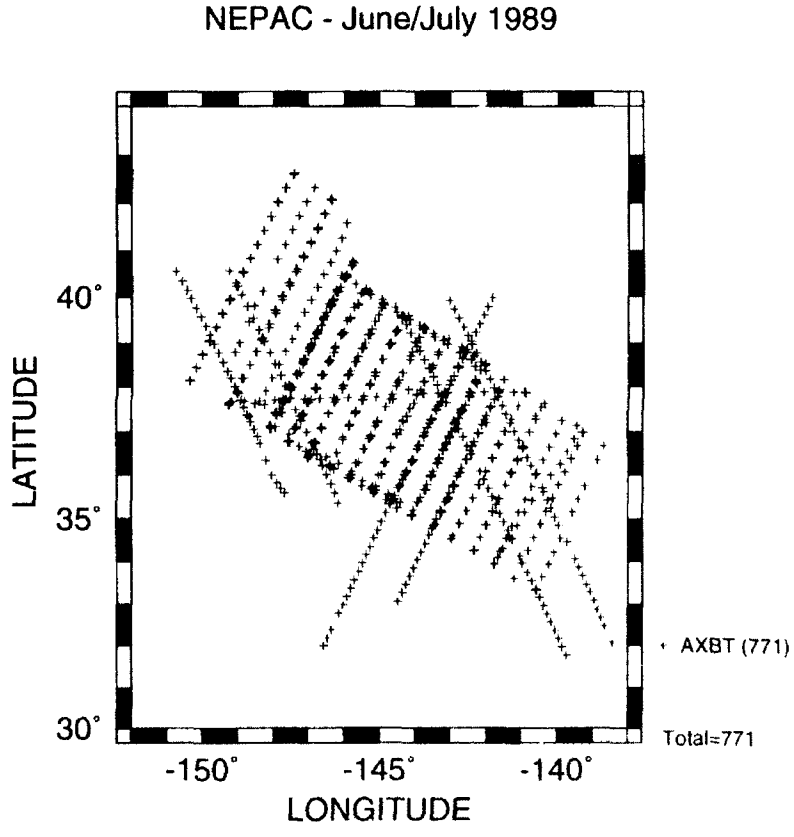

Figure 3-4. Same as in Fig. 3-2 except only NEPAC data is shown.

CTD measurements to about 2000 m depth every 100 km along W and F (the ship track did not go exactly along F, but at an angle). Two CTD casts to about 4000 m were made at the VAST instrumentation site at the beginning and end of the operations. To obtain several nearly-synoptic snapshots of the sound speed field along the tracks, six P-3 aircraft flights dropped deep (nominally 760 m) AXBTs along F, W, and B at a nominal 25 km spacing in lower horizontal gradient regions and at a 12.5 km spacing in higher gradient regions. SUS (air dropped explosive sound sources) were deployed from the aircraft during one flight each along the F and B tracks. The aircraft flights undertaken for VAST, as well as for the NEPAC and Downslope Conversion experiments, are summarized in Table 3-2, and Fig. 3-3 summarizes the total VAST environmental dataset.

The NEPAC environmental dataset was gathered primarily with AXBTs dropped by Navy and research P-3 aircraft. The experimental plan was to obtain three near-synoptic realizations of a more or less rectangular gridded region lying essentially between VAST Tracks B and F (Fig. 3-4). A central portion was designated an intensive study area in which detailed tactical scale modeling was to be attempted; AXBTs were dropped around the boundary of this region between the first and second grids and the second and third grids. Spacing between the drops in the grids was 20 nmi (37 km) along-track and 30 nmi (56 km) between tracks. Spacing between drops on the boundary flights was 20 nmi (37 km). Three pairs of flights were flown along GEOSAT altimetry satellite tracks, with an along-track spacing of 11 nmi (20 km). In general, deep (nominally 760 m) and shallow (nominally 305 m) AXBTs were alternated along the tracks. The NEPAC aircraft flights, along with the other related flights, are summarized in Table 3-2.

Table 3-1. Summary of the environmental measurements made during summer 1989 during the VAST/NEPAC experiments.

Oceanographic Data Acquired:

CTD Stations	29
T-5 XBTs	166
T-7 XBTs	64
XSVs	141
AXBTs	1122
AXSVs	14
XCPs	10

Operation Duration: VAST: 11 days / NEPAC: 25 days

Table 3-2. Environmental measurements made from aircraft during the VAST, NEPAC, and related experiments.

Date 1989	Flt #	Flight Description	Aircraft	AXBTs	AXSVs	SUS	AXCPs	CMODs
25 June	101	NEPAC Grid A1#1	VXN-8	30	--	--	--	--
26 June	102	NEPAC Grid B#1	VXN-8	40	--	--	--	4
	1	NEPAC Grid C#1	NRL	31	--	--	--	--
27 June								
28 June	301	NEPAC Grid D1	VP-9	46	--	--	--	--
	103	NEPAC GEOSAT#1	VXN-8	73	--	--	--	--
	2	NEPAC Special Probes#1	NRL	--	--	--	30	--
29 June								
30 June	3	NEPAC GEOSAT#2	NRL	49	--	--	--	--
	104	NEPAC Boundary#1	VXN-8	42	--	--	--	--
1 July								
2 July								
3 July	4	NEPAC Special Probes#2	NRL	9	--	--	24	--
4 July	105	VAST Line W#1	VXN-8	60	--	--	--	--
5 July	202	Downslope#1	VP-9	56	--	--	--	--
6 July	106	VAST Line W#2	VXN-8	59	--	--	--	--
	203	NEPAC Grid A2	VP-9	27	--	--	--	--
7 July	107	NEPAC Grid C#2	VXN-8	35	--	--	--	4
	304	NEPAC Grid D2#1	VP-46	39	--	--	--	--
	5	NEPAC Grid B#2	NRL	41	--	--	--	--
8 July	205	Downslope(SUS)#2	VP-9	58	--	11	--	--
9 July	6	VAST Line W#3	NRL	59	--	--	--	--
10 July	7	VAST Line F#1	NRL	53	--	--	--	--
	206	Downslope #3	VP-9	58	--	--	--	--
	307	NEPAC Grid E	VP-48	59	--	--	--	--
11 July	308	NEPAC GEOSAT#3	VP-46	66	--	--	--	--
12 July	108	VAST Line F(SUS)#2	VXN-8	68	--	25	--	--
	209	NEPAC Boundary#2	VP-48	39	--	--	--	--
13 July	109	VAST Line B (SUS)	VXN-8	52	14	34	--	--
14 July								
15 July								
16 July								
17 July	8	NEPAC Special Probes#3	NRL	42	--	--	23	--
	210	NEPAC Grid A1#2	VP-48/MAU	30	--	--	--	--
18 July	9	NEPAC Grid C#3	NRL	37	--	--	--	--
19 July	211	NEPAC Grid B#3	VP-48	43	--	--	--	--
	212	NEPAC Grid D2#2	VP-48	48	--	--	--	--

Oceanographic Context

VAST took place in the North Pacific between the Subarctic and Subtropical Frontal zones. The Subarctic region lies north of about 42°N and the Subtropical region south of about 32°N, with a transition region with multiple fronts and mixed subarctic and subtropical waters lying between (Fig. 3-5). In the context of the large scale upper level circulation, the southern part of the area lay on the outer boundary of the westward flowing North Equatorial Current, while the northern boundary lay on the southern edge of the Kuroshio-derived eastward flowing North Pacific Current. (Fig. 3-6).

The upper 1000 m or so of the Subarctic region is made up of the Pacific Subarctic Water (Favorite et al., 1976). The area is characterized by low temperatures and low salinities (<33.8 psu) in the near-surface regime, which ranges from the upper 30 m in summer to 100 m in winter. Below the surface region the salinity increases from about 33.8 psu to 34.0 psu in a well defined permanent halocline between 100 and 150 m. Temperature inversions (temperature increasing temporarily with depth) are often found in the halocline, and the southern limit of the Subarctic region is that beyond which persistent temperature inversions do not occur. During summer a distinct temperature minimum is located between the bottom of the shallow seasonal thermocline and the underlying temperature inversion, resulting in a seasonal shallow sound channel about 50 m thick having its axis in the vicinity of 120 m. (Roden and Robinson, 1988). The main deep sound channel at the longitude of VAST has its axis drop from a depth of about 400 m at 46°N to 800 m at 30°N. Perturbations of 150 m or more in the depth of the sound channel axis are not unusual (Roden and Robinson, 1988).

The southern limit of the of the Subarctic region is the Subarctic Front, which is defined by the abrupt change in the salinity structure. The 33.8 psu isohaline rises from near the base of the Subarctic halocline to the surface in the Subarctic Front. The front extends from the western North Pacific east to North America where it turns southward off California and Baja California and forms what has been called the California Front (Saur, 1980). The location of the frontal zone during any particular time period depends upon the wind stress conditions, but west of 150°W it generally lies between latitudes 40° - 43°N, and then bends southward east of 150°W. The front consists of not one but several meandering temperature, salinity, and density fronts and their associated eddies, all of which are most pronounced in the upper several hundred meters. Rodin and Robinson (1988) review and summarize the properties of the Subarctic Frontal zone.

The Subtropical region lies south of about 32°N, consisting of what Sverdrup et al. (1942) called the North Pacific Central Waters. It has a considerably different temperature and salinity structure from the Subarctic region. At the surface it is characterized by salinities greater than 34.8 psu and has a halocline and associated thermocline between about 100 - 250 m in which salinity decreases with depth.

The northern limit of the North Pacific Central Waters is the Subtropical Front. This front has not been studied as well as the Subarctic Front, but it appears that the average position of the subtropical front may be defined by the position of the 34.8 or 34.9 psu isohaline at

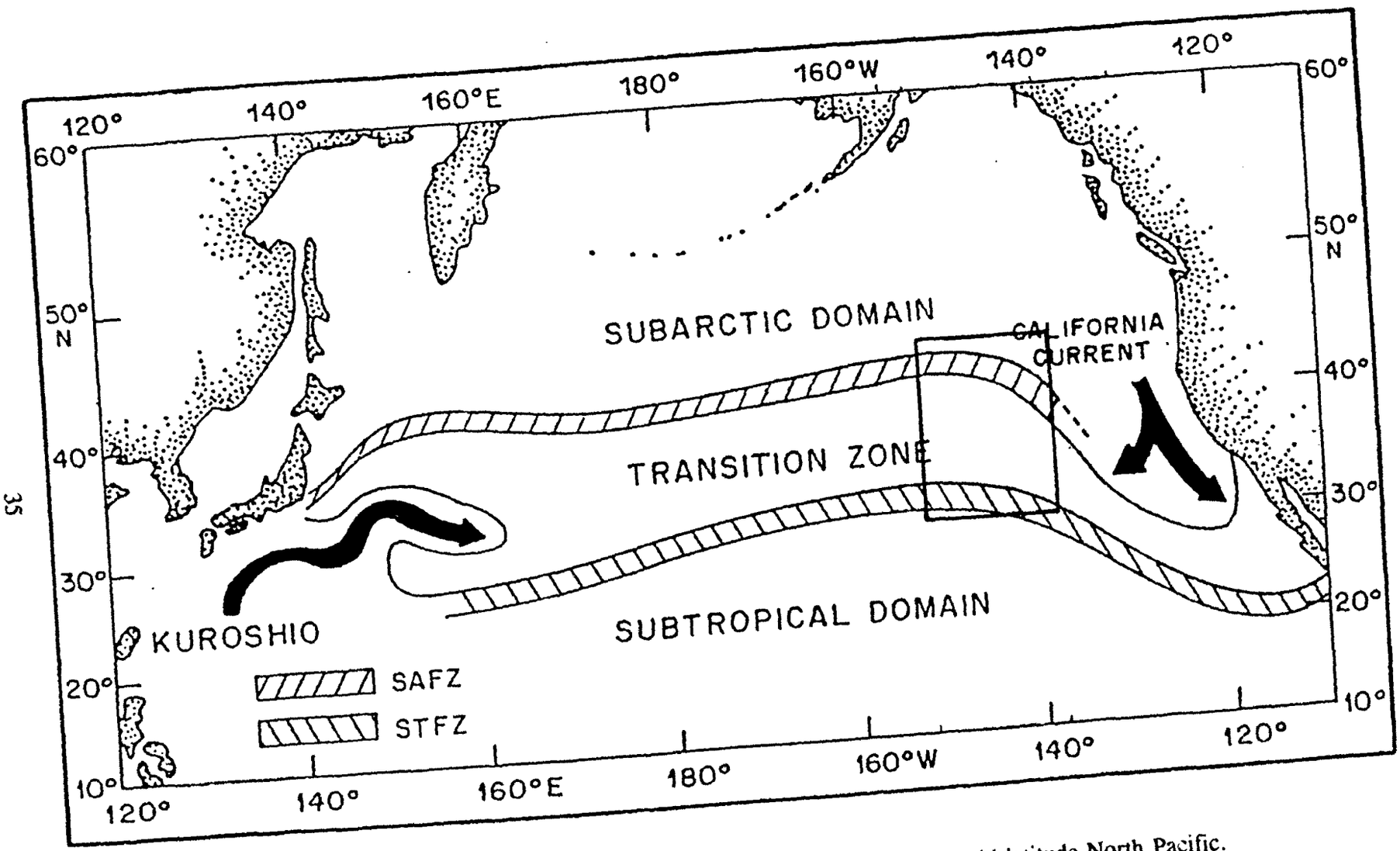

Figure 3-5. Schematic view of the principal oceanic regions in the mid-latitude North Pacific. Arrows indicate prevailing current directions. SAFZ is Subarctic salinity frontal zone; STFZ is the Subtropical temperature frontal zone. The VAST/NEPAC study area during June - July 1989 is shown by the box. (From Roden and Robinson 1989).

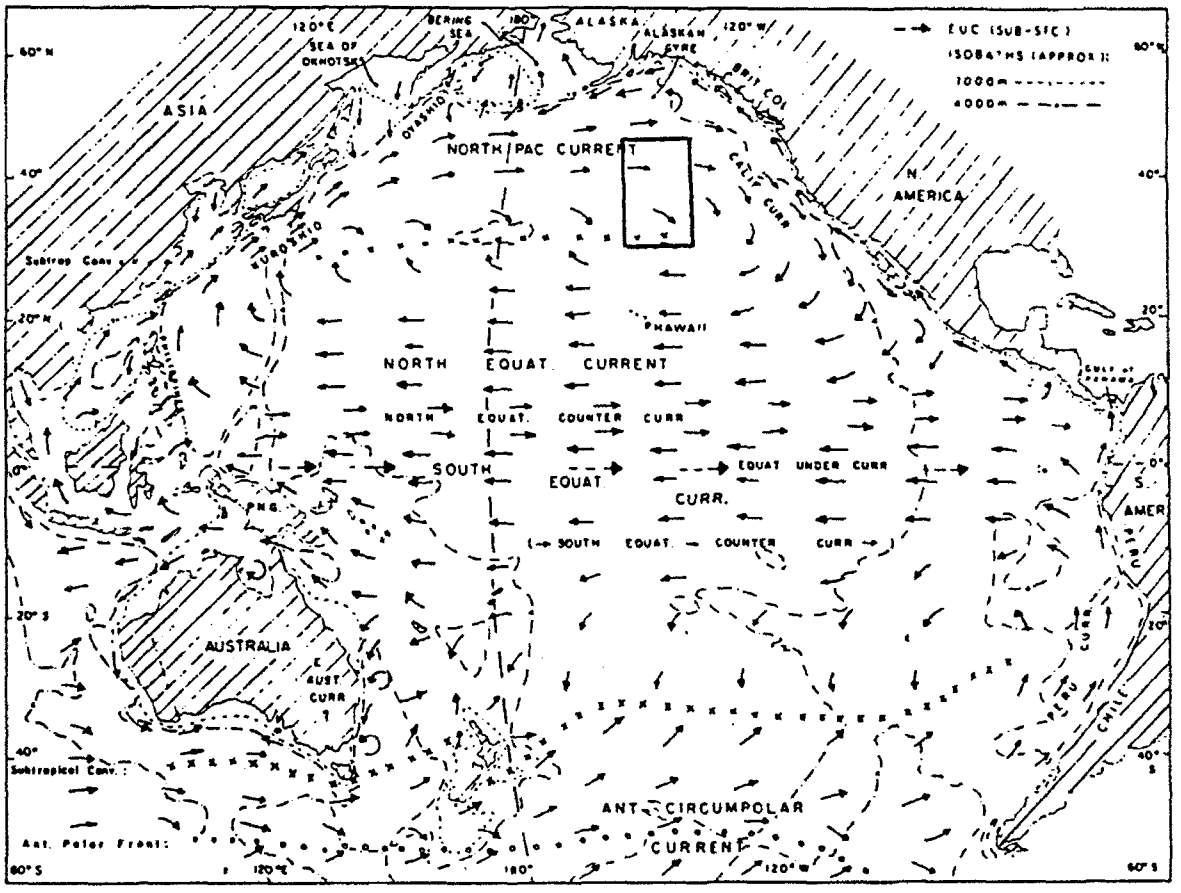

Figure 3-6. Large scale oceanic surface currents in the North Pacific. The general region of the VAST experiment is indicated by the box. (From Pickard and Emery 1990)

or near the surface (Lynn 1986). It lies between about 31° - 33°N. Somewhat north of this, around 33°N, is what Lynn (1986) called the Northern Subtropical Front. It appears to originate in the Kuroshio Extension and is continuous or semi-continuous across the North Pacific, and has a temperature range of 14° - 17° and salinity range of 34.4 - 34.6 psu.

Between the two frontal zones lies the Subarctic-Subtropical transition zone. It contains waters with both Subtropical and Subarctic characteristics, mixed in various proportions depending primarily upon the distance from the source regions. Transient temperature inversions between 100 - 200 m are not uncommon in the northern part where the Subarctic water is more common.

The VAST experiment took place in a region that was quite variable and complex in its upper several hundred meters. It took in the Subarctic Frontal zone of the Northeast Pacific, extended southward into the northern limits of the Subtropical Frontal zone, and included a transition region with multiple fronts. The findings from VAST/NEPAC that are of relevance to investigating the impact of ocean variability on long-range acoustic propagation are summarized in the following sections.

Horizontal Planes

Horizontal planes of sound speed from the 6-7 July 1989 NEPAC flights are given in Fig. 3-7 to give an overview of the structure of the VAST sound speed field. The Subarctic Front is well defined in the upper 200 m, with the characteristic presence of several meandering frontal zones and their associated eddies quite apparent. The surface manifestation of the front is less convoluted, however, than at 100 m. The main portion of the front lies between about 36° - 38° N, but below the surface a southward penetrating meander is seen between 144° - 148°W. There is some evidence from the three separate NEPAC grids that over the three weeks of the VAST/NEPAC experiment, the meander pushed further south and pinched off into an eddy. A second but less intense frontal zone lies to the north of the main front. The presence of several eddies is also suggested, but they are so small that the sampling was too coarse to properly resolve them. This determination of the region of the Subarctic Frontal zone is also borne out by the limits of the 8° and 10° isotherms at 150 m (not shown) (Rodin and Robinson 1988). The southern limit of the Subarctic salinity front may be defined by the surfacing of the 33.8 psu isohaline (Rodin and Robinson 1988), and on the surface salinity plot inferred using T-S relationships with the temperature data (not shown), this lies in the southern portion of the frontal zone as defined by the 8° and 10° degree isotherms.

A second meandering front visible in the data, between 32° - 36°N, lies right over the VAST instrumentation site and the F and B tracks and meanders south of the W track near 143°W. This front may be a northward meander of the Northern Subtropical Front. Its position agrees quite closely with Lynn's (1986) observations except that the temperature range of the frontal region (not shown here) is about 18 - 20° rather than the 14 - 17° quoted by Lynn.

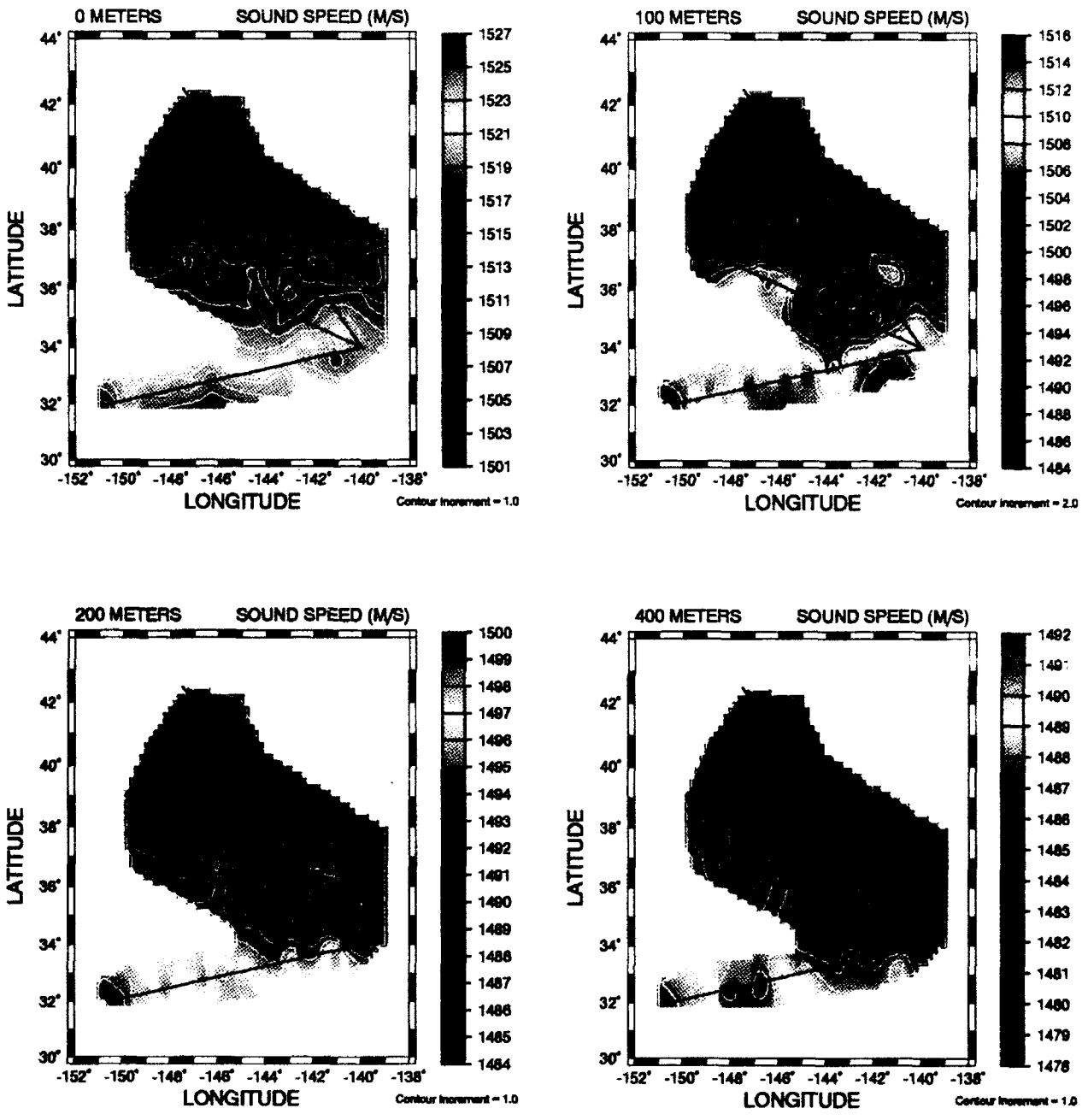

Figure 3-7. Sound speed at 0, 100, 200, and 400 m from the 6 - 7 July 1989 NEPAC AXBT flights and the 6 July VAST flight. The Subarctic Front is particularly apparent at 100 m, lying between about 35° - 38°N, with a weaker filament meandering northward from Track F and forming a frontal zone between about 39° - 40°N. To the south of the Subarctic Front, a northward meander of the Northern Subtropical Front crossed all three tracks (F, B, and W) near the VAST site. (Note the contour increment used at 100 m is twice that used at the other depths.)

Vertical Planes

Sound speed from the three flights along the W (non-frontal) track are presented in Fig. 3-8. While track W was the non-frontal, or benign, track, it was not featureless. The sound speed structure indicates that the track lay largely in the southern limit of the transition zone between the Subarctic and Subtropical regimes. The effect of the northward meander of the Northern Subtropical Front shows in the downward, then upward bowing of the isotachs out to a range of about 300 km. At range 375 km was a persistent subsurface cold core blob that was probably a remnant of an earlier southward meander of the Subarctic Front. Below about 150 m, 50 to 100 m excursions of the isotachs over 50 - 100 km were not uncommon. The shallow sound channel with its axis at about 75 m lay between two sonoclines: one at about 50 m due to the seasonal thermocline and one centered around 125 m due to the permanent halocline. The deep sound channel axis lay at about 800 m.

The frontal track Track F (Fig. 3-9), showed considerably more structure than Track W. The character of the shallow sound channel axis evolved dramatically along the track from south to north. The upper sonocline due to the seasonal thermocline lay at about 50 m along the whole track, but the depth of the lower sonocline due to the halocline jumped from about 150 m up to 100 m at the point the track crossed the Subarctic Front (range of about 450 km). At a range of about 750 km the track passed through another frontal filament and the shallow sound channel disappeared as the deeper sonocline merged with the shallower one at 50 m. Twenty five to fifty-meter excursions of the isotachs were quite common. The deep sound channel axis was found at about 700 m.

The sound speed along track B is given in Fig. 3-10. The shallow sound channel was well behaved along most of the track, although it was best defined between ranges of 500 to 775 km. The track passed through the Northern Subtropical Front at a range of about 125 km and through the meandering Subarctic Front between 145°W (500 km range) and 145.5°W (550 km). The shallow sound channel was best defined and had its greatest width (50 m) between 145.5°W and about 147.5°W (750 km range) when the track passed again into the main Subarctic Front. The deep sound channel lay around 750 m deep. As along the other tracks, fifty-meter or more excursions of the isotachs were not uncommon.

Comparison of Tomographic and Classical Measurements

Matched field processing comparisons were made between sound speed fields derived from the Line W CTD casts only. Because of time constraints, CTD casts had been made only to about 2000 m depth, and several techniques were investigated to extend the profiles to the bottom. The first was to use the GDEM Navy standard climatology and the second was to use the 4000 m VAST site profile extended to bottom with the Levitus climatology. Results and the tomography-generated transect are shown in Fig. 3-11. The two extension techniques appear to give very similar plots; however, the matched field processing results are noticeably different. A more revealing comparison between the fields is given in Fig. 3-12 where the difference between the two extensions and between tomography and each extended field separately are plotted. In the first panel, the difference between the two extended fields, differences are seen to begin at about 2000 m (as would be expected), reach

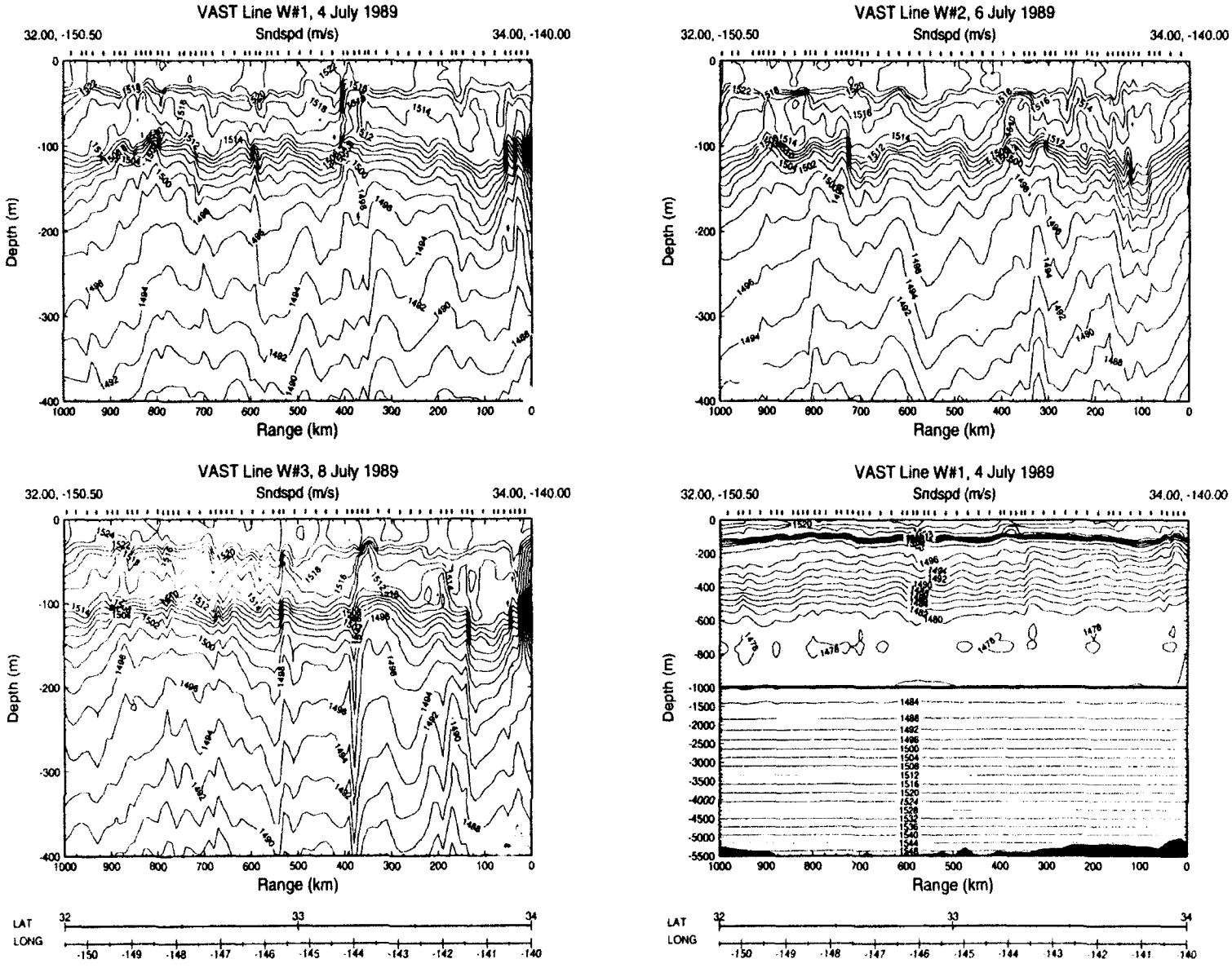

Figure 3-8. Sound speed along track W from the three separate VAST aircraft flights. The first three panels extend from the surface to 400 m to show the upper level structure in more detail. The fourth panel repeats the data in the first panel, but shows the sound speed structure all the way to the bottom. Two sound channels exist: at about 75 m and at about 800 m.

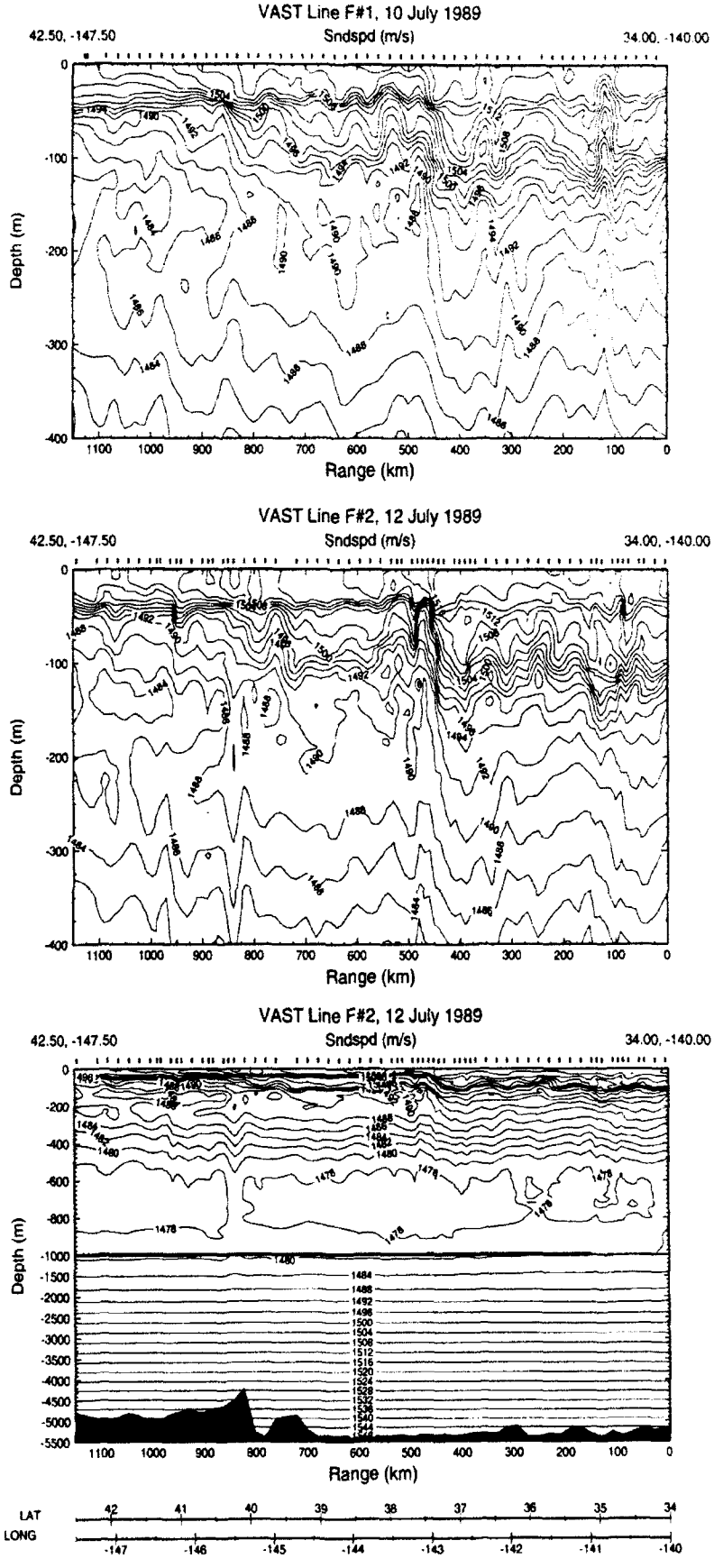

Figure 3-9. Sound speed along track F from the two separate VAST aircraft flights. The first two panels extend from the surface to 400 m to show the upper level structure in more detail. The third panel repeats the data in the first panel, but shows the sound speed structure all the way to the bottom. Ths shallow sound channel at about 75 m disappeared beyond a range of about 750 km. The deep sound channel lay at about 700 m.

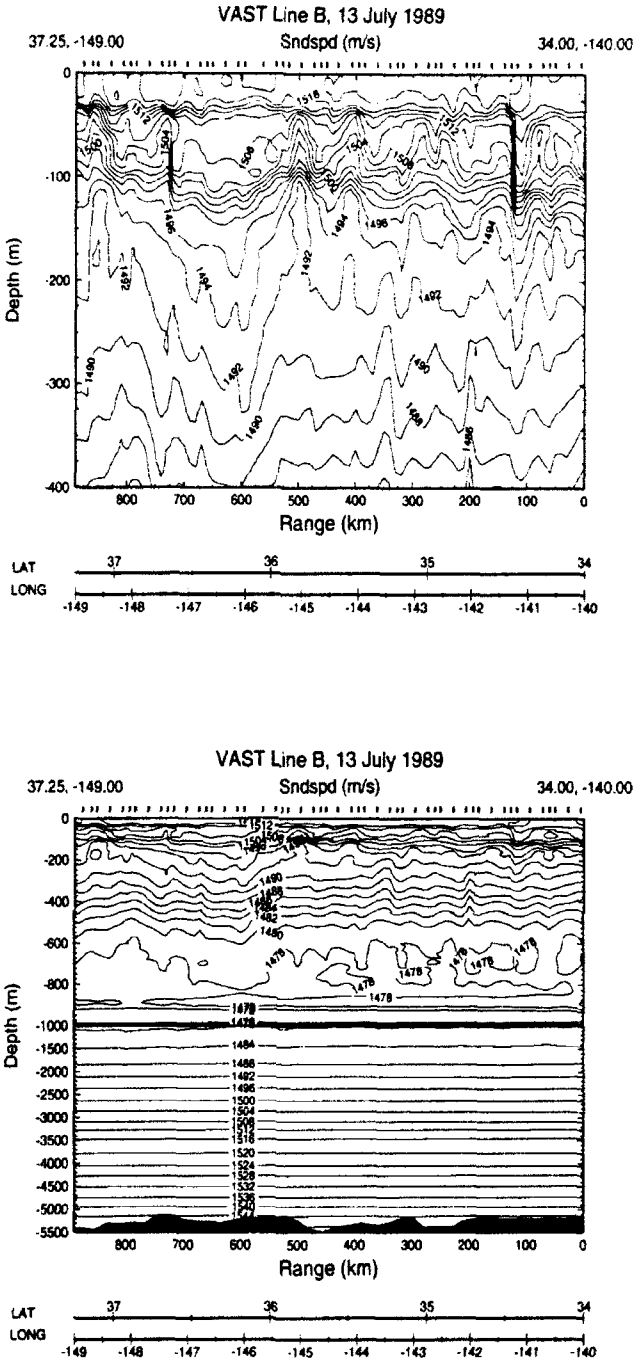

Figure 3-10. Sound speed along track B from the VAST aircraft flight. The track crossed through both the Northern Subtropical Front and the meander of the Subarctic Front. A shallow sound channel existed at about 75 m, and the deep sound channel lay around 750 m.

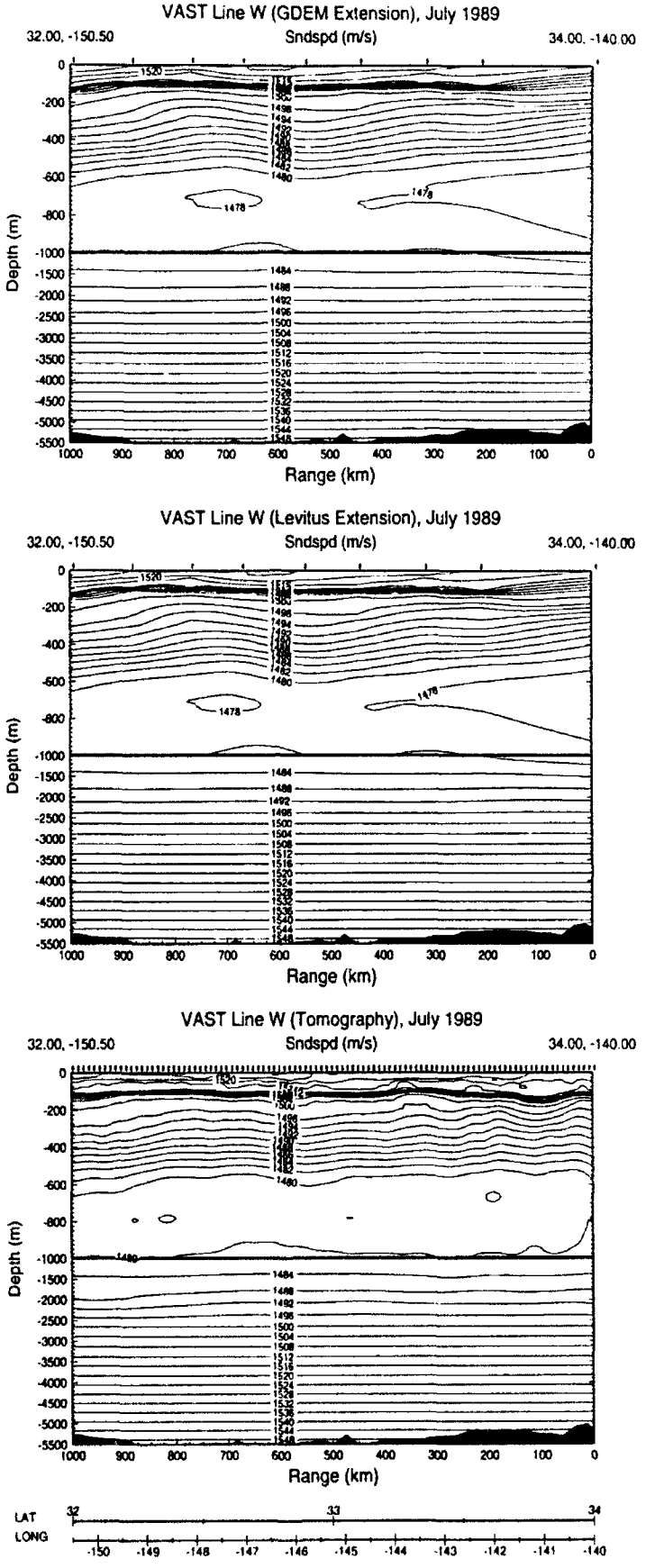

Figure 3-11. Sound speed fields along Line W from CTD casts (first two panels) and from tomography. Except at the VAST site the CTDs extended only to 2000 m, while at the instrumentation site the cast went to 4000 m. In the first panel the fields were extended to bottom using GDEM climatology; in the second panel they were extended using the instrumentation site cast extended to bottom using the Levitus climatology.

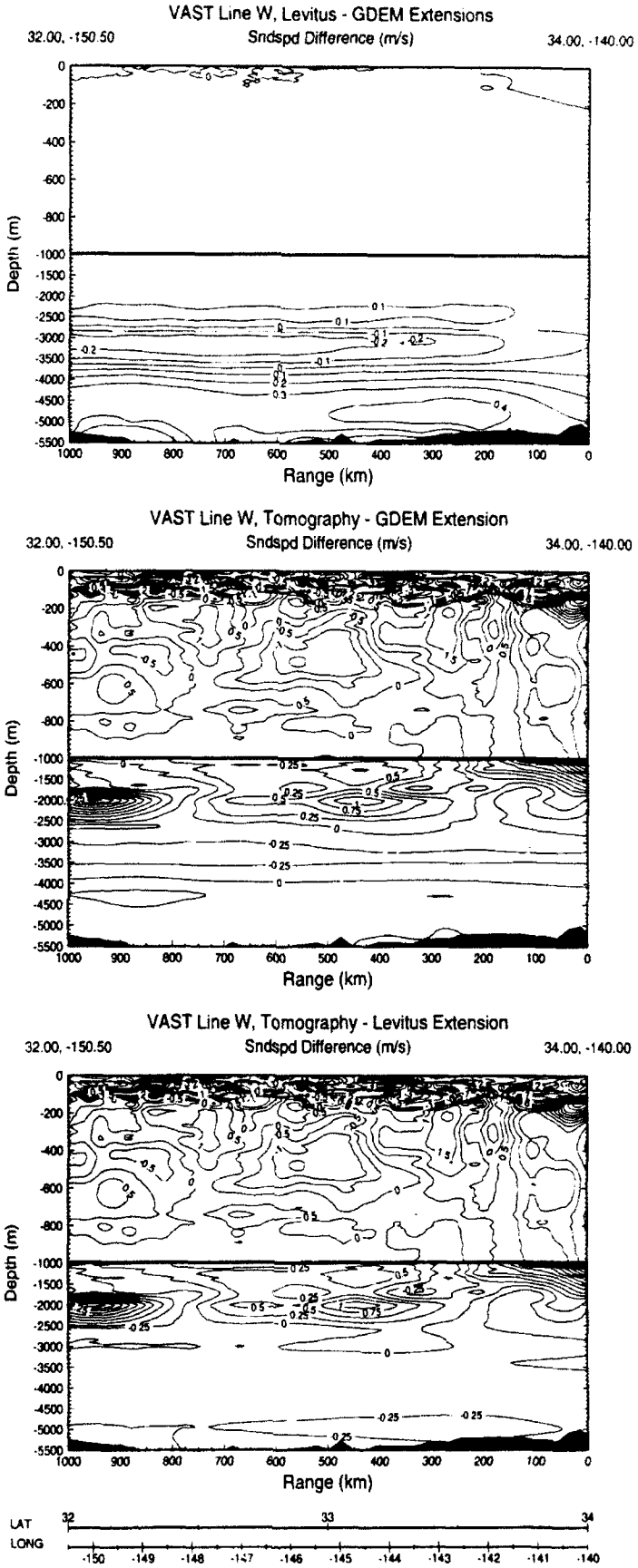

Figure 3-12. Paired differences between the sound speed fields in Fig. 3-11.

-0.2 m s^{-1} at about 3250 m and then increase to greater than +0.4 m s^{-1} near bottom. These apparently minor discrepancies were significant enough to yield different matched field processing results, with the GDEM extension giving poorer results (Livingston and Heitmeyer 1992, unpublished) and the site CTD-Levitus extension and tomography giving comparable results (Heitmeyer 1993, unpublished). The lower two panels show differences from tomography of as much as 7 m s^{-1} in the upper several hundred meters, but since the two classical fields were identical above 2000 m, the matched field processing differences had to be due just to differences in the deep sound speed values.

Comparing Fig. 3-11 with Fig. 3-8 shows that much of the smaller scale structure along Line W was lost in the CTD transect because of the large spacing in both space and time between the CTDs. The impact of the wide spacing is also apparent from the difference from tomography plots in Fig. 3-12. Particularly noticeable variability occurred between ranges 0 - 150 km and 350 - 600 km. The first region included the northward meander of the Northern Subtropical Front. From data not presented here, the feature was seen to be very dynamic and appeared to have moved into the area at about the time VAST began. Two CTDs taken near the site at the end of June showed quite different structure in the upper several hundred meters than CTDs taken in mid-July at the end of the experiment. The second region is probably the smeared impact of the subthermocline features in Fig. 3-8 which led to 75 m or greater excursions of isotachs between 300 and 600 km range.

VAST and MDA Planning

The VAST matched field processing results could not become definitive guidance for planning the third experiment, MDA, because of limitations in the acoustic data collected and the VAST analysis schedule, which coincided with the experiment planning time for MDA. However, one lesson learned concerned experiment siting. The VAST experiment location was quite remote, complicating logistics and reducing the amount of data that could be collected during the available time. For example, aircraft transits typically consumed half the available time: 6 of the 12 hours the aircraft were able to remain aloft. This was taken into account in the design of the next experiment, described in the following section.

3.2.3 MDA

The third experiment in the series was MDA (Multi-Dimensional Array). It took place in July 1991 in the western subtropical Atlantic about 1200 km west of Florida (Fig. 3-13). The tracks (shown on Fig. 3-13) were chosen to represent a continental slope crossing (Track 270) and deep water environments with differing noise and bathymetry (Track 157 and Track 175). The acoustic instrumentation was located at the site where the three tracks intersected.

The MDA environmental measurement program was the most careful and comprehensive sound speed structure determination program ever undertaken for a region of this size. It represents the present state-of-the-art for sound speed structure measurements.

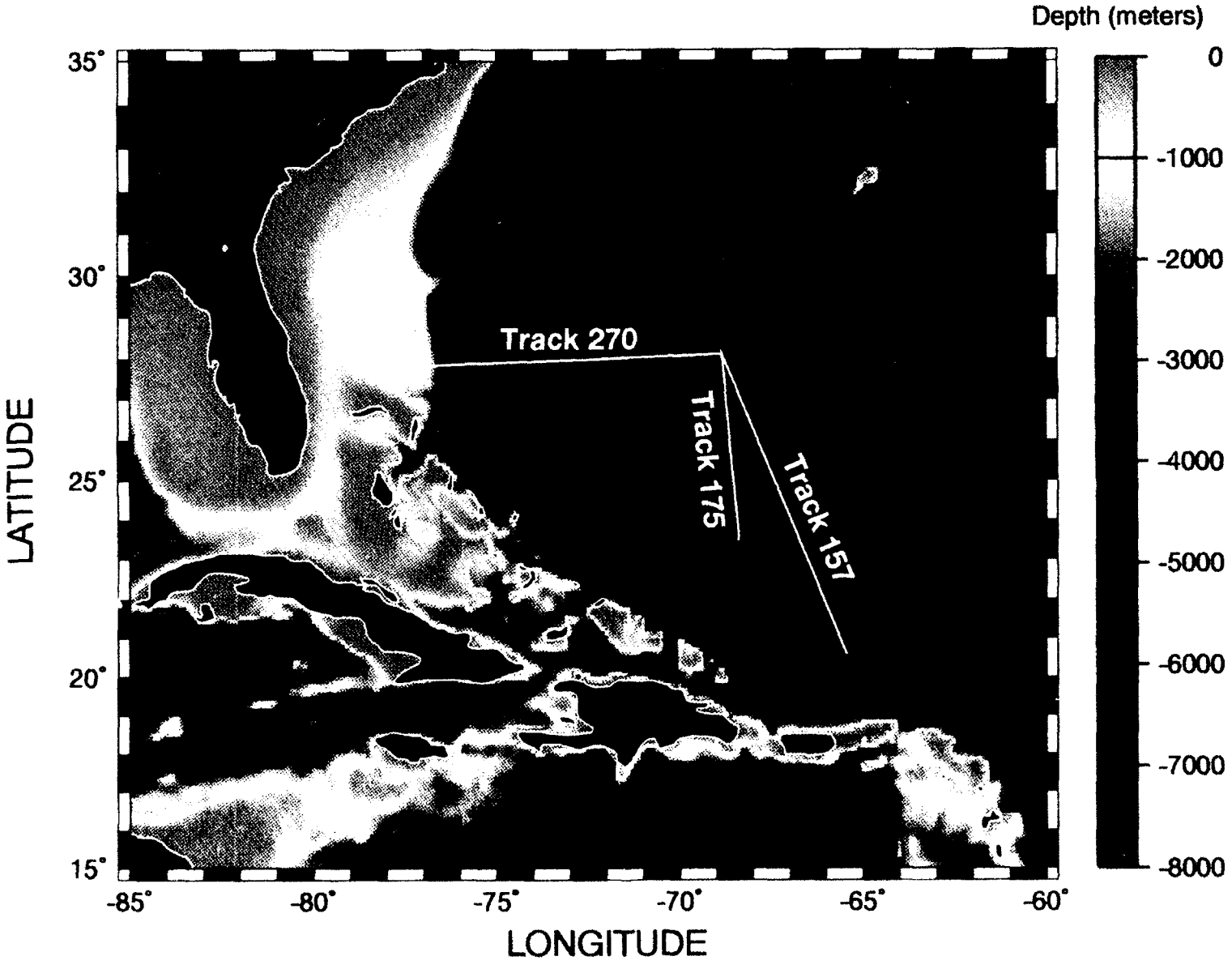

Figure 3-13. Location, bathymetry, and exercise geometry for the MDA experiment.

Environmental measurements were made from aircraft and ships to determine the sound speed field in a classical sense, and a simultaneous set of tomographic measurements was made to determine the sound speed field in a novel manner. (The tomography measurements were part of the joint Scripps/MPL and University of Washington Applied Physics Laboratory's ONT-supported Moving Ship Tomography (MST) and ONR-supported Acoustic Mid-Ocean Dynamics Experiment (AMODE) programs.) Additionally, near real time analysis was conducted in the field to optimize the sampling strategy. Communications between operations centers located in Virginia and Puerto Rico and the at-sea platforms were maintained via MARASAT and fax.

The MDA technical objectives for sound speed measurements were to describe the spatial and temporal evolution of the sound speed field and assess the usefulness of this information in 1) predicting the complex wavefield produced by a source at a given range, depth, and bearing and 2) determining the sensitivity to sound speed structure accuracy of matched field processing. The objectives for the environmental measurements were couched in terms of "matched field processing requirements" and could not be well specified at the time the experimental plan was designed. Even today the specifications for environmental requirements, which depend upon the results of SVLA, VAST, and MDA, for various reasons are still not well defined. As with VAST, the sound speed structure measurements for MDA were a compromise between the best estimate of required accuracy, the best accuracy of available measurement systems and the optimization of resources (dollars and time) available, although lessons learned during VAST were taken to heart. However, as noted, the MDA experiment represents nearly the state-of-the-art limit of present day environmental measurement capabilities. If the sound speed fields determined by MDA are not sufficiently accurate for matched field processing, then it will be extremely difficult if not impossible to achieve those higher accuracies in the foreseeable future.

Lessons learned during VAST regarding the sound speed structure measurements included making full surface to bottom CTD casts so as to fix the deep temperature and salinity relationships which may not be accurately represented in climatologies, the use of only deep AXBTs (850 m) and deep (T-5) XBTs (1850 m) because of the existence of continued variability below the upper several hundred meters, the calibration of the XBTs and AXBTs so as to improve their accuracy, the reduction of spacing between measurement points to the extent allowed by time, money, and aircraft capacity, the deployment at the instrumentation site itself of multiple CTD casts and XBTs during the whole course of the experiment so as to allow the calculation of a site sound speed time series, and the selection of an experiment location closer to available ports and airfields so as to reduce logistical problems and transit times.

The MDA environmental operations took place during two time periods, a limited operation in June and a major undertaking in July 1991. The datasets acquired during both sets of operations are shown in Figs. 3-14 and 3-15. The June work consisted of aircraft flights dropping deep AXBTs (850 m) in a rectangular area to provide an initialization field for the MST/AMODE analysis, and a rendezvous with the MST/AMODE ship to perform a

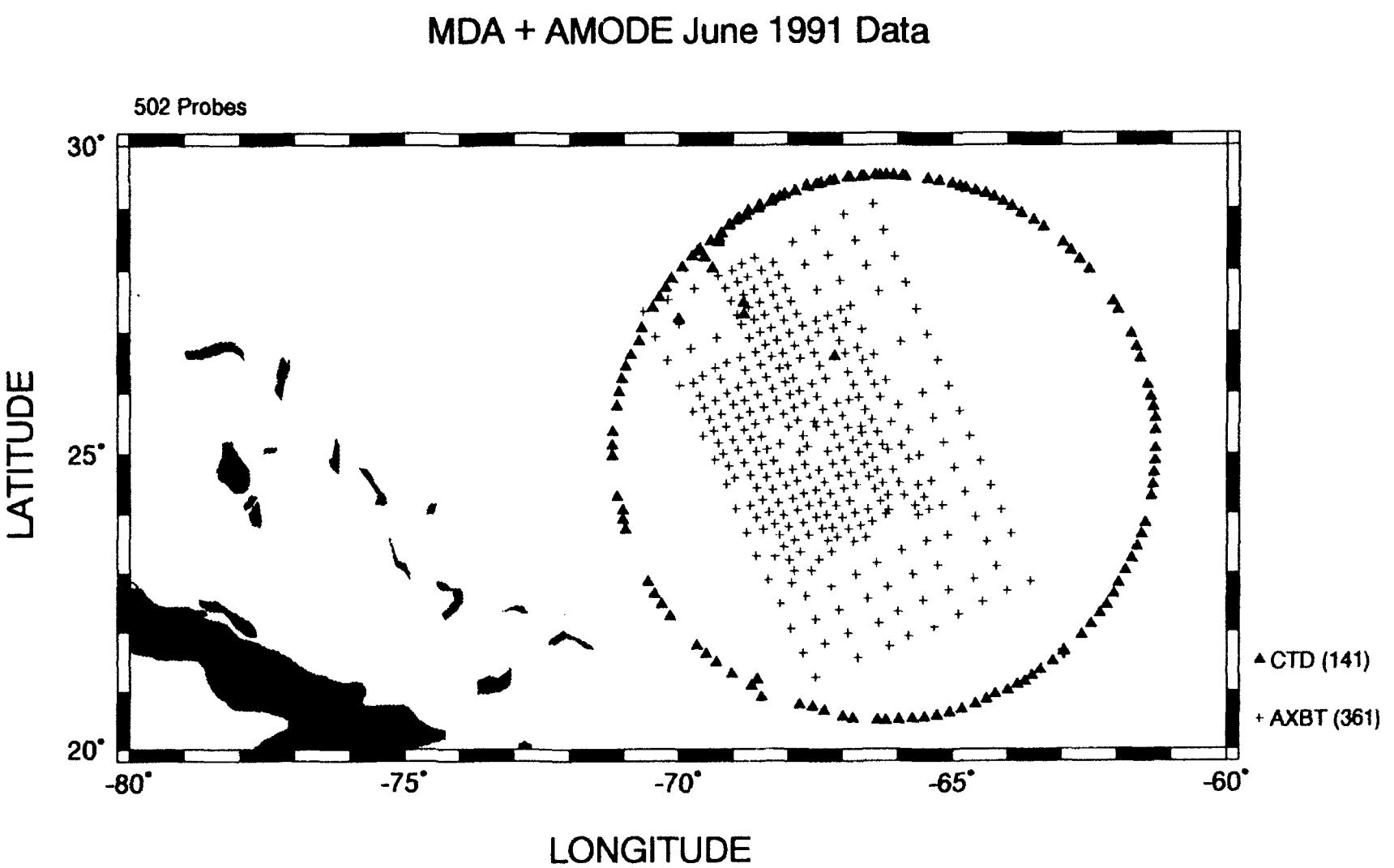

Figure 3-14. Summary of environmental data taken during the June 1991 phase of MDA - MST/AMODE. Only AXBT measurements were made as part of MDA, to be used as an initialization field for the MST/AMODE tomography experiment. All CTDs were taken as part of the MST/AMODE project.

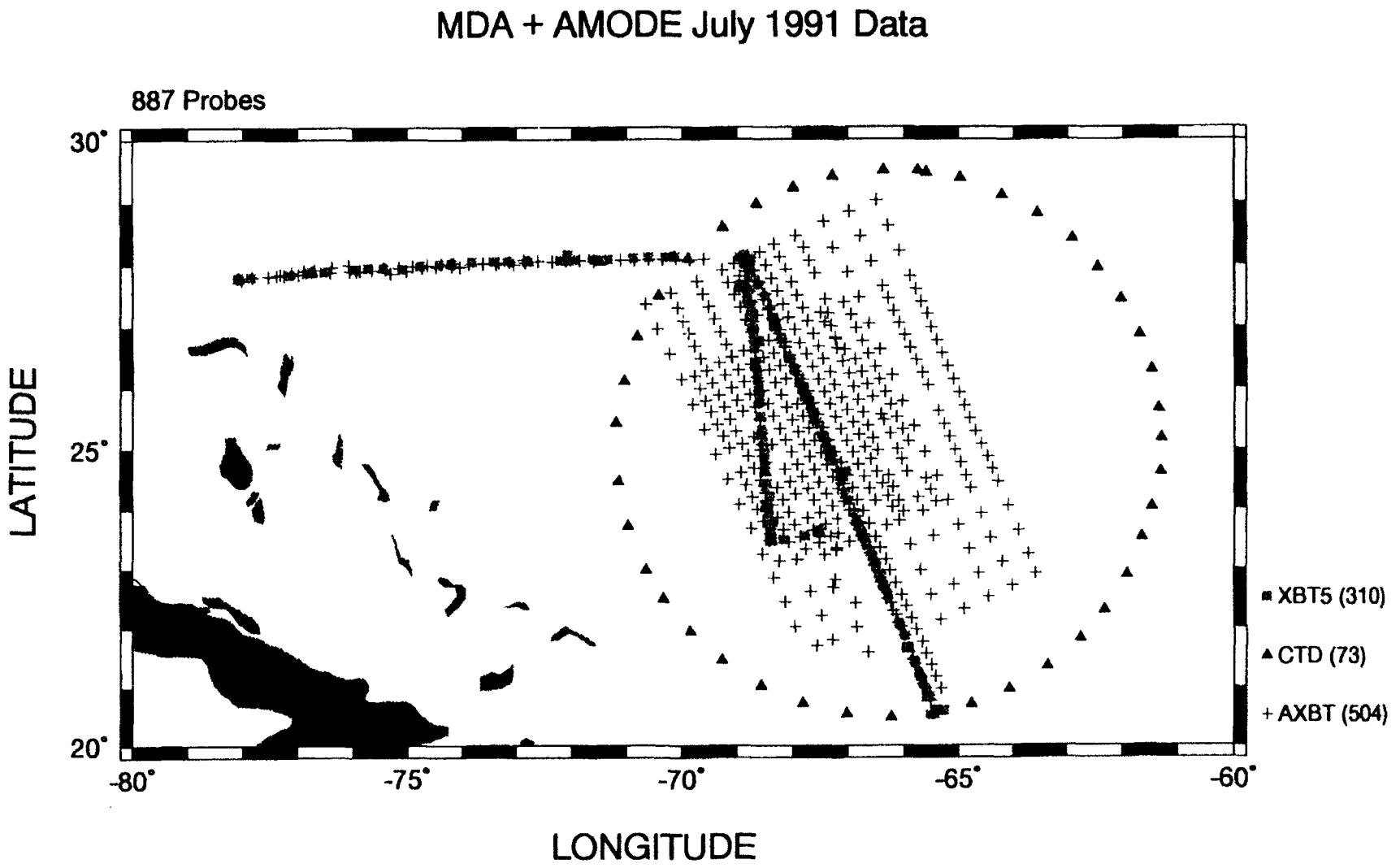

Figure 3-15. Summary of environmental data taken during the July 1991 phase of MDA by both MDA and the MST/AMODE project. The MST/AMODE CTDs form the circular pattern, and only every third one is plotted.

calibration experiment with the new type of AXBTs that were being used for the operations. AXBT spacing was about 25 and 46 km.

The acoustic instrumentation in July was located at the intersection of the 270, 157, and 175 tracks (refer to Fig. 3-13). During July, aircraft flights dropping deep AXBTs (850 m) and deep CTD stations (to bottom, if time allowed) were taken along the three tracks, along with frequent deep (1850 m) ship-deployed XBTs, and the volumetric sound speed field was determined within the rectangular area formed by the 157 and 175 tracks to provide volumetric sound speed fields for acoustic analyses and for comparison with tomographic measurements. The CTDs were taken during the whole course of the experiment, but the AXBT flights were timed to coincide as much as possible with the acoustic operations so as to limit the impact of temporal changes on the resultant sound speed fields used in the analyses. MDA CTD spacing along the tracks was about 100 km, and AXBT spacing was about 25 and 46 km. MST/AMODE CTDs taken on the periphery of the study area were spaced about 25 km apart, but extended to only about 1000 m because of time constraints. The two source ships dropped deep T-5 XBTs every 2 hours during source tows and every 4 hours during source stations.

The importance of knowing the sound speed profile and its temporal variations at the MDA site was factored into the experimental plan. The instrumentation tending ship *Lynch* made two full depth CTD casts at the beginning and end of the experiment and the two source ships made casts periodically as they passed by the site. In addition, multiple T-5 (1850 m) XBT drops were made several times a day and the profiles in each set averaged to produce a more accurate estimation of the temperature profile at that point in time. The CTD and XBT data were combined into one dataset and interpolated in time to give a time series spaced 8 hrs apart of the surface to bottom sound speed field for the full course of the experiment.

The MDA/AMODE dataset is summarized below in Table 3-3. More information is given in Boyd et al. (1992b).

Table 3-3. Summary of the environmental data collected during the summer 1991 MDA and MST/AMODE experiments.

Oceanographic data acquired:

June 1991		
	CTD stations	
	MST/AMODE	85
	AXBTs	361

July 1991

CTD stations		
	Instrumentation site	6
	MDA non-site	25
	MST/AMODE	185
T-5 XBTs		
	Instrumentation site	126
	Non-site	184

Operations duration: June - 14 days/ July - 26 days

Oceanographic Context

The MDA experimental area lay in the southwestern North Atlantic in the vicinity of the Sargasso Sea Subtropical Convergence Zone and the Subtropical Front. Fig. 3-16 gives an overview of the large-scale circulation of most of the Atlantic Ocean, with the MDA region indicated. The circulation in the study area is expected to be dominated by the basin-scale anticyclonic (clockwise) gyre of the North Atlantic between about 15° and 45°N. The climatological wind patterns of westerlies in the north and trade winds to the south produce a meridional convergence of Ekman transport (and hence downwelling) -- the Subtropical Convergence -- within the gyre that is presumed to be a major generating mechanism for the Subtropical Front, which lies typically within a zonally oriented band found between 25° and 32°N. Other mechanisms then act to form and control frontogenesis and frontolysis within the frontal zone. MDA took place in summer. Ekman pumping decreases during summer (Hanson et al. 1991), so the front might be expected to be weaker during this season, although few studies of the front have been done during this time and satellite imagery is of little help because mixed layer warming obscures the surface thermal signature. The frontal zone itself is complex, with multiple fronts within it and significant eddies and meanders on scales of 100 km down to 10 km or even smaller (e.g., Voorhis and Bruce 1982).

As part of the gyre, the climatological near-surface flow patterns in the area are expected to be west and northwest, with speeds increasing to the north and west as the Gulf Stream recirculation region is approached. The major upper level current in the study area is expected to be the west and northwestward flowing Antilles Current, which originates in the vicinity of the Leeward Islands as part of the North Equatorial Current. However, a zonal band of eastward flow, called in the analogous part of the North Pacific the Subtropical Countercurrent (Uda and Hasunuma 1969), has several times been reported occurring in a several degree wide band centered around 25°N (e.g., Iselin 1936; Ebbesmeyer and Taft 1979). Other west and southwestward flowing currents that are part of the lower limb of the gyre bring near-surface, high salinity water down into the study area from its formation region in the subtropics somewhat to the east of the study area. In this region, high evaporation rates lead to surface salinity values exceeding 37 psu. The high salinity water then sinks and spreads south and westward as the Subtropical Underwater. More details

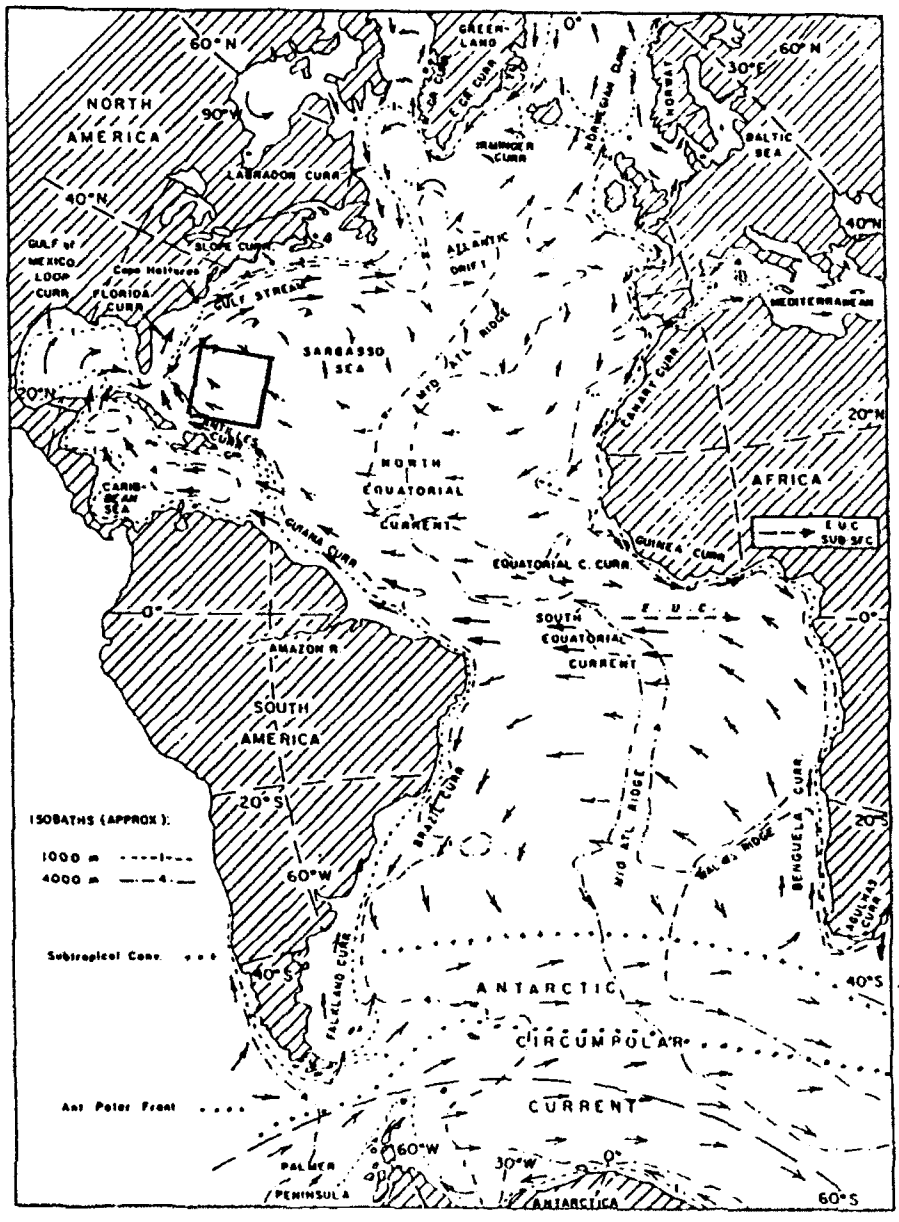

Figure 3-16. Large scale oceanic surface currents in the North Atlantic. The general region of the MDA experiment is indicated by the box. (From Pickard and Emery 1990)

on the oceanographic and meteorological conditions in the MDA region are given in Boyd et al. (1990) and Boyd et al. (1991).

Another way of looking at the oceanographic context of the area is to examine the mean sound speed profile at the instrumentation site and its rms deviation (computed from the six CTD casts) (Fig. 3-17). Regions in the water column with high rms sound speed deviation can be related to the classical oceanographic water masses. Over large areas of the world's oceans, a fairly tight correlation exists between temperature and salinity (that is, a well-behaved T-S diagram exists). Regions where such a correlation does not exist are typically regions of extreme mixing and unstable temperature and salinity (and hence sound speed) values. Outside of these regions of intense mixing, changes in oceanographic properties at a given location and depth are typically quite limited in magnitude. Tight T-S correlations often do not exist, for example, near the surface, or in dynamic frontal zones, regions where values of oceanographic properties can change rapidly and dramatically.

Water types are characteristic inflection points on a T-S diagram. Mixing between several water types leads to region-specific water masses which are particular regions along a T-S diagram. Water masses tend to be identifiable over large geographic regions. The characteristic water masses of this part of the North Atlantic include the Subtropical Underwater (SUW), the 18° Water, the Antarctic Intermediate Water (AAIW), the North Atlantic Deep Water (NADW) (including the Upper, Middle, and Lower Deep water), and the Antarctic Bottom Water (AABW). Fig. 3-17 shows that increased rms sound speed deviations can be associated with the different water masses of the region.

Centered around 80 m is a region of high sound speed variability due to salinity variations in the high salinity Subtropical Underwater. This water mass is formed in the Subtropical region in summer under conditions of low winds, strong solar insolation, and little rainfall. The resulting minimal vertical mixing and excess of evaporation over precipitation causes high salinity values (over 37.2 psu) to occur in the near-surface layers and this dense, high salinity water sinks and spreads throughout the southern North Atlantic and the Caribbean as a high salinity tongue.

The 18° Water is formed in winter at the surface just south of the Gulf Stream, and it sinks and spreads throughout the Sargasso Sea. A small increase in sound speed variability between 300 - 400 m is probably associated with the influx of a larger, deeper mass of 18° Water during the course of the experiment (see later section).

Between about 400 - 1200 m is the low salinity Antarctic Intermediate Water, formed many years earlier at the surface in the Antarctic near the Antarctic Convergence. Its core is located near 800 m, and a peak in sound speed variability around this depth is associated with variations in its salinity.

Between 1200 m and about 4400 m lies the North Atlantic Deep Water. The Upper North Atlantic Deep Water (UNADW) (roughly 1200 - 2000 m) has relatively high salinity due to the effects of the Mediterranean Outflow Water which spreads out from the Straits of Gibraltar throughout the whole North Atlantic. Significant sound speed variability occurred

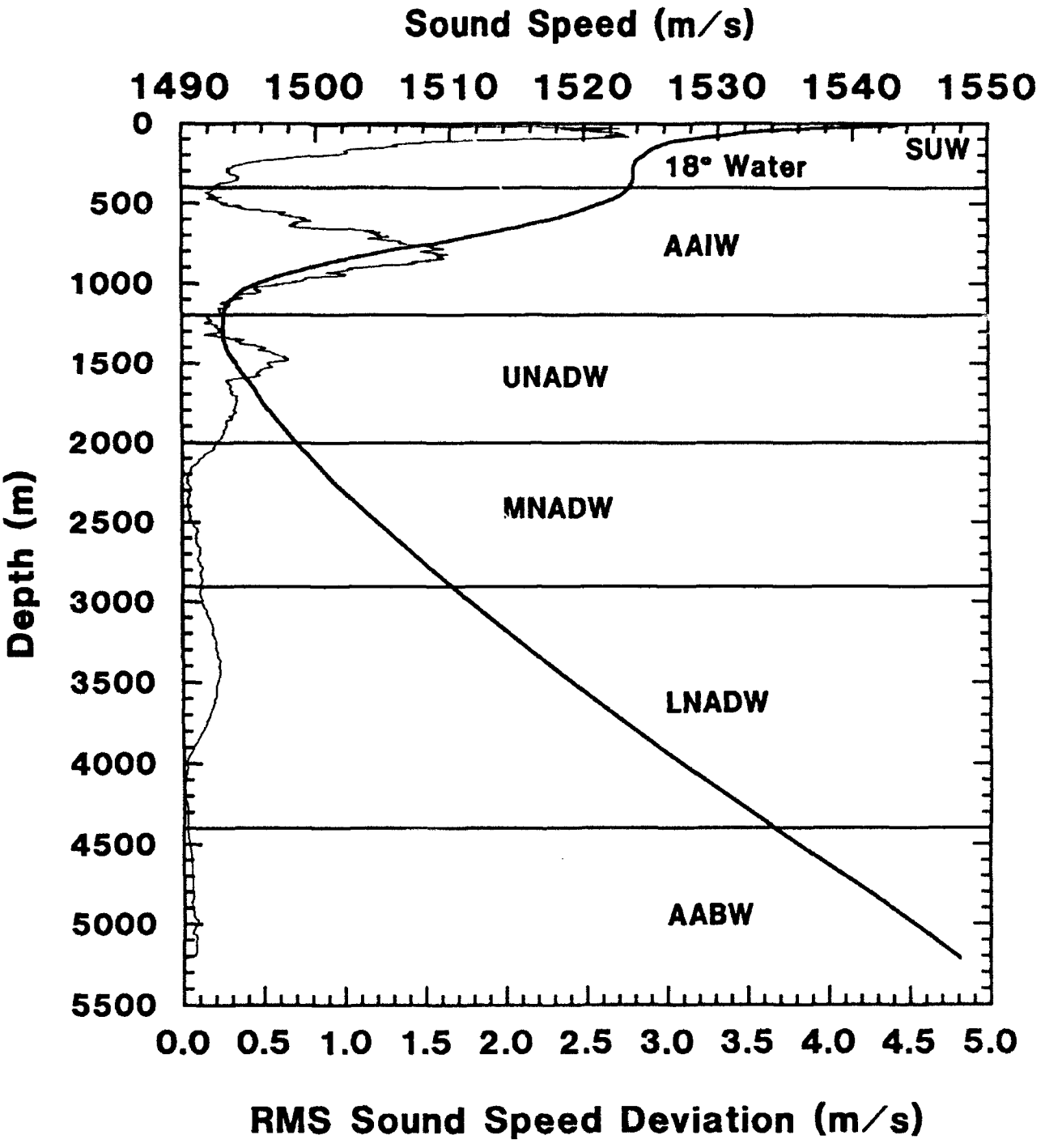

Figure 3-17. Mean sound speed profile and rms sound speed deviation at the MDA site. Depth regimes of the various water masses are indicated. Acronyms are identified in the text.

at the instrumentation site in the UNADW and is discussed in greater detail later. This variability must reflect actual salinity inhomogeneities in the water mass.

The Middle North Atlantic Deep Water (MNADW) (about 2000 - 2900 m) is primarily distinguished from the other water masses by an oxygen maximum, not a relevant parameter here. It is not easily separated from the Lower North Atlantic Deep Water (LNADW) (2900 - 4500 m), although there is a minor increase in sound speed variability at about 3500 m in the LNADW.

Below 4500 m lies the Antarctic Bottom Water, formed in the Weddell Sea of the Antarctic. Wuest (1978) indicates that near the instrumentation site much of the AABW has mixed with NADW, but further to the south along the 157 track a larger percentage of AABW exists at this depth. The observed near-bottom sound speed change along the 157 track of 0.6 m s^{-1} is a result of this N-S gradient in AABW.

Horizontal Planes

Sound speed, estimated sound speed error, and geostrophic currents at 0, 100, 200, and 700 m are plotted in Figs. 3-18 through 3-21 to give an overview of the structure of the sound speed fields and circulation fields during June and July 1991. Although no ships went along the MDA tracks in June, they are shown on the plots for orientation and comparison purposes. Over most of the region surrounding the MDA triangle the estimated sound speed error is less than 0. 5 m s^{-1}.

In June (Figs. 3-18 and 3-19) the Subtropical Front was fairly well defined at 100 and 200 m, centered at around 25°N in the MDA region, with evidence of a number of eddy-like features. Many of the eddies seem to occur in opposite rotating pairs in both months. By July (Figs. 3-20 and 3-21), when the MDA experiment took place, the Front was less well defined and current magnitudes were somewhat less. Other changes in the features can also be identified (Fig. 3-22). The southward extension of the Front passing through the 157 track pinched off by July into a strong cold core (counterclockwise, or cyclonic) eddy centered near 25.5°N. Near the instrumentation site the warm core (clockwise, or anticyclonic) eddy and flow from the north in June shifted northwestward so that in July strong southward currents of nearly a knot passed through the instrumentation site and the anticyclonic eddy was centered near 70.25°W, influencing the environment along the 270 track. The flow through the site was strong enough to cause significant complications during the instrument deployment. There is some indication that the flow consisted of two merging streams: a warmer one from the west and a colder one from the east. In July the eastern part of this flow meandered through the 175 track towards the 157 track, where a portion curved counterclockwise into the eddy formed by the pinching off of the Front, while the rest continued on south. Other warm and cold core eddy-like features are located near the southernmost ends of the 175 and 157 tracks, as well as elsewhere within the study region. The two eddies at the end of the 175 track were identifiable during both months.

The Antilles Current is not apparent in the upper 100 m in either month, but 200 m and below do indicate a general northwestward flow in the southern part of the region. This is

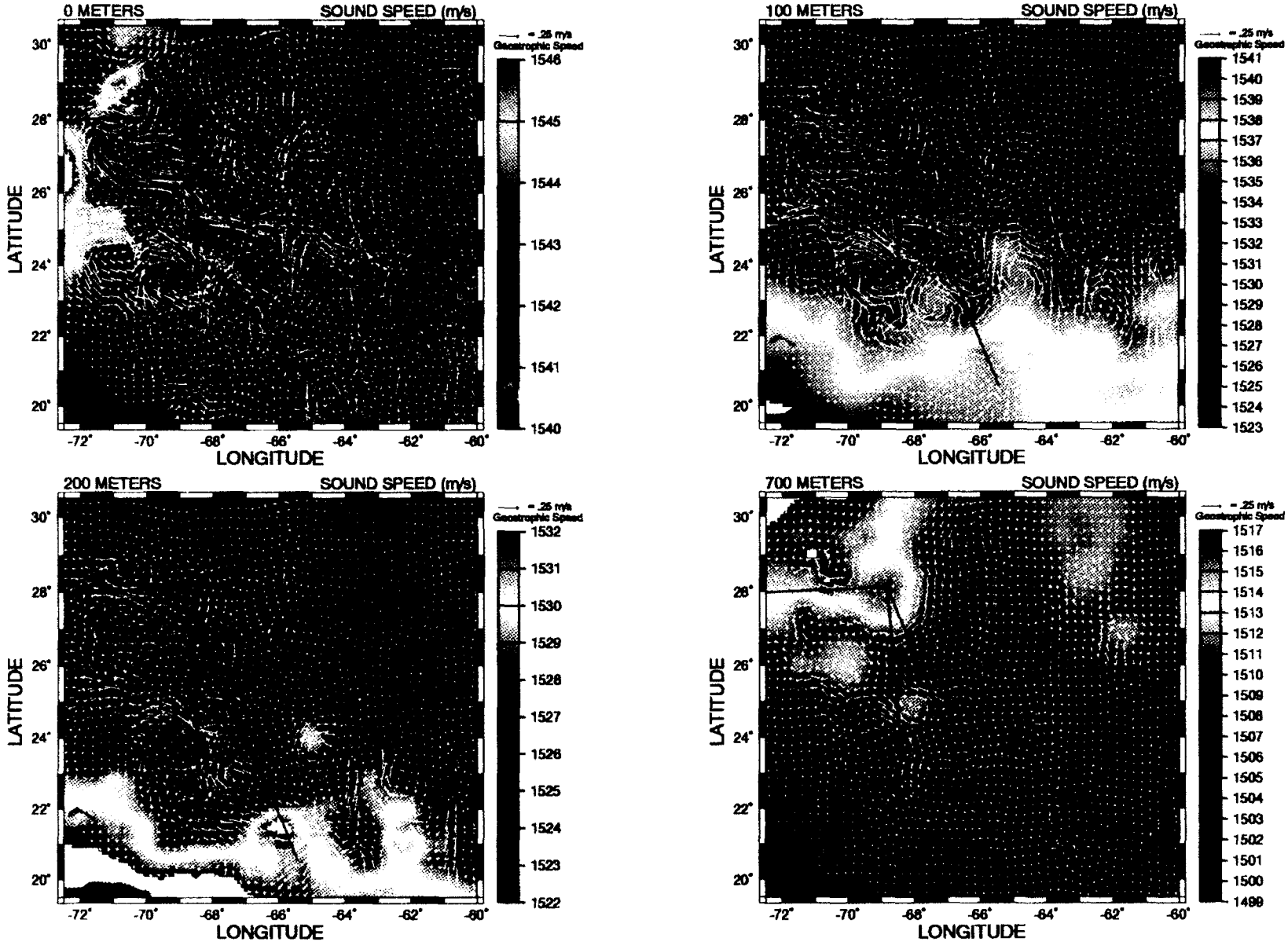

Figure 3-18. Sound speed at 0, 100, 200, and 700 m and geostrophic currents (referenced to 5000 m) in the MDA region during June 1991. Data used were all AXBTs from the four flights on year days 170, 171, 173, and 174 plus one third of the AMODE/MST CTDs during June.

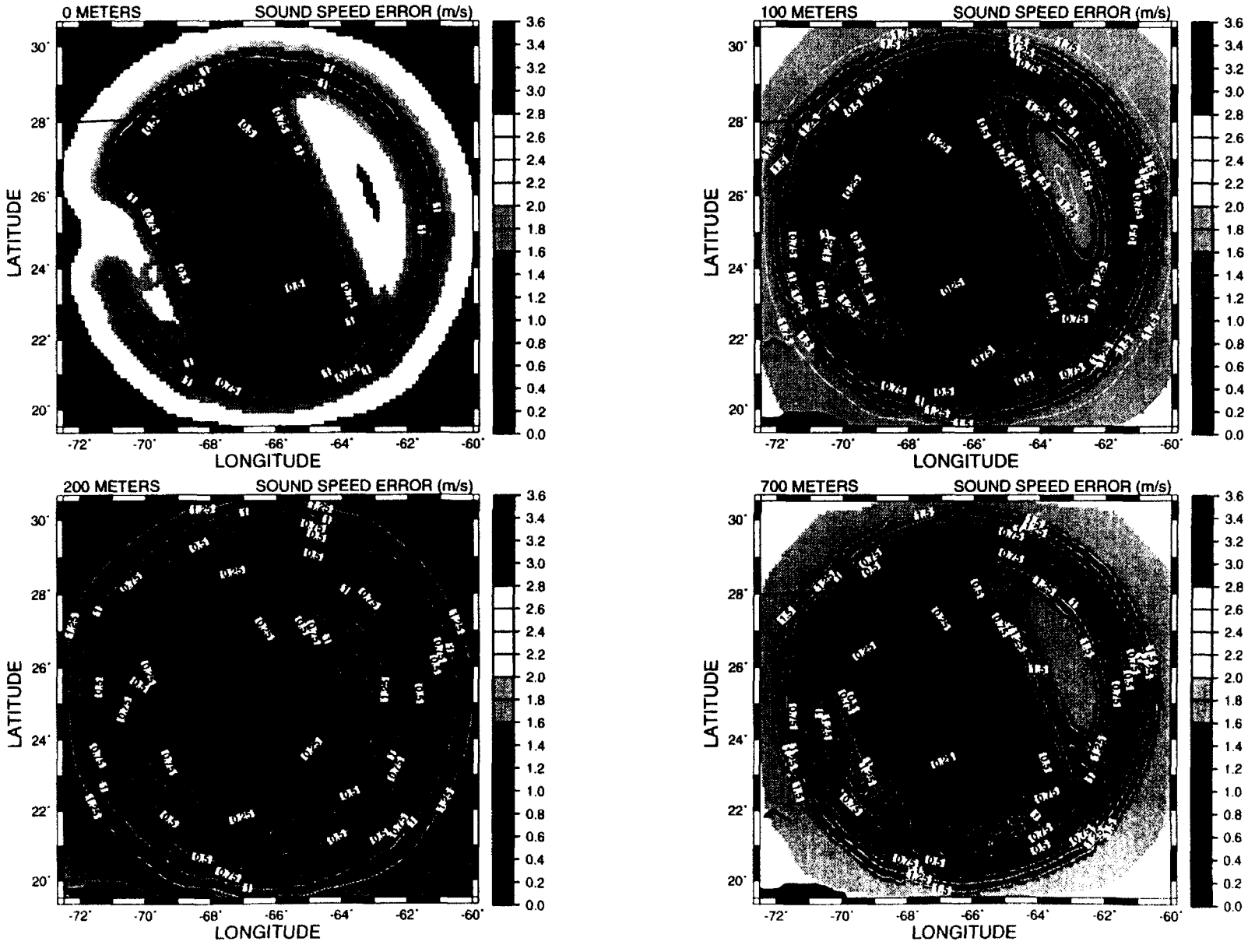

Figure 3-19. Estimated sound speed errors for the fields shown in Fig. 3-18.

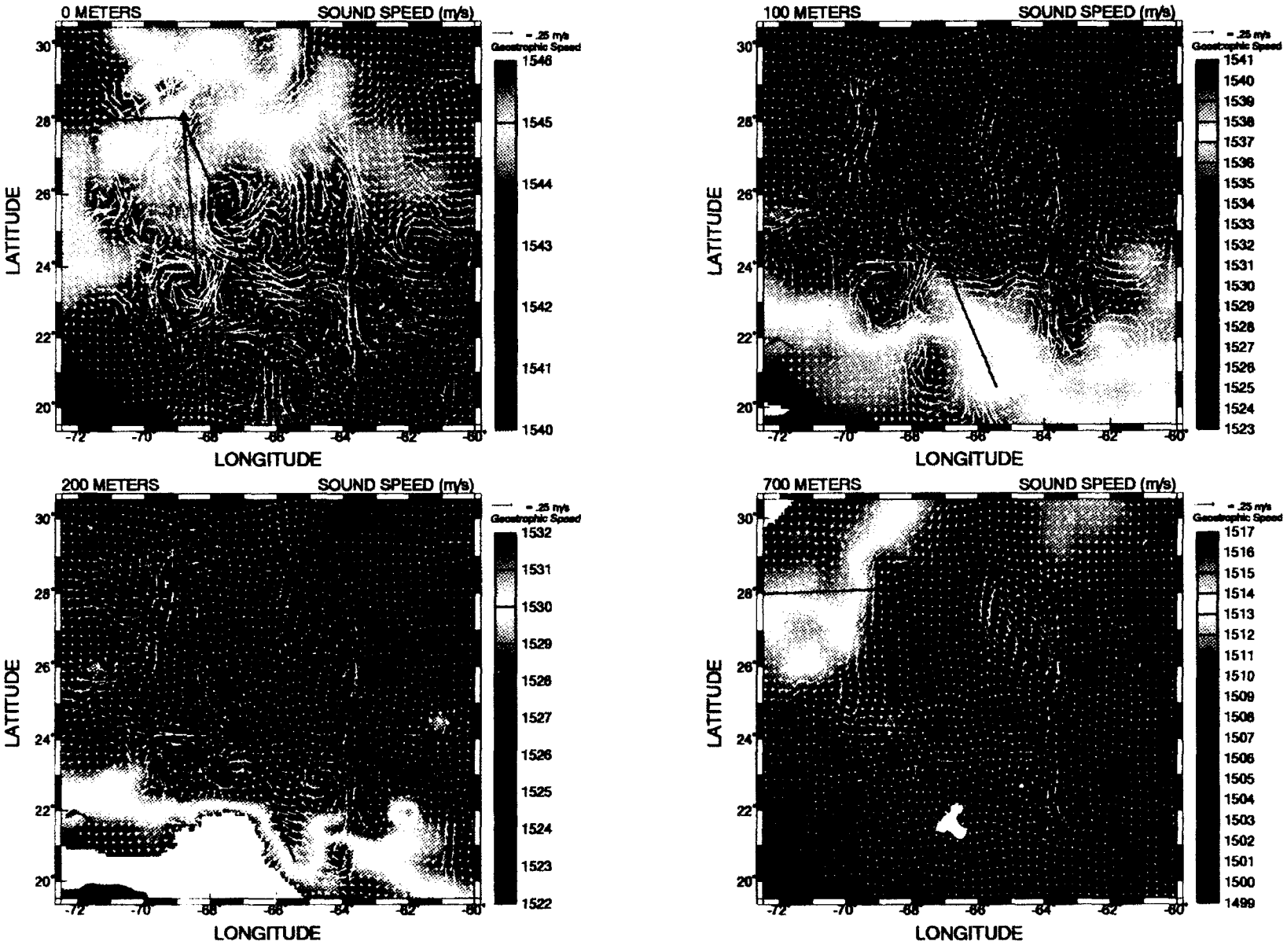

Figure 3-20. Sound speed at 0, 100, 200, and 700 m and geostrophic currents (referenced to 5000 m) in the MDA region during July when the MDA acoustics operations took place. Data used were all AXBT, CTD (MDA only), and XBT data within three days on either side of year day 200.

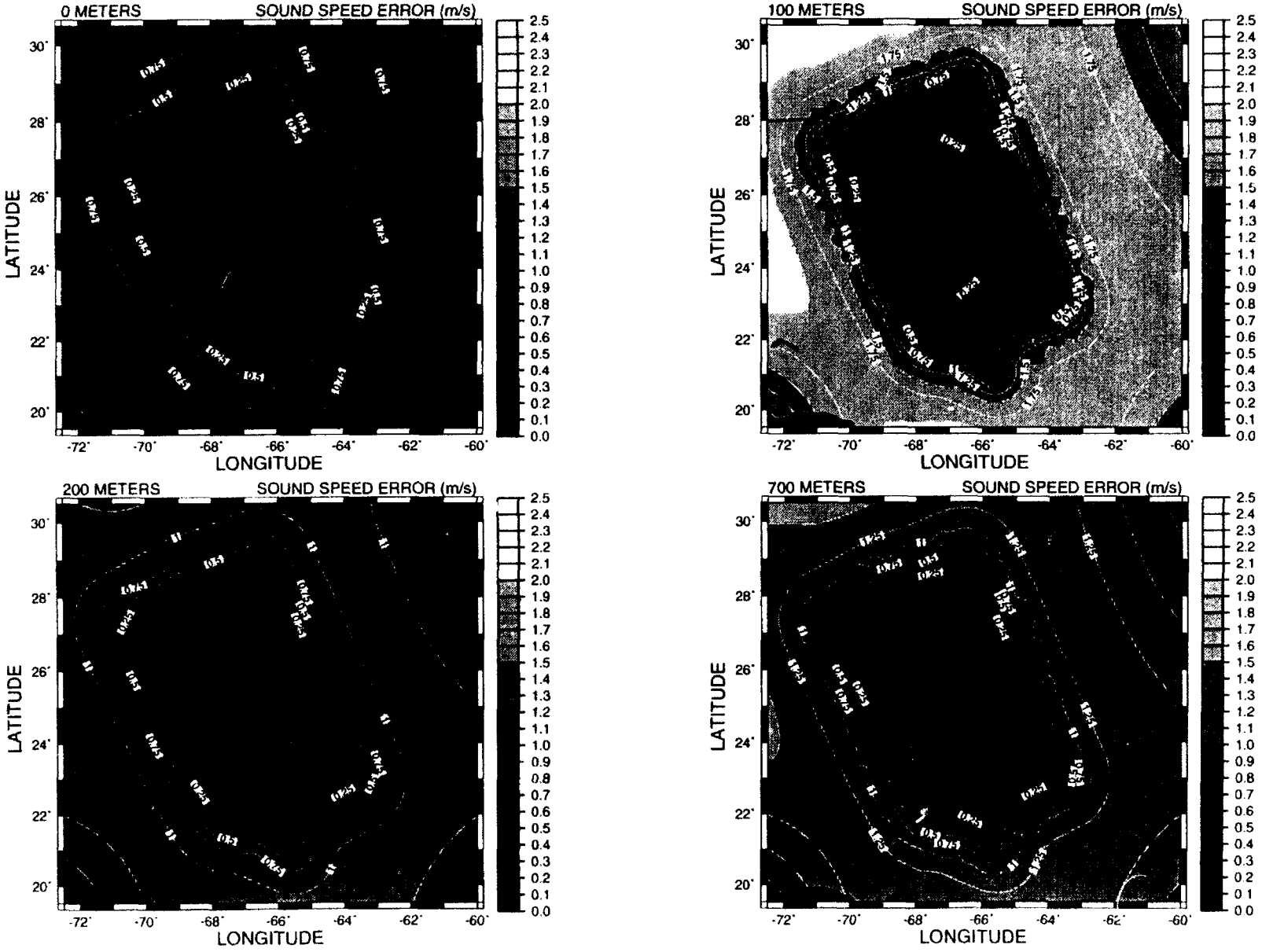

Figure 3-21. Estimated sound speed errors for the fields shown in Fig. 3-20.

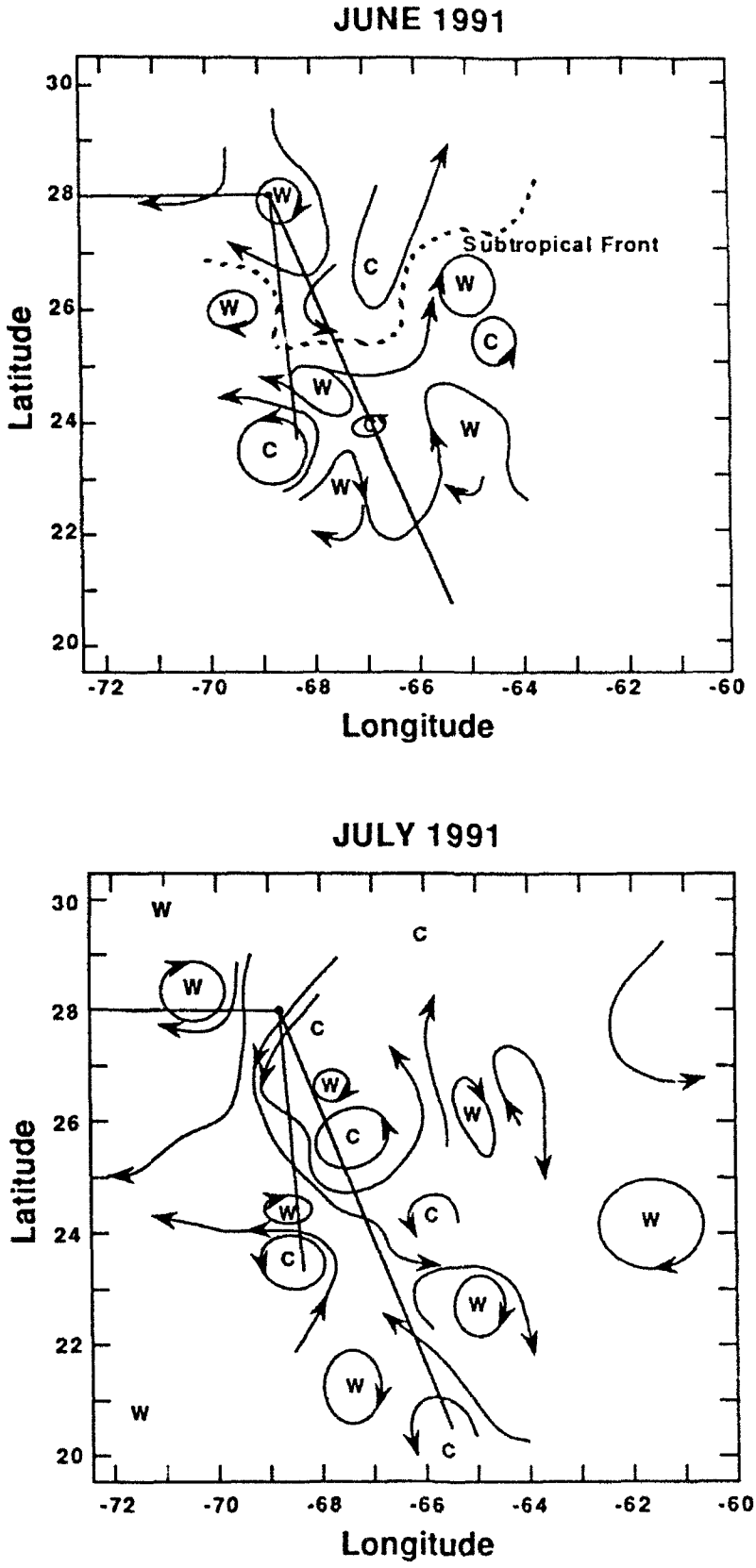

Figure 3-22. Schematic of the upper layer oceanographic features and flow fields in the MDA area for June and July 1991.

outside the region of highest data density, and the plots begin to revert to climatology (Levitus). Probably the most that can be concluded is that there was not a strong Antilles Current through the MDA study region itself, but it could have existed further south.

In the upper right hand portion of the 0 and 100 m plots, a flow from the northeast is seen to enter the area, then curve counterclockwise to form an eastward-directed flow. This feature is primarily climatologically-determined, since there were only a few AMODE/MST CTD stations in the area, but this may be the climatological signature of the Subtropical Counter Current.

Mixed layer depth in June and July as determined from the gridded aircraft flights is shown in Fig. 3-23. In general the layer depth went from shallowest in the north to progressively deeper towards the south. As would be expected from the surface warming that takes place as summer progresses, depths in July were somewhat deeper than depths in June. In June the layer depth ranged from 10 or 15 m in the north to 30 or 35 m in the south. In July depths in the north were about 15 or 20 m and about 45 to 65 m in the south.

270 Track

The 270 track was designed to extend from the instrumentation site westward up onto the continental slope. Mixed layer depth along the 270 track (not shown) ranged from about 15 m near the instrumentation site to about 20 m towards the west. Climatological (GDEM and Levitus) and measured sound speeds along the track are shown in Fig. 3-24 and the differences between the climatological fields and the observed field in Fig. 3-25. The continental shelf and slope are quite apparent. Deviations between GDEM and the observed field tend to be larger than deviations between Levitus and the observed field. Aside from near the surface where large deviations from climatology are expected, the largest differences between measured and both climatological fields occurred in the vicinity of 800 m depth at a range of about 200 km. The maximum difference from GDEM was -5.5 m s^{-1} (observed faster) and from Levitus about -4 m s^{-1}. Another larger deviation from GDEM (about +4 m s^{-1}) was centered at a range of about 600 km. A small region of relatively large (up to -3 m s^{-1}) deviations from Levitus occurred at a range of about 700 km. Below 1500 m all three fields agreed to within 0.25 m s^{-1}.

The topography of the 1524 m s^{-1} isovelocity line may be used to associate features in the oceanography with the sound speed structure. The most noticeable feature is the distinctive downward bowing of the 1524 line and, to a lesser extent, of the other lines in the upper 1000 m or so. This is associated with the general anticyclonic flow through the first 300 km of the 270 line and in particular with the distinctive warm core eddy mentioned above. Otherwise, the sound speed averaged about 1542 m s^{-1} near the surface, 1552 at the deepest part along the track, and about 1491 - 1493 in the deep sound channel at about 1250 m depth.

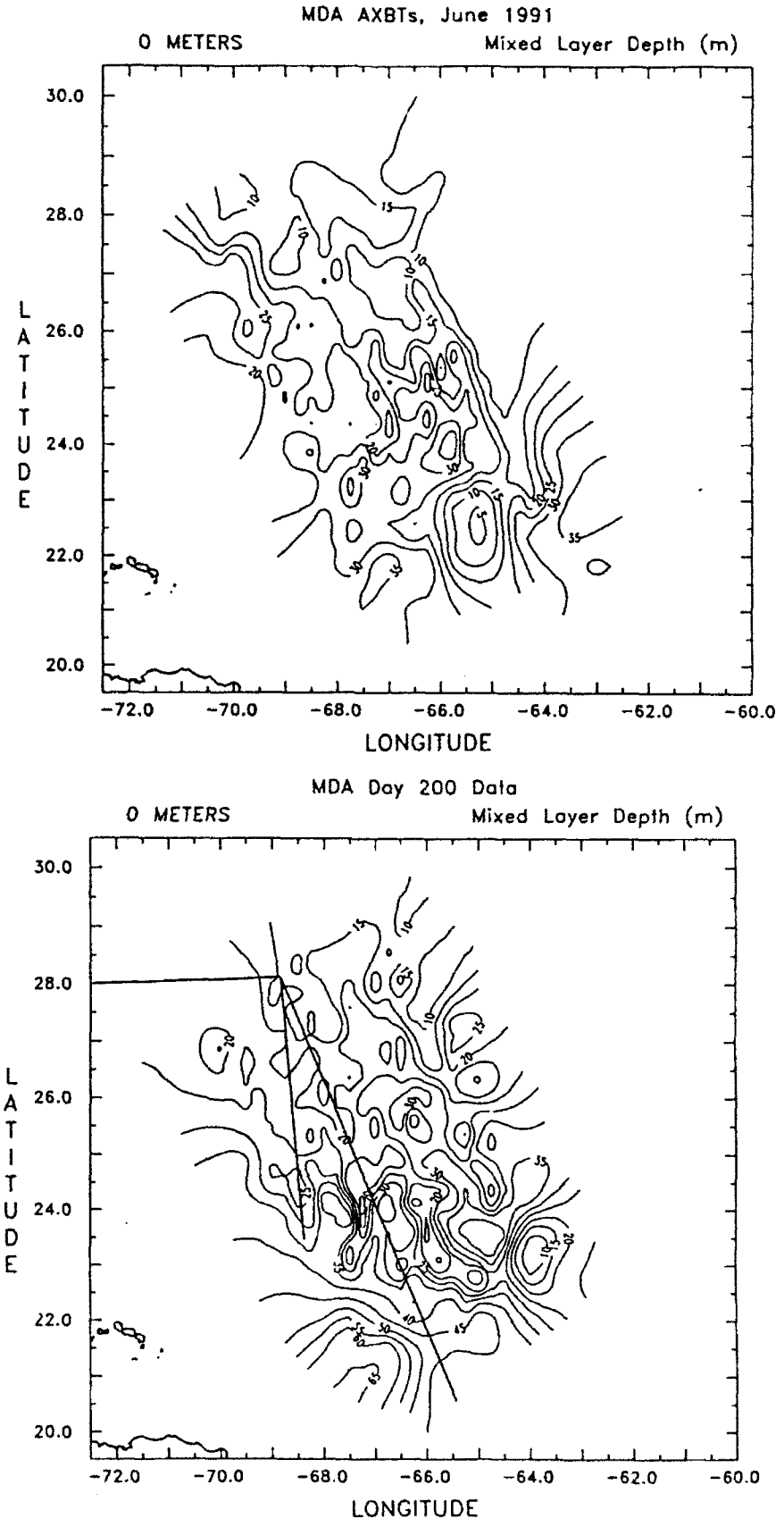

Figure 3-23. Mixed layer depth in June and July 1991 in the study area as determined from aircraft flights. The location of the MDA tracks is shown on the July plot.

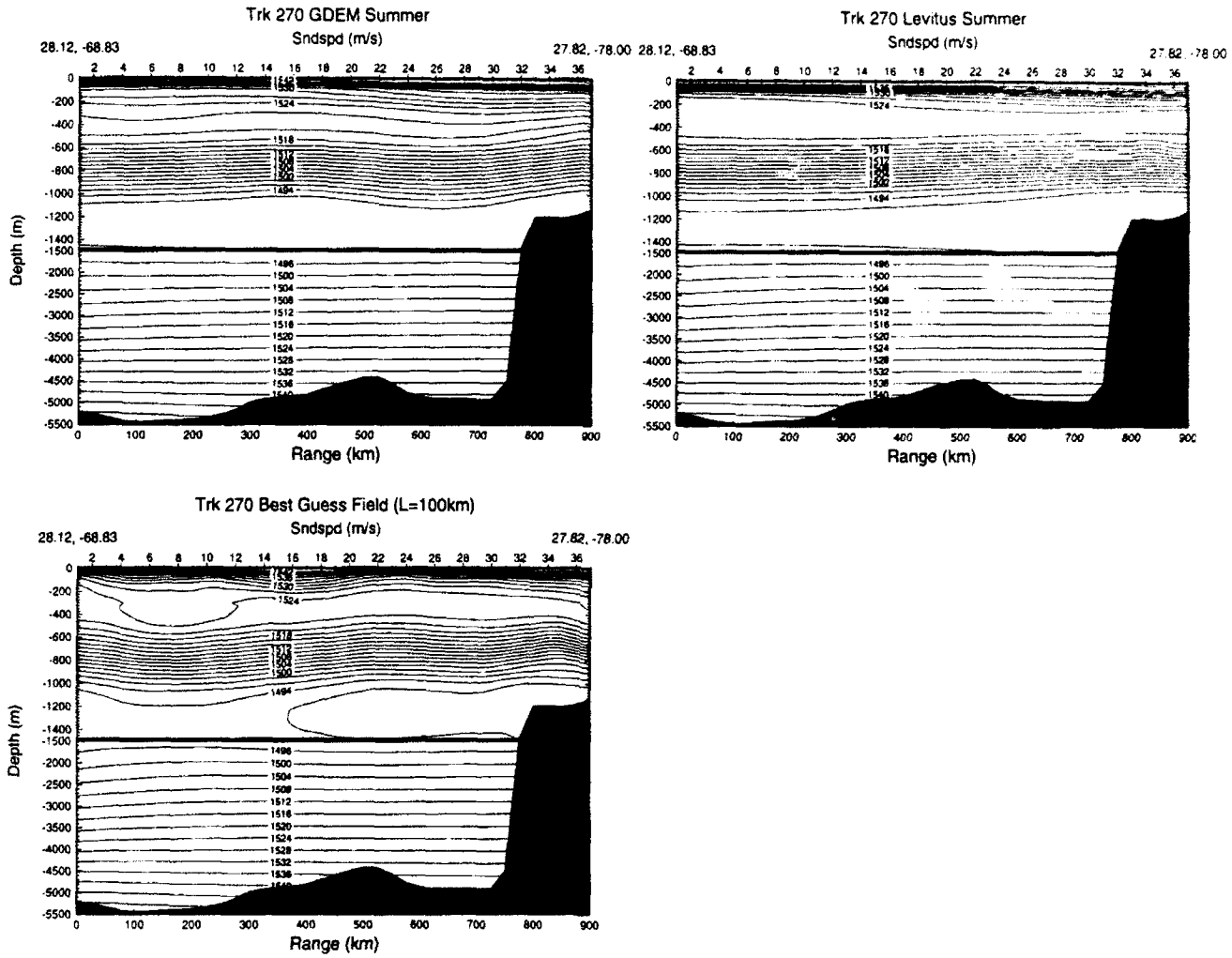

Figure 3-24. GDEM, Levitus, and measured sound speed along the MDA 270 track.

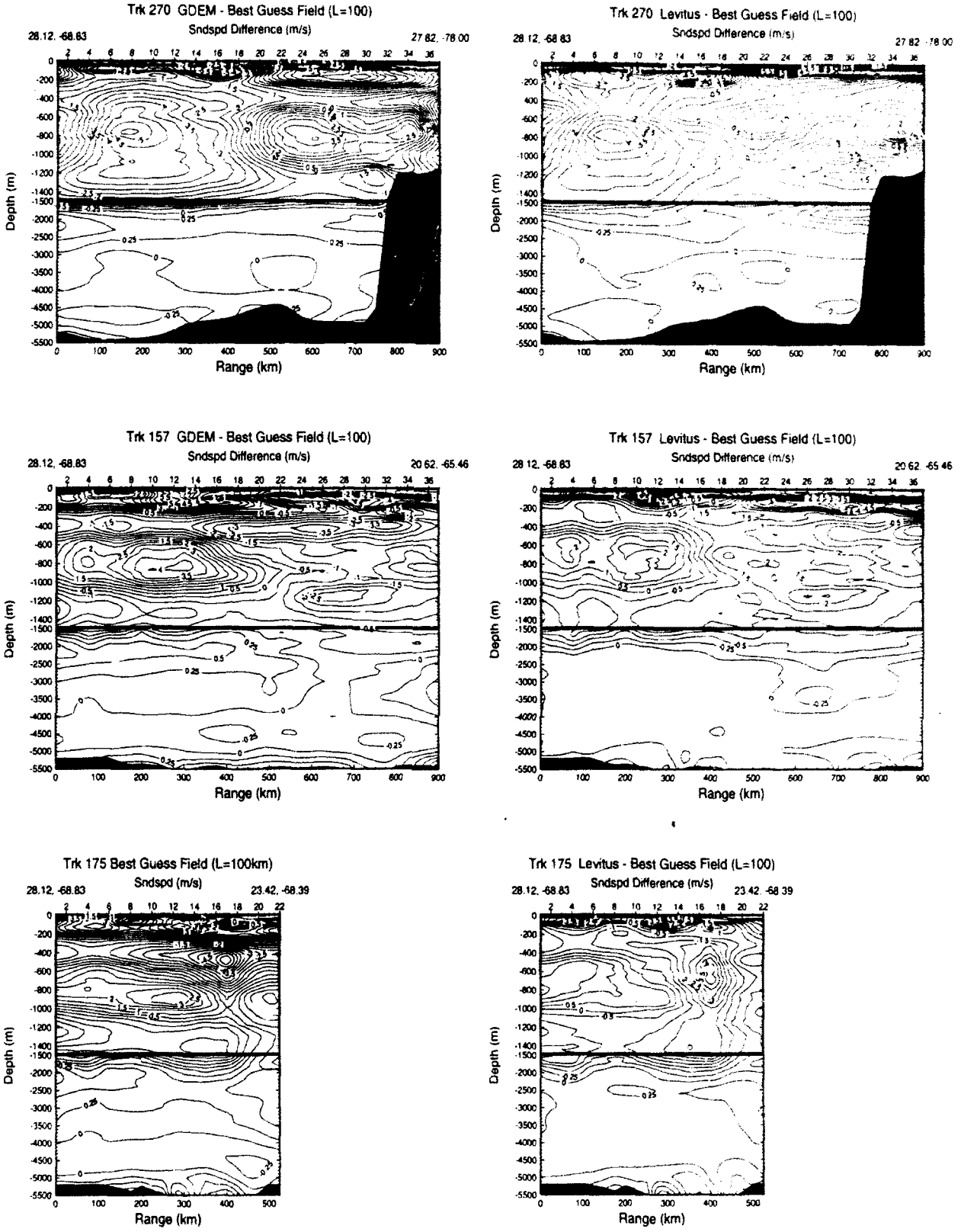

Figure 3-25. Differences between GDEM and Levitus climatologies and the observed fields along all three MDA tracks.

157 Track

The 157 track was the longest track, extending 900 km south southeast of the instrumentation site. Mixed layer depth (from Fig. 3-23) gradually deepened from around 15 m near the site to around 45 m at its southern end. GDEM and Levitus climatological sound speed and observed sound speed centered around day 193 and around day 200 are given in Fig. 3-26. Differences between the climatologies and the observed field at day 200 are shown in Fig. 3-25. Again, deviations between GDEM and the observed field are somewhat larger than between Levitus and the observed field. Below the near-surface region, maximum deviation of GDEM from the observations -- about +4 m s^{-1} -- was centered at a range of about 300 km and depth of 900 m. Levitus showed deviations over much the same broad region as GDEM, but the largest value was about +2 m s^{-1}. GDEM also exhibited fairly large deviations of up to -3.5 m s^{-1} centered around 400 m in depth and over ranges of 400 - 900 km. Levitus' deviations over the same region were about -1.5 to -0.5 m s^{-1}. Below 1500 m deviations were usually within 0.25 m s^{-1}, but in some places were as large as 0.5 m s^{-1}.

The topography of the 1524 m s^{-1} isovelocity line may be related to the oceanographic context given in Figs. 3-20 and 3-22. The upward slope of the line in the first 100 km or so of range is due to the flow from the north through the instrumentation site, and its subsequent downward bowing is related to the weak warm core eddy-like feature seen in Fig. 3-22. Notice in Fig. 3-26 that between day 193 and day 200 the warm signature was reduced in magnitude. This may be attributed to an increase in the width or strength of the flow from the north through the MDA site and/or a move of the warm eddy-like feature to the east. As is noted below, noticeable changes in the site sound speed profile started around day 192 that suggested an increased penetration of 18° Water from the north. Then from a range of 225 km out to 475 km the cold core eddy mentioned earlier is associated with the upward, then downward bowing of the line. Past a range of 475 km few significant oceanographic or acoustic features occur except for the obvious increase of the mixed layer depth. Variations of a few m s^{-1} in the vicinity of the sound channel axis (1492 to 1494 m s^{-1}) are probably associated with slight water mass variations as were observed in the time series at the instrumentation site (discussed below), but the horizontal data coverage does not exist at this depth to associate them with any particular ocean structure. Surface sound speed ranged from about 1543 to 1545 m s^{-1}, while maximum bottom sound speed was about 1551 m s^{-1}.

175 Track

The 175 track was 525 km long. Mixed layer depth (Fig. 3-23) ranged from about 15 m near the instrumentation site to 35 m at the far end of the track. GDEM and Levitus climatological sound speed and measured sound speed are shown in Fig. 3-27, and the differences between the climatologies and the measured sound speed in Fig. 3-25. Both GDEM and Levitus showed large deviations from the observed field centered around 500 m depth and near a range of 400 km. The maximum GDEM deviation was about -5.5 m s^{-1}, while the maximum Levitus deviation was about -4 m s^{-1}. GDEM also had a region of

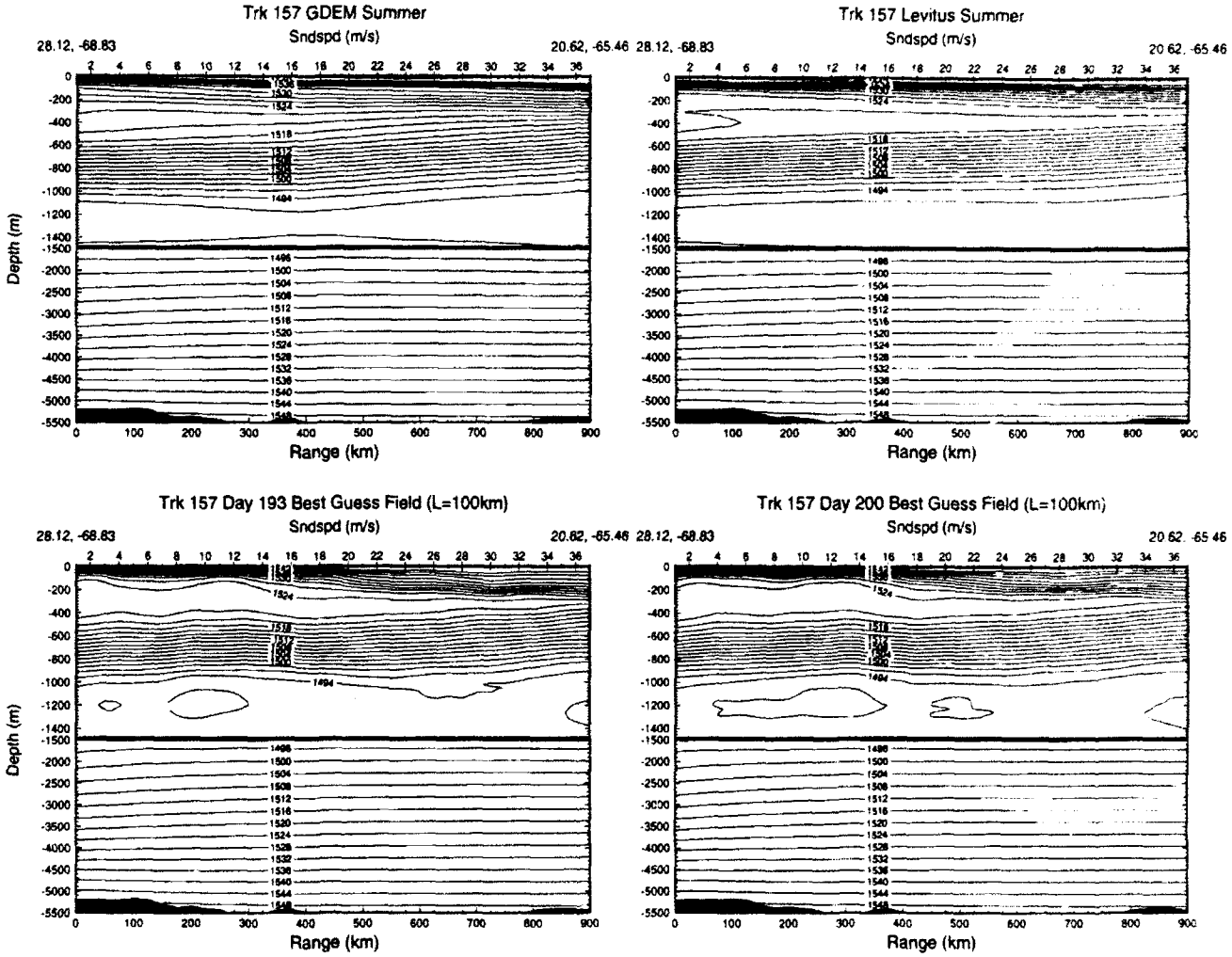

Figure 3-26. GDEM, Levitus, and measured sound speed along the MDA 157 track. Two snapshots of the measured fields were made, one centered around day 193 and one a week later around day 200.

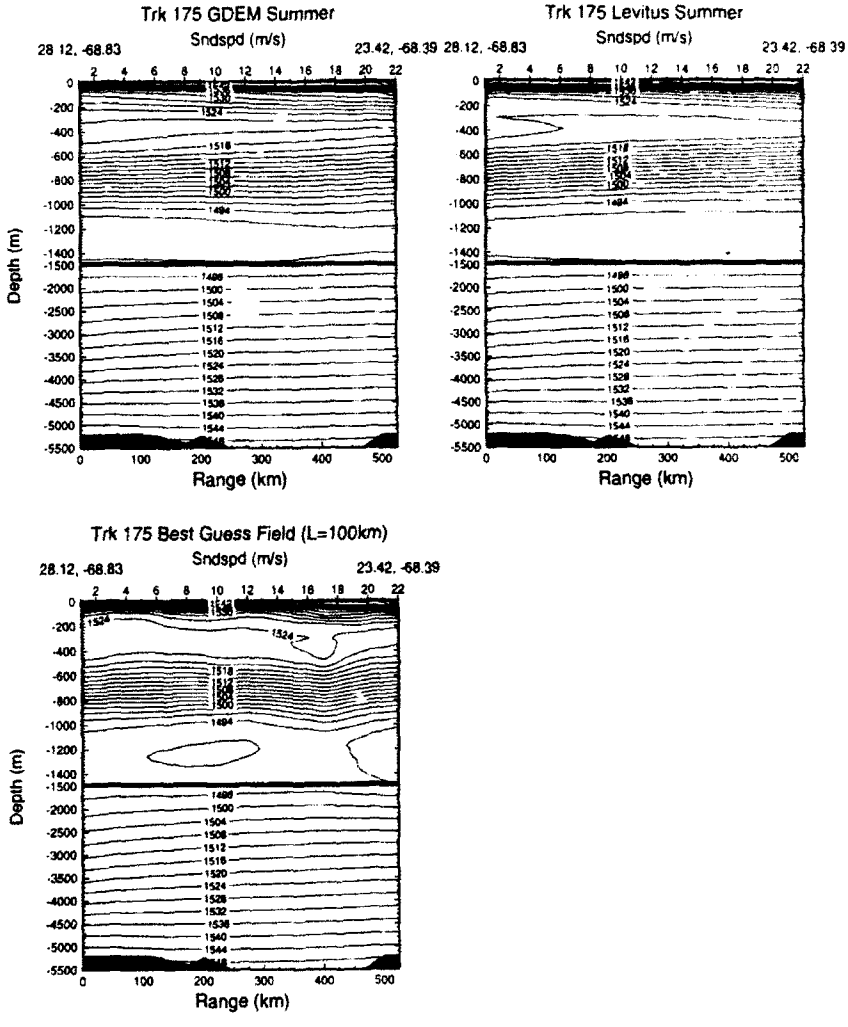

Figure 3-27. GDEM, Levitus, and measured sound speed along the MDA 175 track.

Again, the 1524 m s^{-1} isovelocity line may be related to the oceanographic environment of Figs. 3-20 and 3-22. As along the 157 track, the flow from the north through the instrumentation site is reflected in the upward slope of the line. The bowing and gentle downward slope is a reflection of the meanders and general counterclockwise pattern of the flow as it heads south. The first eddy encountered on the 175 track is a rather small but acoustically significant warm core feature that is reflected in the anvil-shaped excursion of the 1524 line at a range of 350 - 425 km. The weaker cold-core feature at the end of the track accounts for the subsequent upward slope of the line. Note in Fig. 3-20 that the transition between the small warm eddy and the larger cold feature is quite abrupt and results in quite high eastward currents over a narrow region. Surface sound speed along the track was about 1545 m s^{-1}, minimum sound speed at the sound channel axis near 1200 m ranged from about 1491 to 1493 m s^{-1}, and the maximum sound speed in the deepest part of the track was about 1551 m s^{-1}.

Instrumentation-Site Time Series

Because matched field processing is very sensitive to the sound speed profile at the receiver, a time series of surface to bottom sound speed profiles every 6 hours was generated at the site of the acoustic instrumentation (Fig. 3-28). Considerable temporal variability from profile to profile is evident in the figure, and this variability is illustrated even more clearly in Fig. 3-29 where the differences between the mean site profile (Fig. 3-17) and each of the seventy five profiles in the time series are plotted versus depth.

Between about 200 - 400 m lay a region or shelf of nearly constant sound speed (1523 - 1524 m s^{-1}) associated with what is called the 18° Water. The depth extent of this shelf changed over time, as may be seen in Fig. 3-28, and the sound speed itself varied by more than 1.4°C. The profiles from Fig. 3-28 are contoured in the depth-time plane in Fig. 3-30. Using the range between the 1523 and 1524 isovelocity lines in this figure as delimiting the 18° Water region, at the beginning of the experiment the range lay between about 300 and 400 m, while at the end it lay between 150 and 400 m. The changes were first noted around day 192 (Fig. 3-28) (possibly they occurred somewhat earlier but were not picked up until the intensive sampling began). A blob of particularly low sound speed then entered the area around day 194 (13 July), profile #40, and disappeared about two days later (profile #47). Examination of the individual profiles in Fig. 3-28 shows this evolution in more detail. It is almost certain that these changes are associated with advection past the instrumentation site of water of somewhat different characteristics, which is consistent with the strong southerly flow though the region that was discussed in an earlier section. Changes in the sound speed field along the 157 track, for example, are consistent with an increased flow from the north bringing down a more extensive mass of 18° Water.

Not surprisingly, considerable sound speed variation also occurred near the surface, more than 10 m s^{-1} (Fig. 3-29 and 3-31). In the latter figure, the diurnal cycle is clear after about day 192 (July 11) when regular sets of XBTs started to be dropped (prior to then only an occasional CTD or XBT was taken). The cycle is not noticeable at a depth of 6 m or below. Rather drastic sound speed changes appear at 20 m, but this is probably due to variations in the mixed layer depth which was between 15 and 20 m at this location.

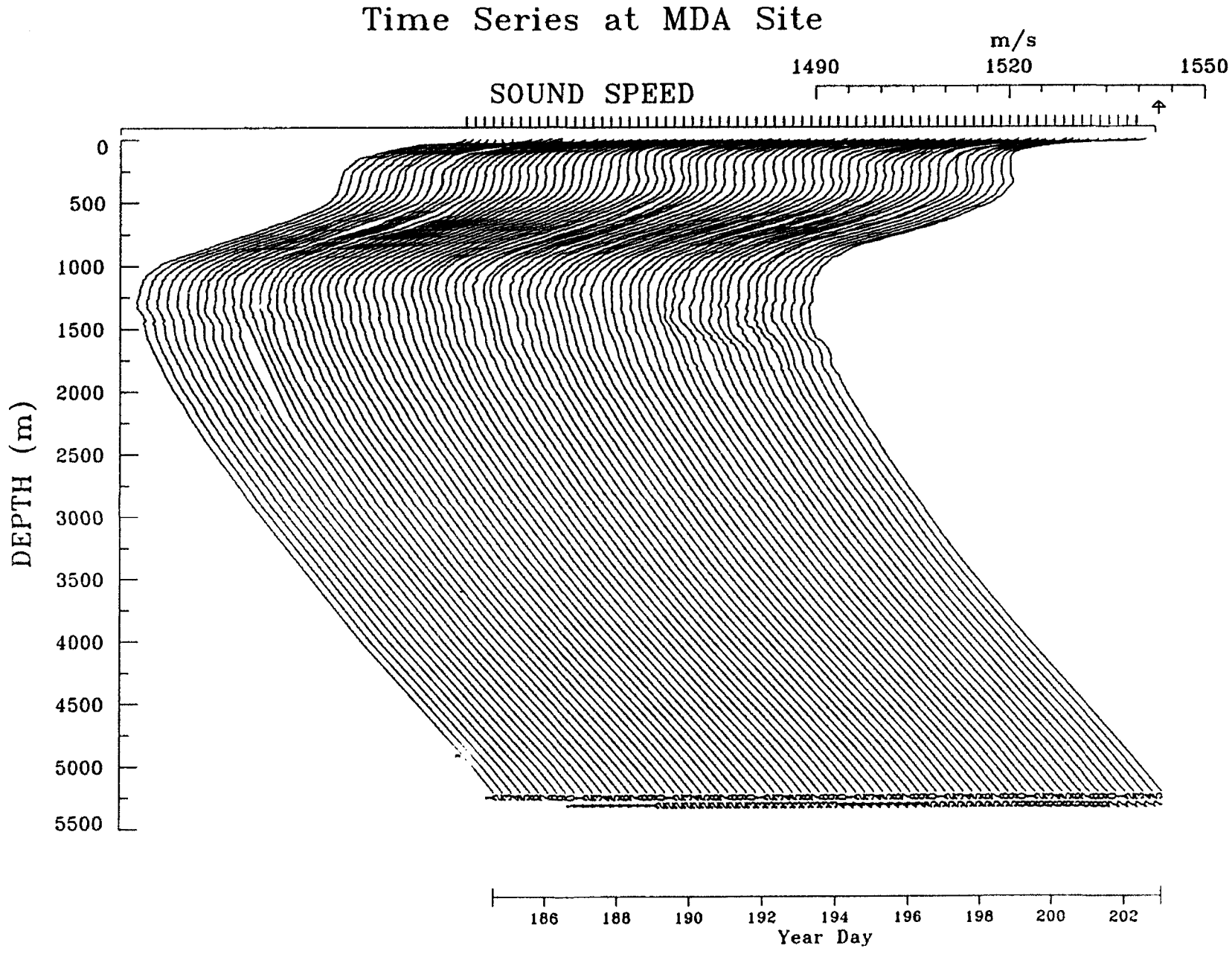

Figure 3-28. MDA site sound speed time series. The series begins on 3 July 1991 (year day 184) 1415 GMT, the second profile is at 1800 GMT, and subsequent profiles are every 6 hours until the last at midnight 22 July (year day 203). Important variations occurred near the surface, between 200 - 400 m, and in the vicinity of the sound channel axis near 1200 m.

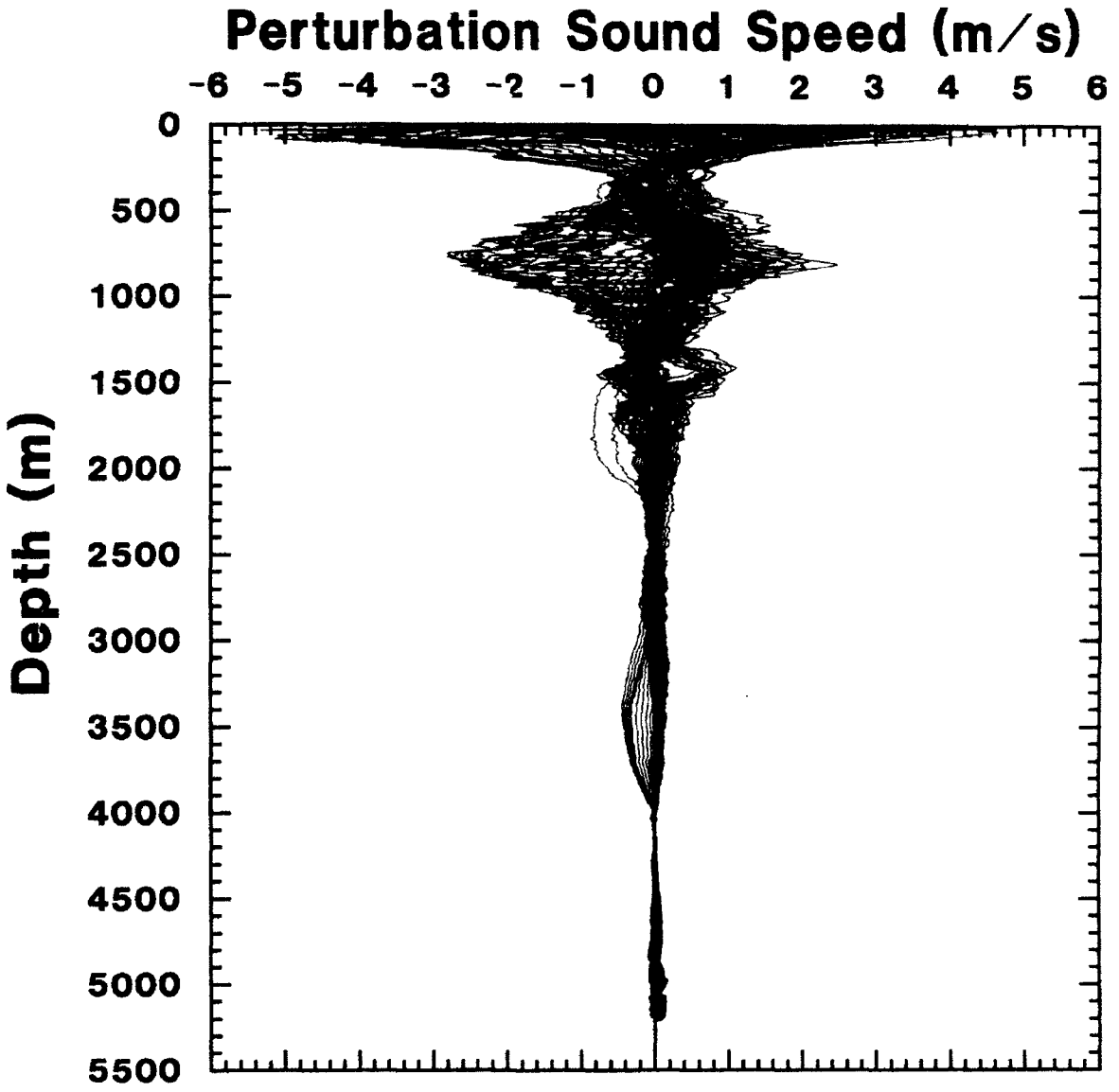

Figure 3-29. Overplot of the difference between the mean MDA site sound speed profile and the seventy five individual profiles in Fig. 3-28. Sound speed near the surface varied by over 10 m s^{-1}, between 200 - 400 m near the 18° Water "shelf" by over 1.4 m s^{-1}, and in the vicinity of the sound channel axis at about 1200 m by over 1.2 m s^{-1}.

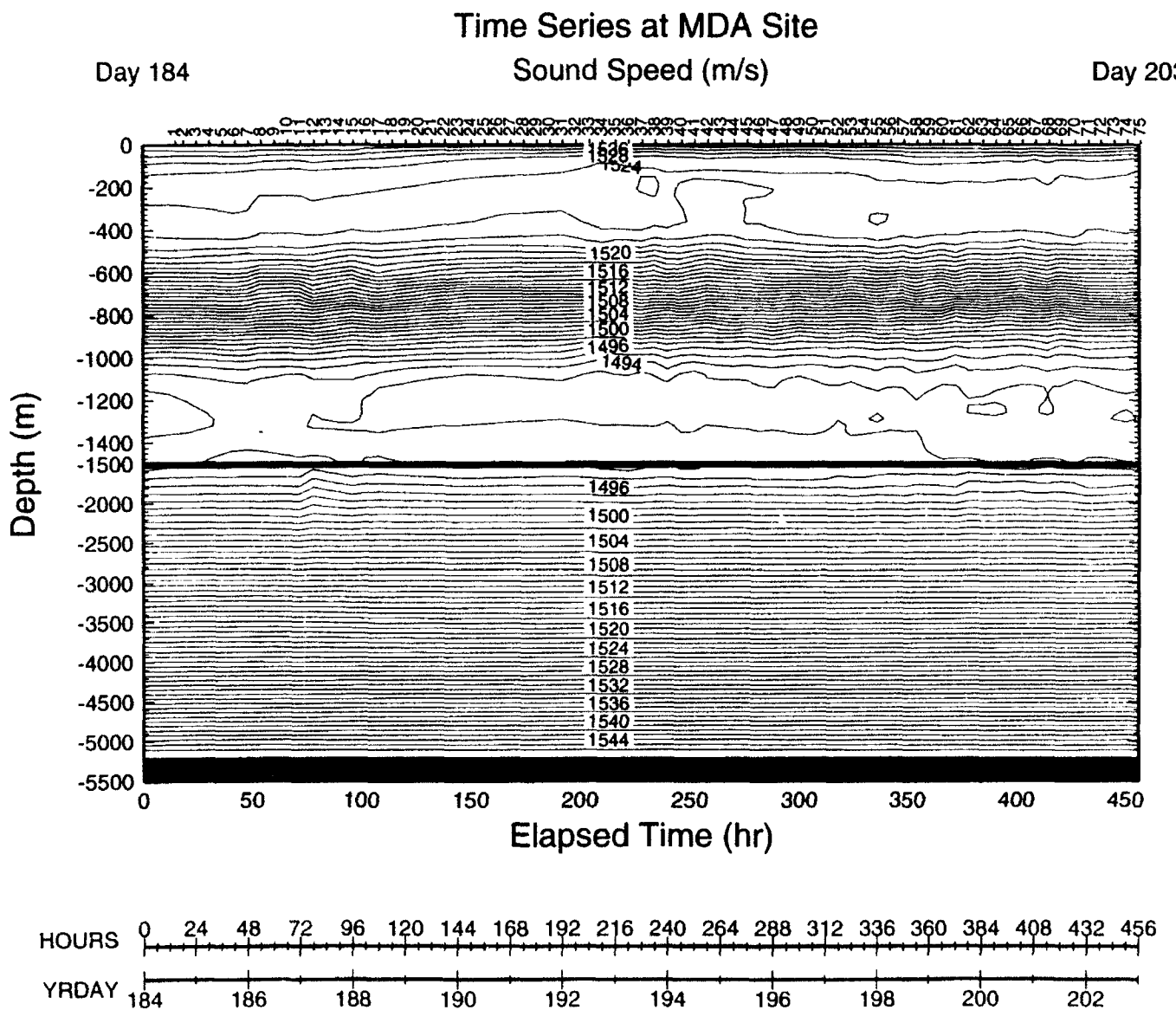

Figure 3-30. Sound speed versus depth at the MDA site from year day 184 1991 (3 July) through year day 203 (22 July). Particular changes in the sound speed structure occurred between about 150 - 400 m and 1000 - 1500 m.

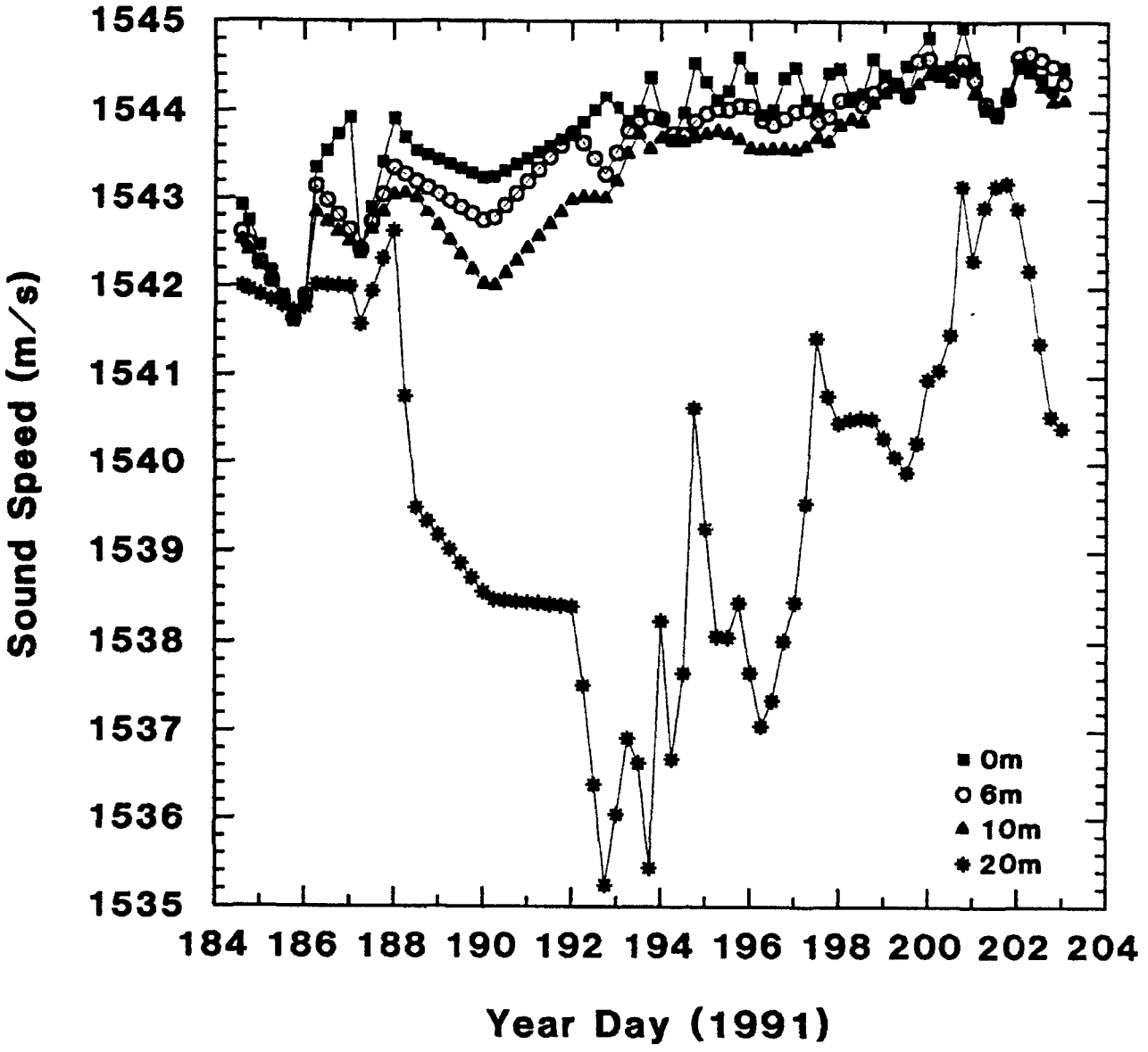

Figure 3-31. Time series of near-surface sound speed at the MDA site at depths of 0, 6, 10, and 20 m. The diurnal cycle is evident only in the surface trace. The large changes at 20 m are due to variations in the sonic layer depth.

Considerable variability of over a meter per second also occurred at depths several hundred meters on either side of the sound channel axis located around 1200 m. The time series in Fig. 3-28 shows some minor fluctuations occurred up to about profile #58 (17 July, 1800 hrs). Then from profile #58 on the shape of the profile near the sound channel axis became much more irregular, as if some blob of water with somewhat different characteristics penetrated into the area. Since data deeper than 1000 m was only taken along the track lines and at the instrumentation site, the horizontal distribution of the data at these depths is inadequate for us to associate the changes with any particular intermediate depth ocean circulation patterns or property inhomogeneities. The conclusion can be drawn, however, that horizontal inhomogeneities of over a meter per second must exist.

Comparison of Tomographic and Classical Measurements

Tomography sound speed along the 157 track, computed using a Levitus initialization field and incorporating only the travel time data and MST/AMODE CTDs is shown in Fig. 3-32, along with the data measured with classical techniques from day 200, and the differences between the two. Maximum differences ranged from about -2 to +2 m s^{-1}. The regions of highest difference are near the surface, around 200 m, and between 400 - 900 m. The differences in the latter regime seem to have a periodicity of about 250 km. One way of comparing the two different pictures of the sound speed environment is through comparing their effects on matched field processing. This comparison is presently underway (Heitmeyer and Boyd, in preparation for Journal of Underwater Acoustics), but the findings can be summarized by saying that there were not striking differences between the results from both the classical sound speed fields and the tomographic fields.

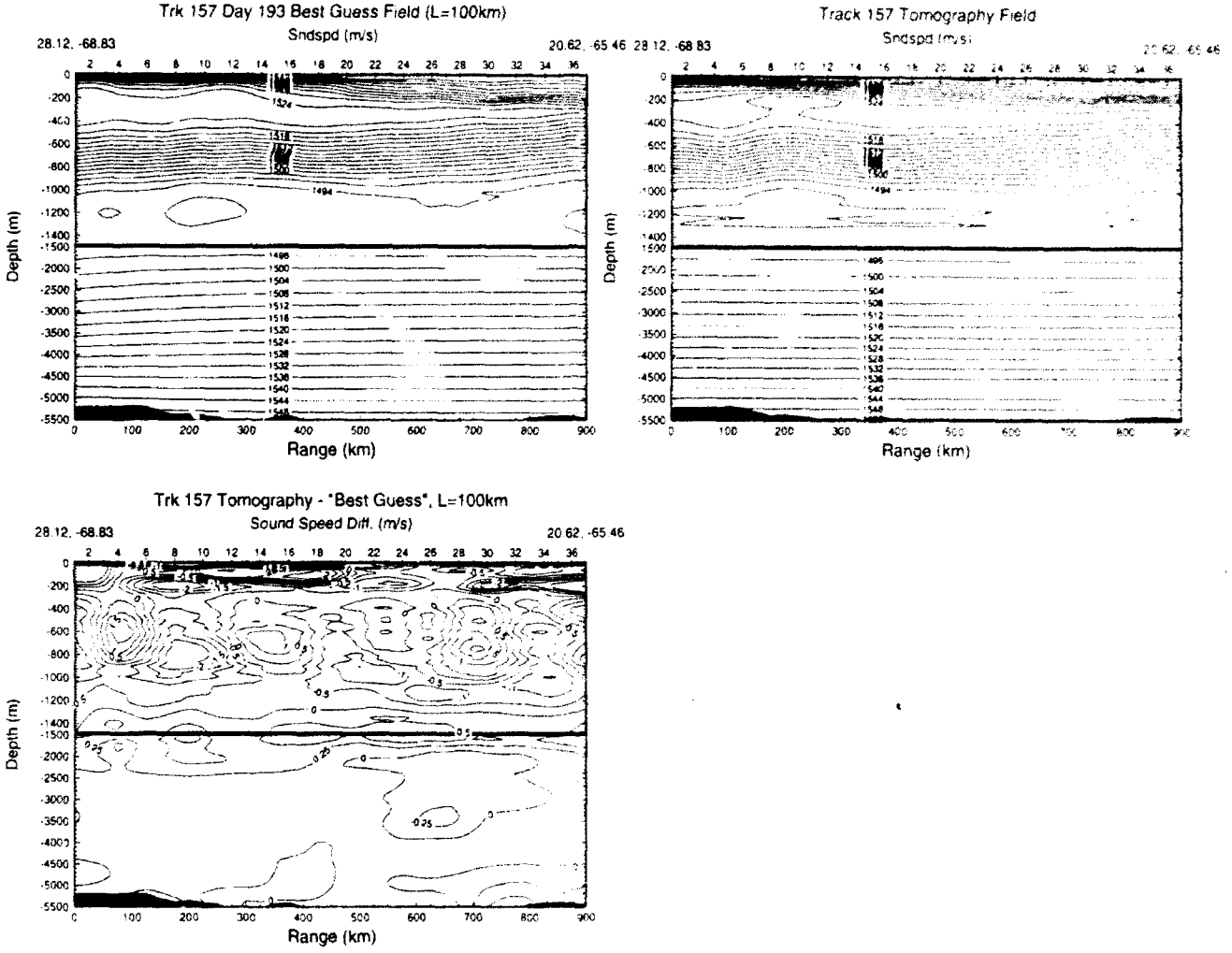

Figure 3-32. Tomography derived and direct measurement sound speed fields along the 157 track, and the difference between the two.

4.0 CONCLUSIONS FROM THE HGI EXPERIMENTS

In the Introduction it was pointed out that mesoscale and submesoscale variability in the oceanic sound speed field significantly effects long-range acoustic propagation. Two major issues were identified. First, how should the sound speed fluctuations due to mesoscale and larger/slower processes be determined and what sampling errors are tolerable for selected applications such as matched field processing? Is it feasible with present day techniques to determine the sound speed field this accurately over long ranges? Second, what limits are imposed by the submesoscale and smaller/faster processes (primarily internal waves)? Is the rule of thumb that submesoscale processes do not seriously limit analyses at propagation distances of 20,000 wavelengths more or less correct?

The answers to these questions are still being explored in the ongoing analyses of the datasets obtained from VAST and MDA, but all indications are promising. The VAST and MDA sound speed measurement programs were among the most extensive ever undertaken, and MDA/AMODE/MST combined probably represents the present limit to how well the sound speed field can be measured over regions of comparable size. Combinations of various classical techniques utilizing high accuracy nonexpendable instrumentation and lesser accuracy expendable instrumentation deployed from ships and aircraft, combined with carefully chosen databases and proper analysis techniques can yield sound speed errors of a meter per second or less, and the results seem to be quite adequate for matched field processing applications. Fields determined in this manner are as good as fields determined using present-day acoustic tomography or even slightly better. Matched field processing up to ranges of 20,000 wavelengths was successful.

However, several important lessons have come out of the analyses to date of the VAST and MDA datasets. First, sound speed variations of half a meter per second are common in the very deep ocean. Variations of several meters per second may be found as deep as 1000 - 2000 m. It is important for matched field processing to capture this variability, and the procedure of making only shallow measurements to 300 m or even 1000 m with expendables and shallow CTD casts and then extending the profiles to the bottom using a standard climatology may not always be satisfactory. Measurements should be taken as deep as possible, with a good number extending all the way to the bottom. When extension with a climatology is used, the selection of the proper climatology may be important. The experiences with VAST and MDA have indicated that the Levitus climatology in the Northeast Pacific and the Sargasso Sea gives somewhat better results than GDEM.

Second, instrument errors from oceanic instrumentation can be reduced by proper calibration procedures, although there is a limit to how accurately a sound speed profile can be determined under the best of conditions because of inherent oceanic variability, largely internal waves. However, the use of proper averaging procedures such as averaging several rapidly collected XBTs or using optimal statistical interpolation procedures can reduce the overall error of the sound speed field down to less than a meter per second.

The extensive sea tests conducted to date as part of the High Gain Program were essential for gathering the databases necessary to address the questions posed by the program regarding ocean variability and long-range acoustic transmission. However, the experiments are too large and expensive to be conducted on anything like a routine basis. In particular, operational systems which require frequent updates of the three dimensional sound speed field will need to depend upon operational sound speed products produced by the Fleet Numerical Oceanography Center or the Naval Oceanographic Office, probably augmented periodically with direct measurements made in crucial areas and rapidly assimilated into the field. While steady progress is being made in this technology, it will be some years (if indeed ever) before operational products will approach the accuracy needed without significant in situ input. This is the case with the assimilation and prediction of meteorological fields, and there is no reason to think the situation will be different with oceanographic fields.

5.0 ACKNOWLEDGMENTS

Over the course of five years a great many people contributed to this work. Among those crucial to its success were Dick Heitmeyer (NRL), Bill Hodgkiss (Scripps Marine Physical Laboratory), Bob Hearn (Naval Command, Control and Ocean Surveillance Center, RDT&E Division), Orest Diachok (NRL, now at the SACLANT Undersea Research Center), Herb Freese (Science Applications, Inc), and Martin Fagot (NRL) for the leadership they exhibited in the High Gain program and the various forms of support they knowingly and unknowingly provided the author. Richard Myrick, Dennis Lavoie, Steve Sova, Dan Kennedy, Walter Brundage, Tim Howell, Don Burns, Bruce Gomes (all at NRL); Irene DePalma (formerly of NRL); Mike Wilcox, John Cartmill, Peter Flynn, and Shirley Baker (all at Planning Systems, Inc.); and Bob Linzell (Neptune Sciences, Inc) assisted in data collection and processing during the field experiments at the field processing stations and on board both ships and aircraft. Bob Linzell and Shirley Baker were primarily responsible for the later data analysis. Richard Myrick and Bob Linzell are especially to be thanked. Aircraft from NRL, VXN-8, VP-9, VP-46, and VP-48 participated in the data collection phases, and Gary Athey of the Naval Oceanographic Office served as Senior NAVOCEANO Representative on the VXN-8 aircraft during both VAST and MDA and provided invaluable assistance and advice. Crew members and other scientists on the various ships and aircraft involved in the experiments must remain nameless, but without their enthusiastic work and cooperation the massive High Gain Experiments never would have succeeded.

Jim Paquin (Neptune Sciences, Inc), Laurie Jugan, Dick Crout, Alan Wallcraft (all at Planning Systems, Inc), Herb Freese (SAIC), and Ted Bennett (Naval Oceanographic Office) provided valuable input and comments for this document.

Program Managers Newell Booth (now at Naval Command, Control and Ocean Surveillance Center, RDT&E Division) and Dick Doolittle at the Office of Naval Technology (now part of the Office of Naval Research, Code 451) provided very tangible support in the form of financial resources. This work was funded under program elements 0602435N and 0602314N.

6.0 REFERENCES

Bennett, Jr., T.J., M.R. Carnes, P.A. Phoebus, and L.M. Riedlinger (1989). Feature modeling: The incorporation of a front and eddy map into optimum interpolation-based thermal analyses. NORDA Report 242, Naval Research Laboratory, Stennis Space Center, MS.

Bennett, Jr,T.J., J. Boyd, L. Knauer, G. Dawson, and W. Wilson (1992). A feature model of the Iceland Faeroe Front. *MTS Journal*, 26(2), 44-52.

Boyd, J.D. (1987). Improved temperature and depth conversion equations for Sippican AXBTs. *J. Atmos. Ocean. Techn.*, 4(3), 545-551.

Boyd, J.D. (1989). Aircraft Measurements in the Northeast Pacific in Support of the Downslope Conversion Experiment. NORDA Technical Note 470, Naval Research Laboratory, Stennis Space Center, MS.

Boyd, J.D. (1990a). Aircraft Measurements in the Northeast Pacific, Summer 1989. NOARL Technical Note 40, Naval Research Laboratory, Stennis Space Center, MS.

Boyd, J.D. (1990b). Environmental Data Inventory, VAST-I, July 1989. NOARL Technical Note 13, Naval Research Laboratory, Stennis Space Center, MS, 53 pp.

Boyd, J.D., L.A. Jugan, and P. Fleischer (1990). An Environmental Summary of the Sargasso Sea for the Month of July. NOARL Technical Note 62, Naval Research Laboratory, Stennis Space Center, MS.

Boyd, J.D., L.A. Jugan, B.J. Roser (1991). Comparison of Environmental Conditions at Two Sargasso Sea Locations During February. NOARL Technical Note 121, Naval Research Laboratory, Stennis Space Center, MS.

Boyd, J.D., E.P. Kennelly, and P. Pistek (1992a). Estimation of EOF Expansion Coefficients from Incomplete Data. NOARL Technical Note 291, Naval Research Laboratory, SSC, MS.

Boyd, J.D., D. M. Lavoie, R. K. Myrick, R. S. Linzell (1992b). Environmental Data Catalog: MDA-91, June - July 1991. NOARL Technical Note 225, Naval Research Laboratory, SSC, MS.

Boyd, J.D., and R. S. Linzell (1993a). Temperature and depth accuracy of Sippican T-5 XBTs. *Jour. Atm. Ocean. Techn.*, 10(1), 128-136.

Boyd, J.D., and R. S. Linzell (1993b). Evaluation of the Sparton Tight-Tolerance AXBT. *Jour. Atm. and Ocean. Techn.*, accepted.

Bucker, H.P. (1976). Use of calculated sound fields and matched-field detection to locate sound sources in shallow water. *J. Acoust. Soc. Am.*, 59, 368-373.

Carnes, M.R., J.L. Mitchell, and P.W. DeWitt (1990). Synthetic temperature profiles derived from GEOSAT altimetry: Comparison with air-dropped expendable bathythermographic profiles. *J. Geophys. Res.*, 95, 17979-17992.

Chen, C., and F.J. Millero (1977). Speed of sound in seawater at high pressures. *J. Acoust. Soc. Am.*, 62, 1129-1135.

Clancy, R.M, and W.D. Sadler (1992). The Fleet Numerical Oceanography Center suite of oceanographic models and products. *Weather and Forecasting*, 7, 307-327.

Cummings, J.A. and M.J. Ignazewski (1991). The Fleet Numerical Oceanography Center Regional Ocean Thermal Analysis System, Proceedings MTS'91, An Ocean Cooperative: Industry, Government, and Academia, New Orleans, Nov. 10-14, 1123-1129.

Daley, R. (1991). *Atmospheric Data Analysis.* Cambridge University Press, 456 pp.

Davis, T.M., K.A. Countryman and M.J. Carron (1986). Tailored acoustic products utilizing the NAVOCEANO GDEM (a Generalized Digital Environmental Model). Proc. 36th Naval Symposium on Underwater Acoustics, Naval Ocean Systems Center, San Diego, CA.

Del Grosso, V.A. (1974). New equation for the speed of sound in natural waters (with comparisons to other equations). *J. Acoust. Soc. Am.*, 56, 1084-1091.

DeWitt, P.W. (1987). Modal decomposition of the monthly Gulf Stream/Kuroshio temperature fields. NAVOCEANO Technical Report NOO TR 298, Naval Oceanographic Office, Stennis Space Center, MS.

Dushaw, B.D., P.F. Worcester, B.D. Cornuelle, and B.M. Howe (1993). On equations for the speed of sound in sea water. *J. Acoust. Soc. Am.*, 93, 255-275.

Ebbesmeyer, C.C., and B.A. Taft (1979). Variability of potential energy, dynamic height, and salinity in the main pycnocline of the western North Atlantic. *J. Phys. Oceanogr.*, 9, 1073-1089.

Favorite, F., A.J. Dodimead and K. Nasu (1976). *Oceanography of the Subarctic Pacific Region, 1960-71.* Bulletin 33, International North Pacific Fisheries Commission, 187 pp.

Flatte, S.M., ed. (1979). *Sound Transmission through a Fluctuating Ocean.* Cambridge University Press, 299 pp.

Fofonoff, N.P., and R.C. Millard (1983). Algorithms for computation of fundamental properties of seawater. UNESCO Tech. Pa. in Mar. Sci, No. 44, 53 pp.

Frye, H.W. and J.D. Pugh (1971). A new equation for the speed of sound in seawater. *J. Acoust. Soc. Am.*, 50, 384-386.

Hanson, H.P., P. Cornillon, G.R. Halliwell, Jr., and V. Halliwell (1991). Climatological perspectives, oceanographic and meteorological, on variability in the Subtropical Convergence Zone in the northwestern Atlantic. *J. Geophys. Res.*, 96, 8517-8529.

Horton, C.W., M. Clifford, D. Cole, J.E. Schmitz, and L.E. Kantha (1992). Operational modeling: Semi-enclosed basin modeling at the Naval Oceanographic Office. *Oceanography*, 5, 69-72.

Hurlburt, H.E., A.J. Wallcraft, Z. Sirkes and E.J. Metzger (1992). Modeling of the global and Pacific Oceans: On the path to eddy-resolving ocean prediction. *Oceanography*, 5, 9-18.

Iselin, C.O.D. (1936). A study of the circulation of the western North Atlantic. *Pap. Phys. Oceanogr. Meteorol.*, 4.

Jugan, M.J. and H. Beresford (1991). Editing approach for the Navy's Master Oceanographic Observation Data Set. Proc. MTS '91, vol 2, 1164-1168.

Kao, T.W. (1987). The Gulf Stream and its frontal structure. *J. Phys. Oceanogr.* 17(1), 123-133.

Khedouri, E., C. Szczechowski, and R.E. Cheney (1983). Potential Oceanographic Applications of Satellite Altimetry for Inferring Subsruface Thermal Structure, OCEANS'83, Proceedings Marine Technology Society, 274-280.

Levitus, S. (1982). Climatological Atlas of the World. NOAA Prof. Pap. No. 13, 173 pp.

Lynn, R.J. (1986). The Subarctic and Northern Subtropical Fronts in the eastern North Pacific Ocean in Spring. *J. Phys. Oceanogr.*, 16, 209-222.

Munk, W., and C. Wunsch (1979). Ocean acoustic tomography: A scheme for large scale monitoring. *Deep-Sea Res.*, 26A, 123-161.

Nelson, C.A, and W.T. Aldinger (1992). An overview of Fleet Numerical Oceanography Center Operations and Products. *Weather and Forecasting*, 7, 204-219.

Pickard, G.L., and W.J. Emery (1990). *Descriptive Physical Oceanography*. Pergamon Press, 320 pp.

Porter, M.B, R.L. Dicus, and R.G. Fizell (1987). Simulations of matched-field processing in a deep-water Pacific environment. *IEEE J. Oceanic Eng.*, OE-12, 173-190.

Roden G.I. and A. R. Robinson (1988). *Subarctic Frontal Zone in the North-Eastern Pacific: Mesoscale Structure and Synoptic Description.* Harvard Open Ocean Model Report # 31, Harvard University, Cambridge MA 02138, 27 pp. + figures.

Saur, J. F. T. (1980). Surface salinity and temperature on the San Francisco-Honolulu route, June 1966-December 1970 and January 1972-December 1975. *J. Phys. Oceanogr.*, 10, p. 1669-1680.

Spindel, R.C., and P.F. Worcester (1990). Ocean acoustic tomography. *Scientific American*, Oct., 94-99.

Stoughton, R.B., S.M. Flatte, and B.M. Howe (1986). Acoustic measurements of internal wave rms displacement and rms horizontal current off Bermuda in late 1983. *J. Geophys. Res.*, 91, 7721-7732.

Sverdrup, H.U., M. W. Johnson and R. H. Fleming (1942). *The Oceans.* Prentice Hall, 1087 pp.

Teague, W.J., M.J. Carron, and P.J. Hogan (1990). A comparison between the Generalized Digital Environmental Model and Levitus climatologies. *J. Geophys. Res.*, 95, 7167-7183.

Thompson, J.D., T.L. Townsend, A.J. Wallcraft, W.J. Schmitz (1992). Ocean prediction and the Atlantic basin: Scientific issues and technical challenges. *Oceanography*, 5, 36-41.

Uda, M., and K. Hasunuma (1969). The eastward subtropical countercurrent in the western North Pacific ocean. *J. Oceanogr. Soc. Japan*, 25, 201-210.

U.S. Department of Commerce (1992). National Oceanographic Data Center Users Guide, Key to Oceanographic Records Documentation No. 14.

Voorhis, A.D., and J.G. Bruce (1982). Small scale stirring and frontogenesis in the subtropical convergence of the western North Atlantic. *J. Mar. Res.*, 40(suppl.), 801-821.

White, W.B., and R.L. Bernstein (1979). Design of an oceanographic network in the midlatitude north Pacific. *J. Phys. Oceanogr.*, 9, 592-606.

Wilson, W.D. (1960). Equation for the speed of sound in water. *J. Acoust. Soc. Am.*, 32, 1357.

Wuest, G. (1978). *The Stratosphere of the Atlantic Ocean.* Amerind Publishing Co., New Delhi. 112 pp.

7.0 RESULTING PUBLICATIONS

The publications listed below include those published or submitted in the course of this work through August 1993.

Boyd, J.D. (1989). Aircraft Measurements in the Northeast Pacific in Support of the Downslope Conversion Experiment. NORDA Technical Note 470, Naval Research Laboratory, Stennis Space Center, MS.

Boyd, J.D. (1990a). Aircraft Measurements in the Northeast Pacific, Summer 1989. NOARL Technical Note 40, Naval Research Laboratory, Stennis Space Center, MS.

Boyd, J.D. (1990b). Environmental Data Inventory, VAST-I, July 1989. NOARL Technical Note 13, Naval Research Laboratory, Stennis Space Center, MS.

Boyd, J.D., L.A. Jugan, and P. Fleischer (1990a). An Environmental Summary of the Sargasso Sea for the Month of July. NOARL Technical Note 62, Naval Research Laboratory, Stennis Space Center, MS.

Boyd, J.D., L.A. Jugan, M.A. Rich and B.J. Roser (1990b). Environmental Conditions in the Gulf of Mexico during November-December. NOARL Technical Note 83, Naval Research Laboratory, Stennis Space Center, MS.

Boyd, J.D., L.A. Jugan, B.J. Roser (1991a). Comparison of Environmental Conditions at Two Sargasso Sea Locations During February. NOARL Technical Note 121, Naval Research Laboratory, Stennis Space Center, MS.

Boyd, J.D. (1991b). Critical Experiment Review: EVA Analysis and Support. NOARL Technical Note 217, Naval Research Laboratory, SSC, MS.

Boyd, J.D., E.P. Kennelly, and P. Pistek (1992a). Estimation of EOF Expansion Coefficients from Incomplete Data. NOARL Technical Note 291, Naval Research Laboratory, SSC, MS.

Boyd, J.D., D. M. Lavoie, R. K. Myrick, R. S. Linzell (1992b). Environmental Data Catalog: MDA-91, June - July 1991. NOARL Technical Note 225, Naval Research Laboratory, SSC, MS.

Boyd, J.D., and R. S. Linzell (1993a). Temperature and depth accuracy of Sippican T-5 XBTs. *Jour. Atm. Ocean. Techn.*, 10(1), 128-136.

Boyd, J.D., and R. S. Linzell (1993b). Evaluation of the Sparton Tight-Tolerance AXBT. *Jour. Atm. and Ocean. Techn.*, accepted.

Boyd, J.D., E. P. Kennelly, and P. Pistek (1993). Estimation of EOF expansion coefficients from incomplete data. Deep-Sea Research, submitted.

Cornuelle, B.D., P.F. Worcester, J.A. Hildebrand, W.S. Hodgkiss, Jr., T.F. Duda, J.D. Boyd, B.M. Howe, J.A. Mercer, and R.C. Spindel (1994). Ocean acoustic tomography at 1000-km range using wavefronts measured with a large aperture vertical array. *J. Geophys. Res.*, accepted.

Worcester, P.F., B.D. Cornuelle, J.A. Hildebrand, W.S. Hodgkiss, Jr., T.F. Duda, J.D. Boyd, B.M. Howe, J.A. Mercer, and R.C. Spindel (1994). A comparison of measured and predicted broadband acoustic arrival patterns in travel time-depth space at 1000-km range. *Jour. Acous. Soc. Am.*, submitted.

The AMODE-MST Group (1993). Moving ship tomography in the Northwest Atlantic Ocean. *EOS: Trans. AGU*, submitted.